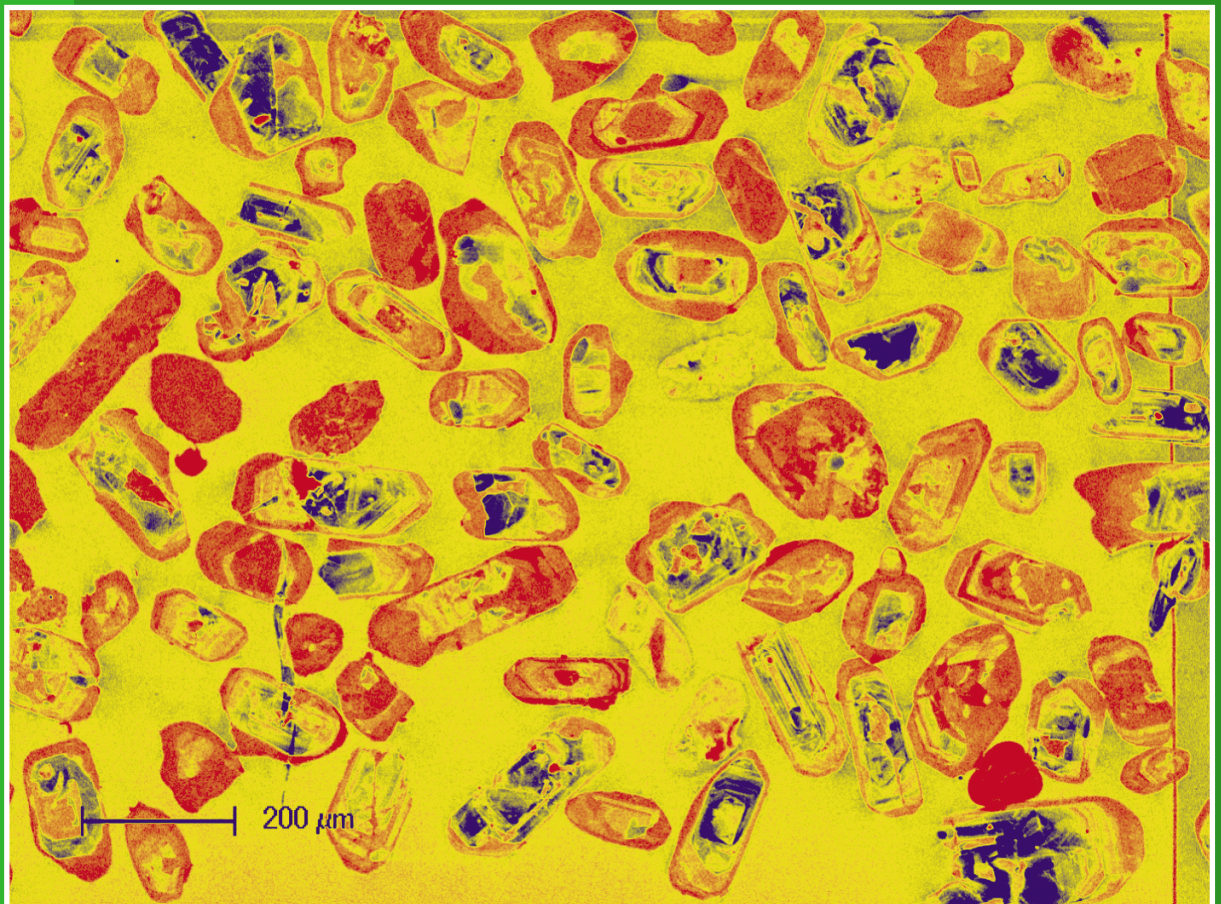


**REPORT
115**

**A MULTI-ISOTOPIC APPROACH TO THE CRUSTAL
EVOLUTION OF THE WEST MUSGRAVE PROVINCE,
CENTRAL AUSTRALIA**

by CL Kirkland, RH Smithies, A Woodhouse,
HM Howard, MTD Wingate, EA Belousova, JB Cliff,
RC Murphy, and CV Spaggiari





Government of **Western Australia**
Department of **Mines and Petroleum**

REPORT 115

A MULTI-ISOTOPIC APPROACH TO THE CRUSTAL EVOLUTION OF THE WEST MUSGRAVE PROVINCE, CENTRAL AUSTRALIA

by

**CL Kirkland, RH Smithies, A Woodhouse¹, HM Howard, MTD Wingate,
EA Belousova², JB Cliff³, RC Murphy², and CV Spaggiari**

¹ Continental Evolution Research Group, School of Earth and Environmental Sciences, The University of Adelaide

² GEMOC, Department of Earth and Planetary Sciences, Macquarie University

³ Centre for Microscopy, Characterisation and analysis, The University of Western Australia

Perth 2012



**Geological Survey of
Western Australia**

MINISTER FOR MINES AND PETROLEUM
Hon. Norman Moore MLC

DIRECTOR GENERAL, DEPARTMENT OF MINES AND PETROLEUM
Richard Sellers

EXECUTIVE DIRECTOR, GEOLOGICAL SURVEY OF WESTERN AUSTRALIA
Rick Rogerson

REFERENCE

The recommended reference for this publication is:

Kirkland, CL, Smithies, RH, Woodhouse, E, Howard, HM, Wingate, MTD, Belousova, EA, Cliff, JB, Murphy, RC and Spaggiari, CV 2012,
A multi-isotopic approach to the crustal evolution of the west Musgrave Province, central Australia: Geological Survey of Western
Australia, Report 115, 47p.

National Library of Australia Cataloguing-in-Publication entry

Title: A multi-isotopic approach to the crustal evolution of the
West Musgrave Province, Central
Australia [electronic resource] / C L
Kirkland ... [et al.]

ISBN: 9781741684551 (ebook: pdf)

Series: Report (Geological Survey of Western
Australia), 115

Subjects: Geology, Structural--Western Australia--Musgrave Province.
Soil crusting--Western Australia--Musgrave Province.
Earth--Crust.
Soil mineralogy--Western Australia--Musgrave Province.
Soil ecology--Western Australia--Musgrave Province.

Other Authors/Contributors: Kirkland, C. L.
Geological Survey of Western Australia

Dewey Number: 551.1409941

Grid references in this publication refer to the Geocentric Datum of Australia 1994 (GDA94). Locations mentioned in the text are referenced using Map Grid Australia (MGA) coordinates, Zone 52. All locations are quoted to at least the nearest 100 m.



U–Pb measurements were conducted using the SHRIMP II ion microprobes at the John de Laeter Centre of Isotope Research at Curtin University in Perth, Australia. Isotope analyses were funded in part by the Western Australian government Exploration Incentive Scheme (EIS). Lu–Hf measurements were conducted using LA-ICPMS at the ARC National Key Centre for Geochemical Evolution and Metallogeny of Continents (GEMOC), via the ARC Centre of Excellence in Core to Crust Fluid Systems (CCFS), based in the Department of Earth and Planetary Sciences at Macquarie University, Australia.

Copy editor: K Hawkins
Cartography: M Prause
Desktop publishing: B Hitchings

Published 2012 by Geological Survey of Western Australia

This Report is published in digital format (PDF) and is available online at <<http://www.dmp.wa.gov.au/GSWApublications>>.

Further details of geological publications and maps produced by the Geological Survey of Western Australia are available from:

Information Centre
Department of Mines and Petroleum
100 Plain Street
EAST PERTH WESTERN AUSTRALIA 6004
Telephone: +61 8 9222 3459 Facsimile: +61 8 9222 3444
www.dmp.wa.gov.au/GSWApublications

Cover photograph: Proterozoic zircon crystals from GSWA 194768, many showing evidence of multi-stage growth.

Contents

Abstract	1
Introduction	2
Geological setting	2
Magmatic suites of the west Musgrave Province	5
Papulankutja Supersuite	5
Wankanki Supersuite	5
Pitjantjatjara Supersuite	5
Warakurna Supersuite	6
Younger events	6
Analytical methodology	6
U–Pb	6
Lu–Hf	6
Sm–Nd	7
Oxygen	24
Petrography, Hf isotopic signatures, and U–Pb geochronology of the Papulankutja Supersuite and related rocks	24
GSWA 194767: psammitic enclave in gneiss	27
GSWA 194768: migmatitic gneiss	27
GSWA 187195: leucogranitic gneiss	27
GSWA 194765: granite dyke	27
GSWA 194764: foliated monzogranite	29
GSWA 194766: granitic pegmatite dyke	29
GSWA 194759: dolerite dyke	29
Results and interpretation	30
The c. 1400 Ma Papulankutja Supersuite	30
Metasedimentary rocks related to the Papulankutja Supersuite	30
Inheritance in the dolerite dyke	30
Evolution of Hf isotope ratios within individual zircons	31
Evolution of Hf isotope ratios between samples: the case for c. 1900 Ma crust formation	31
Whole-rock Sm–Nd isotopic record of the Musgrave Province: support for c. 1900 Ma crust formation	35
Oxygen isotopes in zircons: evaluating the degree of crustal input into mantle magma sources	36
Masking of juvenile Hf input by high-field-strength element (HFSE) magma enrichment	37
Isotopic constraints on the geological architecture of Proterozoic Australia	38
Comparison with the Albany–Fraser Orogen	39
Comparison with the Arunta Orogen	39
Comparison with the Gawler Craton	39
The Proterozoic development of the Musgrave Province	41
Conclusions	42
References	43

Figures

1. Simplified geological map of the west Musgrave Province	3
2. Primitive-mantle-normalized trace and REE plot	5
3. U–Pb analytical data for zircons from Papulankutja Supersuite samples	28
4. U–Pb zircon geochronology of Papulankutja Supersuite samples	29
5. Intragrain Hf isotopic values in zircons from GSWA 194767	31
6. $^{176}\text{Hf}/^{177}\text{Hf}(i)$ evolution diagram for zircons from the west Musgrave Province	32
7. Hf-evolution diagram for magmatic rocks of the west Musgrave Orogen	32
8. Histograms of $^{176}\text{Lu}/^{177}\text{Hf}$ values for a range of different geological settings	32
9. Probability density diagram of two-stage model ages from the west Musgrave Province	33
10. Two-stage model-age evolution of magmatic supersuites of the west Musgrave Province	33
11. Schematic initial Hf evolution diagram	34
12. Whole-rock ϵNd vs zircon ϵHf for samples from the west Musgrave Province	35
13. Nd-evolution plot for whole-rock samples from the west Musgrave Province	35
14. Zircon $\delta^{18}\text{O}_{\text{VSMOW}}$ against Hf crustal model age from the same zircon grains	36
15. Mixture-modelling of batch melts and bulk melting between Musgrave lithologies and average mid-ocean ridge basalt	38
16. Time–space diagram for the west Musgrave Province, Albany–Fraser Orogen, and west Arunta Orogen	40
17. Event signature diagram	41
18. Schematic continental reconstruction of Proterozoic Australia for the interval 1900–1600 Ma	42

Tables

1.	Summary of U–Pb SIMS geochronology.....	7
2.	LA-ICPMS Lu–Hf analytical results for zircon from the west Musgrave Province.....	8
3.	LA-ICPMS Lu–Hf analytical results for zircon from magmatic rocks of the west Musgrave Province.....	11
4.	Compilation of TIMS Sm–Nd analytical results for whole rock samples from the west Musgrave Province.....	18
5.	Oxygen isotope analyses from zircons of the west Musgraves.....	25
6.	Statistical time series analysis of Nd and Hf model ages from magmatic rocks of west Musgrave Province.....	34

A multi-isotopic approach to the crustal evolution of the west Musgrave Province, central Australia

by

CL Kirkland, RH Smithies, E Woodhouse¹, HM Howard, MTD Wingate,
EA Belousova², JB Cliff³, RC Murphy², CV Spaggiari

Abstract

Both the timing and mechanism of crust formation are important factors in understanding the mineral wealth of a region, as juvenile addition of material from the mantle into the crust directly or indirectly controls the mineral endowment. Studies of Hf and Nd isotopic evolution can constrain the timing of crust formation, provided that the recorded isotopic signal does not represent a mixture between materials formed at different times. Hence two caveats have been widely considered important with respect to this: (i) crust formation events can only be ascribed to periods when crystallization ages correspond to model ages; and (ii) trends along normal crustal evolution lines reflect reworking of the same source. However, with respect to the first point, a match between model ages and the timing of reworking of evolved material implies either a real crust formation event or early source homogenization and, in either case, a coupling between lower and upper crustal processes. This is even the case where no juvenile material has been preserved from the mantle extraction event. With respect to the second point, intracontinental rifts and other regions with sustained very-high-temperature crustal recycling processes generate magmatic provinces with extreme enrichment in high-field-strength elements (HFSE). This can have a profound influence on isotope evolution trends, suppressing typical juvenile addition patterns. Isotope mixture modelling indicates that a significant volume of mantle-derived material can be accommodated within HFSE-enriched magmas without divergence of isotopic signatures from apparent reworking trends.

In order to illustrate these points we present a case study from the west Musgrave Province in Western Australia. The oldest exposed basement in the west Musgrave Province has traditionally been considered to be calc-alkaline igneous rocks of the 1345–1293 Ma Wankanki Supersuite, interleaved with near-contemporaneous paragneisses of the Wirku Metamorphics. However, new geochronology has revealed the presence of exposed 1402 ± 4 Ma crystalline rocks. Hf isotopes in zircons from these magmatic rocks and others throughout the Musgrave Orogen indicate major juvenile crust formation events at 1950–1900 Ma and 1600–1550 Ma. Although no juvenile rocks or crystals are known from 1950 to 1900 Ma, radiogenic addition into the crust at this time is required to account for consistent Nd and Hf evolution patterns that show no indication of an initially heterogeneous source. Measurements of oxygen isotopes in zircons confirm that much of the Hf isotope signal is not compromised by mixtures. Furthermore, the correspondence between mantle extraction ages and the commencement of reworking of Archean material is consistent with generation of new crust at 1950–1900 Ma. This timing of juvenile addition is dissimilar to that observed in the Albany–Fraser and Arunta Orogens and may reflect continental arc development on the margin of a continent to the south. The general Hf isotopic evolution trend apparently reflects reworking from a dominant 1950–1900 Ma source with only minor unradiogenic and radiogenic input after that time. However, the Musgrave Province crust had become so HFSE enriched during the prolonged intracontinental Musgrave Orogeny (1220–1150 Ma) that it was insensitive to mantle input, which is estimated to have been 85–60% during this event.

KEYWORDS: Lu–Hf, model age, Musgrave Province, oxygen isotopes, Proterozoic Australia, Sm–Nd, U–Pb, zircon

Introduction

The formation of continental crust is the process by which generally basaltic material is extracted from the mantle, differentiated, and emplaced as an andesitic to dacitic upper surface on Earth (Hofmann, 1988). This important process is responsible for producing stabilized continental crust that is able to support terrestrial life, and ultimately endows the mineral wealth of a region. For example, periods of juvenile crust formation (Condie, 1998) coincide with periods of enhanced orogenic gold volume (Goldfarb et al., 2001; Groves et al., 2003). Active continental margins are typically regarded as the principal sites of continental crust formation, as new juvenile material is generated and pre-existing crust is recycled at these margins (Arculus, 1999; Hawkesworth and Kemp, 2006a,b). However, new additions to the continental crust also occur in extensional settings, such as continental large igneous provinces and in major rift systems (Ernst et al., 2005; Paul, 1992; Rogers et al., 2000; Wörner, 1999).

The collision of an intra-oceanic volcanic arc with the margin of a continent along a subduction zone is an important tectonic setting within which continental crust, enriched in incompatible elements, differentiates over time. However, it is also an important setting within which pre-existing crust is reworked. Arc–continent collisions have formed many of the world’s mountain belts including the Urals, the Appalachians, the Variscides, and the Tethyides. On present-day Earth, arc–continent collision occurs along tectonically active plate boundaries such as those in the southwest Pacific Ocean and the Caribbean Sea. Arc–continent collision zones host significant quantities of the world’s mineral wealth, including large deposits of massive sulfides, gold, and platinum group elements. Despite the importance of arc-accretion events, their identification in the geological record is complicated by selective preservation of certain types of terranes within the arc system.

Specific arc-related tectonic environments, reflecting either juvenile input or reworking, or a combination of these processes, would be expected to produce unique Hf isotopic evolution patterns (Collins et al., 2011). For example, in a simple situation of arc accretion onto a craton margin, juvenile signatures would be predicted to diminish over time as melts penetrate through a thickening crustal volume. On the other hand, back-arc development would increase the juvenile input into isotopic systems with greater influence of asthenospheric mantle. Intra-oceanic arc creation would be expected to produce juvenile melts over the duration of compression. Although these are simple scenarios, magmatic isotopic and chemical patterns over time should indicate the dominant tectonic process. Furthermore, some intracontinental rifts, particularly those of Proterozoic age, due to a supercontinental plate configuration at this time, can present interesting environments within which there were very high (or ultra high) temperature crustal recycling processes (Smithies et al., 2011). These processes result from enhanced mantle heat flow and form magmatic provinces characterized by extreme enrichment in high-field-strength elements (HFSE) (Evins et al., 2010; Smithies et al., 2010). This work demonstrates that the

compositions of magmas in these provinces can suppress changes in isotopic evolution trends.

The Mesoproterozoic Musgrave Province in central Australia possibly represents one of the most extreme cases of an extension-related, HFSE-enriched magmatic province (Smithies et al., 2011). Magmatism in this region extends from c. 1400 Ma to c. 1040 Ma and is divided into four major events, of which at least two were intracontinental (Smithies et al., 2010). Apparent Nd- and Hf-isotopic trends for these magmatic rocks suggest recycling of the same isotopically homogeneous regional source, itself formed at some stage before c. 1800 Ma. This suggestion, however, is significantly at odds with local and regional geological relationships, and with Hf-isotopic data drawn from magmatic, inherited, and detrital zircon datasets. These contrasting interpretations arise because significant quantities of juvenile material (HFSE-poor, low Hf concentration) can be contributed to crustal sources within a HFSE-enriched (high Hf concentration) magmatic province before evolution trends diverge from apparent reworking trends.

Hf- and Nd- evolution trends can be considered as a function of either of two end-member scenarios; that is, resulting from direct extraction from the mantle or related to mixing of juvenile material with unradiogenic sources to produce mixed evolution arrays. It is widely believed that juvenile crust-formation events are indicated by the coincidence of crystallization ages and model ages (e.g. Arndt and Goldstein, 1987). However, this is not always an easy rule to apply. There are geological environments in which direct mantle-derived melts might stagnate in the deep crust for extended periods prior to zircon crystallization or where zircon crystals are either dissolved and the record of crystallization is lost (Hawkesworth et al., 2009), or do not develop in the first place (Watson, 1996). In such cases, strong linear isotopic evolution arrays and a lack of model age scatter through time indicates either effective early homogenization of disparate sources or a source from an early mantle extraction event. In the case of the Musgrave Province, the data suggest a crust-forming event between 1950 and 1900 Ma. To distinguish between different tectonic settings and to understand their development through time in the west Musgrave Province, measurements of Lu–Hf isotopes in zircons from magmatic rocks and Sm–Nd isotopes in whole-rock samples are compared with similar data from other parts of the West, North, and South Australian Cratons.

Geological setting

The Mesoproterozoic Musgrave Province is an east-trending belt up to 800 km long and 350 km wide, bounded to the north and south by Neoproterozoic to Paleozoic basins. The province lies at the convergence of several of Australia’s main Proterozoic structural trends, which are thought to reflect the amalgamation of the North, West, and South Australian Cratons (Fig. 1) (Myers et al., 1996). The broad lithological framework of the province is largely established (Camacho and Fanning, 1995; Camacho et al., 2002; Clarke and Powell, 1991;

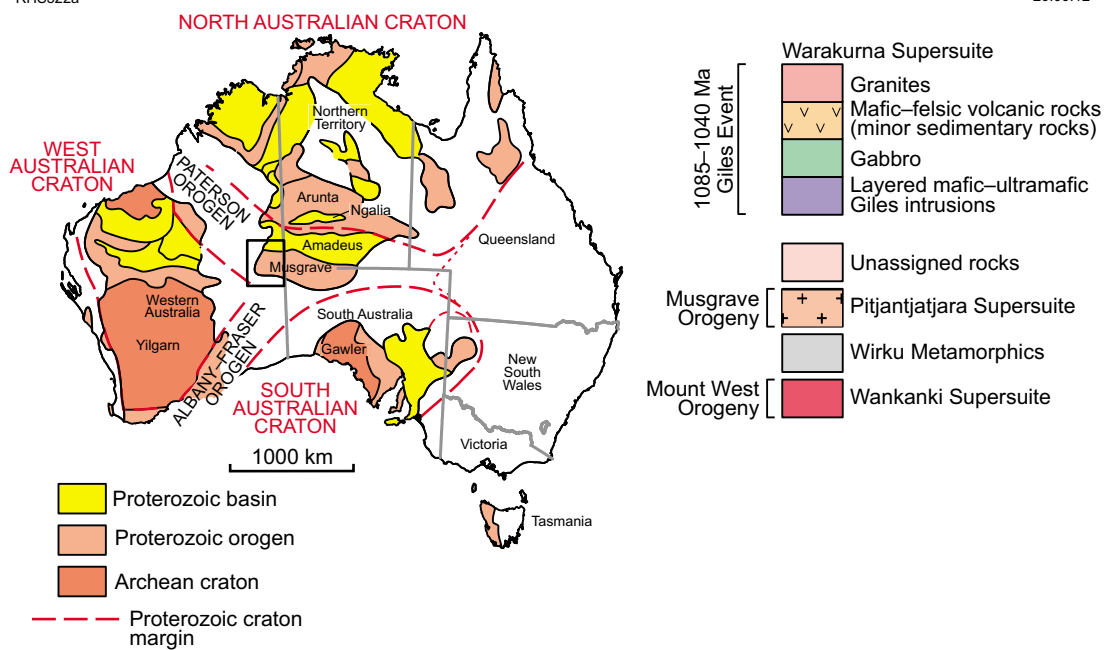
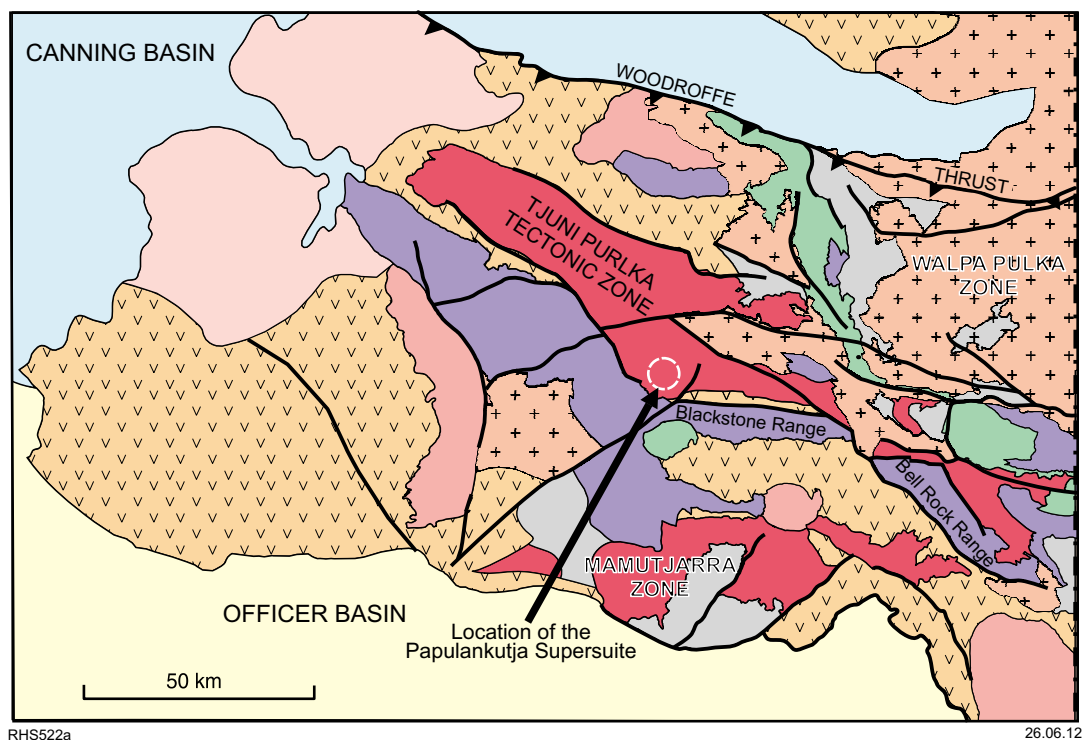


Figure 1. Simplified geological map of the west Musgrave Province, showing the three lithotectonic zones. Inset shows the location of the Musgrave Province with respect to North, South, and West Australian Cratons (modified from Myers et al., 1996).

Daniels, 1974; Evins et al., 2010; Glikson et al., 1996; Gregory et al., 2009; Kelly et al., 2006; Smithies et al., 2011; Smithies et al., 2010; White et al., 1999), although its paleogeographic and tectonic evolution remain uncertain. In particular, the time of craton amalgamation is debated (Aitken and Betts, 2009; Betts and Giles, 2006; Wade et al., 2006; Wade et al., 2008), although the current consensus is that it was complete by c. 1290 Ma. Possibly of direct relevance to this debate is the observation that the Musgrave Province, in general, represents Proterozoic Australia's most isotopically juvenile region (Wade et al., 2006).

The nature of the basement to the Musgrave Province is cryptic due to intense reworking during numerous Mesoproterozoic events. However the Nd- and Hf-isotopic evolution of nearly all rocks in the province requires the presence of an early Mesoproterozoic to Paleoproterozoic juvenile basement, along with a minor Archean component (Smithies et al., 2010; Wade et al., 2006). Banded gneisses, mainly preserved as rafts in granite, locally form a significant component throughout the Musgrave Province (Gray, 1978; Gray and Compston, 1978). These are typically interpreted to have been derived from volcanic, volcanoclastic, or clastic protoliths deposited mainly between 1600 and 1540 Ma (Edgoose et al., 2004; Gray, 1978; Gray and Compston, 1978). However, Evins et al. (in press) considered that protoliths to all banded gneisses in the west Musgrave Province, and many in the east (e.g. those discussed in Wade et al., 2006), were supracrustal deposits with maximum depositional ages younger than c. 1400 Ma. Protoliths to many of the gneisses within the west Musgrave Province were deposited between c. 1345 and 1293 Ma, and were derived from sources that included three major detrital zircon age ranges: c. 3200–2630 Ma, c. 1790–1590 Ma, and c. 1570–1470 Ma. These paragneisses are now assigned to the Wirku Metamorphics (Howard et al., 2011a). Nevertheless, rare exposures of c. 1600–1540 Ma orthogneiss elsewhere in the province (in South Australia and the Northern Territory, e.g. Edgoose et al., 2004) confirm the presence of basement of this age, although its extent and tectonic setting remain poorly constrained. Based on juvenile incompatible trace element compositions and radiogenic Nd-isotopic compositions, an arc setting for the orthogneiss protoliths (or, in the case of the Wirku Metamorphics, for the igneous hinterland to the detritus in those paragneisses) has been inferred (Wade et al., 2006). This arc was considered to have accreted to the southern margin of the Paleoproterozoic to Mesoproterozoic Arunta Province to the north (Wade et al., 2006).

Outcrop in the west Musgrave Province is dominated by granite formed during several Mesoproterozoic events. The oldest of these is a recently identified, and hitherto unnamed, event that involved intrusion and possible extrusion of felsic, calc-alkaline magmas of the c. 1400 Ma Papulankutja Supersuite and contemporaneous redistribution of this material into localized sedimentary basins (Howard et al., 2011b). Subsequent major magmatic events include the 1345–1293 Ma Mount West Orogeny, the 1220–1150 Ma Musgrave Orogeny and the 1085–1040 Ma Giles Event (Camacho et al., 2002; Evins

et al., 2010; Glikson et al., 1996; Howard et al., 2011b; Smithies et al., 2010; Smithies et al., 2011; Wade et al., 2008).

In the west Musgrave Province, granites are distributed between three lithotectonic zones (Smithies et al., 2010). The Walpa Pulka Zone (Fig. 1) in the northeast is dominated by granites generated during the Musgrave Orogeny. In the southwest, the Mamutjarra Zone (Fig. 1) is dominated by granites of the Mount West Orogeny. Between these zones, the Tjuni Purlka Tectonic Zone (Fig. 1) is a broad northwest-trending zone that was a focus for deformation from at least c. 1220 Ma to c. 1050 Ma (Smithies et al., 2010). Its faulted boundaries provided pathways for mafic to felsic magmas during the Giles Event.

The Mount West Orogeny produced calc-alkaline granites of the Wankanki Supersuite (Fig. 1), which were emplaced mainly within the Tjuni Purlka Tectonic Zone and the Mamutjarra Zone (Evins et al., 2009; Smithies et al., 2009). Crystallization ages range from c. 1345 to c. 1293 Ma, although they are concentrated between c. 1326 and 1312 Ma (Smithies et al., 2011). Rocks of the Wankanki Supersuite and of the older Papulankutja Supersuite are compositionally indistinguishable. They are typically metaluminous, calcic to calc-alkaline granodiorites and monzogranites with strong compositional similarities to Phanerozoic granites of the Andean continental arc (Smithies et al., 2010). The Mount West Orogeny may reflect a final subduction and accretionary event in the amalgamation of the North, West, and South Australian Cratons (Betts and Giles, 2006; Giles et al., 2004; Smithies et al., 2011). However, a lack of associated gabbroic rocks, together with calculated Nd- T_{DM} and Hf- T_{DM}^2 model ages (c. 2000–1900 Ma) that pre-date intrusion ages by >700 Ma, suggest either a continental arc setting or the intracontinental remelting of calc-alkaline basement (Smithies et al., 2011; Smithies et al., 2010). T_{DM} refers to the model age of a sample based on the time that the isotopic composition of the sample was equivalent to the model-depleted mantle (e.g. Griffin et al., 2004).

The Musgrave Orogeny produced intense deformation and widespread granulite-facies metamorphism. The dominant northwest structural trend within the Tjuni Purlka Tectonic Zone reflects a crustal architecture established during or before the Musgrave Orogeny and was locally modified and reactivated during later events. There is no clear evidence for significant compressional deformation associated with the prolonged Musgrave Orogeny, which appears to have been essentially intracontinental (Fishwick and Reading, 2008; Smithies et al., 2010; Wade et al., 2008).

Orthopyroxene-bearing (charnockitic) and locally rapakivi-textured granites of the Pitjantjatjara Supersuite intruded the mid-crust more or less continuously throughout the Musgrave Orogeny. Their distribution is essentially antithetic to that of the Wankanki Supersuite. They are ferroan and typically alkali-calcic granites (Frost et al., 2001; Frost and Frost, 2008) with a wide silica range (56.8–78.0 wt% SiO_2) and extreme enrichments in rare earth elements (REE) and HFSE, which clearly

distinguishes them from older calc-alkaline rocks of the Wankanki and Papulankutja Supersuites (Fig. 2). These anhydrous, Ti- and P-enriched granites, like compositionally similar granites elsewhere (e.g. Kilpatrick and Ellis, 1992), were intruded at very high temperatures (approximately $>900^{\circ}\text{C}$; Smithies et al., 2010). Their intrusion coincided with, although it was not the heat source for, a 70–100 Ma period of regional ultrahigh-temperature (UHT) metamorphism (Smithies et al., 2011). This metamorphism was characterized by temperatures in the lower crust of $>1000^{\circ}\text{C}$ along a geothermal gradient of $\geq 35\text{--}40^{\circ}\text{C}/\text{km}$ (Kelsey et al., 2009).

Rocks of the Warakurna Supersuite, emplaced during the 1085–1040 Ma Giles Event, extend over at least 1.5 million km^2 in central and western Australia, forming the Warakurna Large Igneous Province (Howard et al., 2009; Wingate et al., 2004). Giant mafic–ultramafic bodies (Giles intrusions) intruded the boundary between the Mamutjarra and Tjuni Purlka Tectonic Zones between c. 1080 and 1075 Ma (Evins et al., 2010; Smithies et al., 2011). From c. 1075 to 1070 Ma, mafic and felsic magmatism continued to be focused along synmagmatic shear zones that mark the boundaries of the Tjuni Purlka Tectonic Zone, and a thick (approximately 10 km) succession of bimodal volcanic rocks was deposited on the western part of the Musgrave Province from c. 1075 to <1050 Ma. Like the earlier rocks of the Pitjantjatjara Supersuite, the felsic rocks of the Warakurna Supersuite are ferroan and typically alkali-calcic (Frost and Frost, 2008), with extreme enrichments in REE and HFSE (Fig. 2).

The Giles Event has been interpreted as the result of a mantle plume (Wingate et al., 2004), although continuous

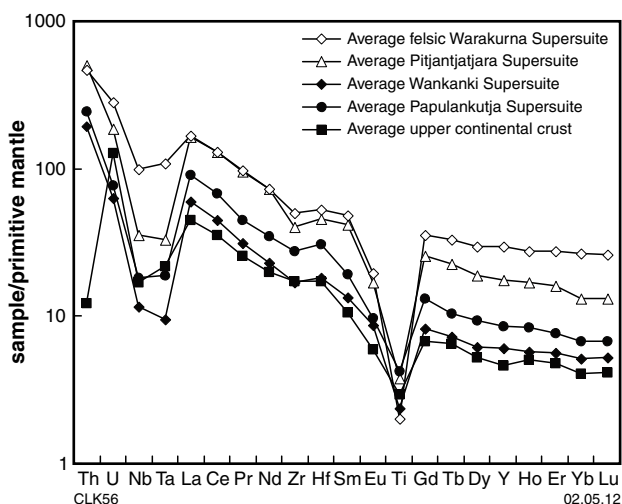


Figure 2. Primitive-mantle-normalized trace and REE plot showing average whole-rock compositions for magmatic supersuites of the west Musgrave Province. Average upper continental crust (Rudnick et al., 2005) is shown for comparison. Normalization values are from Sun and McDonough (1989). Data from individual samples are available for download from <http://geochem.dmp.wa.gov.au/geochem/>

mantle-derived igneous activity from c. 1080 to <1050 Ma has been suggested to require a more complex geodynamic setting (Evins et al., 2010). One interpretation is that the Giles Event reflects a long-lived, failed intracontinental rift called the Ngaanyatjarra Rift (Evins et al., 2010). An intracontinental setting is indicated for the Musgrave Province for at least 150 Ma prior to the Giles Event, and the region has remained in such a setting to the present day (Evins et al., 2010; Smithies et al., 2011).

Magmatic suites of the west Musgrave Province

Outcrop in the west Musgrave Province is dominated by granitic rocks produced during several Mesoproterozoic events, including an unnamed c. 1400 Ma event, the 1345–1293 Ma Mount West Orogeny, the 1220–1150 Ma Musgrave Orogeny, and the 1085–1040 Ma Giles Event (Smithies et al., 2009; Wade et al., 2008). Magma compositions range from dominantly calc-alkaline during the Mount West Orogeny to dominantly alkaline-calcic during the Musgrave Orogeny and Giles Event, and have been interpreted to correspond to a transition from subduction and accretionary orogenesis (Mount West Orogeny; Betts and Giles, 2006; Giles et al., 2004; Smithies et al., 2010; Smithies et al., 2009) to intracontinental events (Musgrave Orogeny and Giles Event; Wade et al., 2006; Wade et al., 2008).

Papulankutja Supersuite

At c. 1400 Ma, granodiorites and monzogranites were intruded into a limited area south of Mount Scott, in the southwestern part of the Holt map sheet (Tjuni Purlka Tectonic Zone; Fig. 1). These intrusive rocks are chemically indistinguishable from calc-alkaline granites of the Wankanki Supersuite. As discussed below, the Papulankutja Supersuite formed principally through dehydration melting of c. 1950–1900 Ma juvenile lower crust, most likely in a continental arc setting.

Wankanki Supersuite

During the Mount West Orogeny, c. 1345 to c. 1293 Ma granites of the Wankanki Supersuite were emplaced (Smithies et al., 2009; White et al., 1999). Intrusions of the Wankanki Supersuite are metaluminous, calcic to alkali-calcic granodiorites to monzogranites (Smithies et al., 2010).

Pitjantjatjara Supersuite

The Musgrave Orogeny caused intense deformation, widespread granulite facies reworking, and granitic magmatism of the Pitjantjatjara Supersuite (Edgoose et al., 2004). In the west Musgrave Province, magmatism mainly occurred between c. 1220 and c. 1150 Ma (Smithies et al., 2009) and produced a suite of ferroan, alkali-calcic granitic magmas. The absence of clear evidence for significant compressional deformation associated with

the prolonged Musgrave Orogeny implies an essentially intracontinental setting (Wade et al., 2008). Pitjantjatjara magmas include voluminous monzodiorite to alkali-feldspar granite, and less voluminous schlieric biotite–orthopyroxene leucogranites within the monzogranite to syenogranite compositional range. These rocks formed through melting of a homogenized 1950–1900 Ma source that was refertilized by mantle input.

Warakurna Supersuite

Mafic–ultramafic Giles intrusions were emplaced between c. 1080 and 1070 Ma between tectonic zones of the west Musgrave Province, together with ferroan, alkali-calcic granites and rhyolites (Evins et al., 2010; Smithies et al., 2010; Smithies et al., 2009). The Giles event is considered to include at least 10 magmatic pulses with hiatus of up to 10 Ma, consistent with a long-lived intracontinental rift setting (the Ngaanyatjarra Rift; Evins et al., 2010).

Younger events

Following deep burial of the Musgrave Orogen beneath Neoproterozoic basins, the Musgrave Province was deformed during several uplift events. These uplift events include the c. 550 Ma Petermann Orogeny, broadly coincident with Gondwana assembly (Edgoose et al., 2004), and the c. 400–350 Ma Alice Springs Orogeny (Haines et al., 2001).

Analytical methodology

We present Hf, Nd, and oxygen isotopic datasets, constrained by U–Pb zircon geochronology, for material recording the earliest magmatic evolution in the west Musgrave Province. The mean square of the weighted deviates (MSWD; York, 1966) is provided with results. The MSWD is used as a measure of consistency of the dataset. In simple terms a value of one suggests that the scatter can be explained by analytical uncertainties alone and that if geologically caused variation is present, it cannot be resolved within the precision of the individual analyses. Values less than one suggest that analytical uncertainties have been overestimated. Values greater than one can indicate that either underestimated analytical uncertainties or another source of uncertainty (typically related to geological complexity) is present in the dataset. However, the actual MSWD value depends on the number of data points (Wendt and Carl, 1991). As an example, consider a dataset of five analyses. For 95% confidence that the scatter is due to analytical errors in this dataset, the MSWD would range from 0.2 to 2.2. However, for 25 analyses the MSWD range would be less, from 0.6 to 1.5. Regressions have r^2 values provided, which refers to the degree of correlation between x and y variables. P values are cited which describe the probability (from 0 to 1) of a statistical significance test. The 95% confidence level (P value; $1.00 - 0.95 = 0.05$) is widely regarded as indicating statistical significance.

U–Pb

The analytical method for secondary ion mass spectroscopy (by the sensitive high-resolution ion microprobe) (SIMS–SHRIMP) zircon U–Pb analysis is described in detail in Wingate and Kirkland (2010) and only a brief summary is provided here. Zircons were separated by crushing and elutriation followed by heavy-liquid and magnetic separation. The resulting hand-picked zircon crystals were mounted with zircon standards (CZ3, OG1, BR266, and Temora 2) in epoxy and ground to half-grain thickness to expose crystal interiors. Transmitted, reflected-light, and cathodoluminescence (CL) images of all grains were produced to guide positioning analytical locations. The zircon standard BR266 was used for concentration calibration and also U–Pb calibration (559 Ma, 903 ppm 238U; Stern, 2001). The accuracy of $^{207}\text{Pb}^*/^{206}\text{Pb}^*$ ratios was verified by comparison with the Archean OG1 zircon standard (Stern et al., 2009). No correction for $^{207}\text{Pb}^*/^{206}\text{Pb}^*$ fractionation is deemed necessary. A summary of geochronology results is presented in Table 1.

Lu–Hf

Hafnium isotope analyses were conducted on previously dated zircons using a New Wave/Merchantek LUV213 laser-ablation microprobe attached to a Nu Plasma laser ablation multi-collector inductively coupled plasma mass spectrometer (LA-MC-ICP-MS) at Macquarie University, Sydney. The analyses used a beam diameter of approximately 55 μm and a 5 Hz repetition rate, which resulted in ablation pits typically 40–60 μm deep. The ablated sample material was transported from the laser cell to the ICP-MS torch by a helium carrier gas. Interference of ^{176}Lu on ^{176}Hf was corrected by measurement of interference-free ^{175}Lu , and using the invariant $^{176}\text{Lu}/^{175}\text{Lu}$ correction factor 1/0.02669 (DeBievre and Taylor, 1993). Interference of ^{176}Yb on ^{176}Hf was corrected by measuring the interference-free ^{172}Yb isotope, and using the $^{176}\text{Yb}/^{172}\text{Yb}$ ratio to obtain the interference-free $^{176}\text{Yb}/^{177}\text{Hf}$ ratio. The appropriate value of $^{176}\text{Yb}/^{172}\text{Yb}$ was determined by spiking the JMC475 hafnium standard solution with ytterbium, and finding the value of $^{176}\text{Yb}/^{172}\text{Yb}$ required to yield the $^{176}\text{Hf}/^{177}\text{Hf}$ value for non-spiked solution. Thirty zircons from the Mud Tank carbonatite locality were analysed, together with the samples, as a measure of the accuracy of the results. Most of the data and the mean $^{176}\text{Hf}/^{177}\text{Hf}$ value (0.282532 ± 25 ; $n = 50$) are within 2 standard deviations of the recommended value (0.282522 ± 42 (2σ); Griffin et al., 2007). Eight analyses of the 91500 zircon standard analysed during this study indicated $^{176}\text{Hf}/^{177}\text{Hf} = 0.282326 \pm 26$ (2σ), which is well within the range of values reported by Griffin et al., (2006). The Temora 2 zircon standard yielded an average $^{176}\text{Hf}/^{177}\text{Hf}$ ratio of 0.282685 ± 37 (2σ ; $n=148$), which is consistent with the accepted value. Calculation of initial $^{176}\text{Hf}/^{177}\text{Hf}$ is based on the ^{176}Lu decay constant of $1.867 \times 10^{-11}/\text{y}$ (Scherer et al., 2001). Initial $^{176}\text{Hf}/^{177}\text{Hf}$ isotopic ratios normalized to the chondritic uniform reservoir (CHUR); ϵHf are based on the present-day

Table 1. Summary of U–Pb SIMS geochronology

Sample	Lithology	Easting	Northing	Metamorphism (Ma)	Migmatization (Ma)	Detrital (Ma)	Magmatic (Ma)	Inheritance (Ma)
194767	Psammitic enclave in gneiss	405044	7142426	1205–1154	1313 ± 15	1463–1375 (1404)		
194768	Migmatitic gneiss	404249	7141068	1206–1167	1311 ± 21	1423–1361 (1402)		
187195	Leucogranitic gneiss	405582	7140874	1196, 1179	1298 ± 26	1561–1351 (1409, 1375)		
194764	Foliated monzogranite	404125	7130441	1316 ± 8			1402 ± 4	
194765	Granite dyke	404124	7130433				1318 ± 9	1835–1340 (1340, 1370, 1390, 1416, 1681)
194766	Granitic pegmatite	404250	7130586				1197 ± 4	1879–1347 (1428)
194759	Dolerite dyke	477976	7118435					1372 ± 14

NOTES: Significant detrital / inherited age components indicated within parentheses. Age ranges denoted with dashes. Coordinates refer to MGA zone 52. SIMS = secondary ion mass spectrometry

chondritic measurement of 0.282772 (Blichert-Toft and Albarede, 1997). Calculation of model ages (T_{DM}) is based on a depleted-mantle source with $(^{176}\text{Hf}/^{177}\text{Hf})_i = 0.279718$ at 4.56 Ga and $^{176}\text{Lu}/^{177}\text{Hf} = 0.0384$ (Griffin et al., 2004). T_{DM}^2 (crustal) ages were calculated assuming that the Hf within each zircon resided within a reservoir with $^{176}\text{Lu}/^{177}\text{Hf}$ ratio of 0.015 (Griffin et al., 2004; Griffin et al., 2002), consistent with the ratio determined from the best-fit array on a Hf evolution diagram. Lu–Hf data from the Papulankutja Supersuite and its related rocks are presented in Table 2 and a regional compilation is presented in Table 3.

Sm–Nd

Sm–Nd isotope measurements were determined on crushed whole-rock samples by isotope dilution at several different laboratories over several years. Samples were spiked with ^{150}Nd – ^{149}Sm mixed solutions and dissolved in HF–HNO₃. REE were separated using solution column chemistry. Sm and Nd were separated and collected by passing the solution through an additional set of ion exchange columns. Sm and Nd were loaded with acid onto filaments and analysed using mass spectrometry. In each analytical session, the unknowns were analysed together with isotope standards. All analyses of the unknowns are adjusted to a nominal $^{143}\text{Nd}/^{144}\text{Nd}$ value of 0.511850 for the La Jolla standard. Mass fractionation was monitored and corrected using the value for $^{146}\text{Nd}/^{144}\text{Nd}$ of 0.7219 (O’Nions et al., 1979). Procedural blanks analysed during these analyses were always less than <200 pg and are considered to be negligible compared to the total quantity of Nd in the samples. A compilation of whole-rock Sm–Nd isotope analyses from the west Musgrave Province <<http://www.geochem.dmp.wa.gov.au/geochem/>> is provided in Table 4.

Table 2. LA-ICPMS Lu–Hf analytical results for zircon from the Papulankutja Supersuite and its related rocks

Analysis No.	Group ID	$^{207}\text{Pb}^*/^{206}\text{Pb}^*$ (Ma)	$^{176}\text{Hf}/^{177}\text{Hf}$	1 SE	$^{176}\text{Lu}/^{177}\text{Hf}$	$^{176}\text{Yb}/^{172}\text{Hf}$	$^{176}\text{Hf}/^{177}\text{Hf}$ (i)	ϵ_{Hf}	1 SE	T_{DM} (Ga)	$T_{\text{DM}} \pm 2$
194767-4.1	I	1405	0.281992	0.000020	0.000680	0.02107	0.281974	2.96	0.70	1.76	1.99
194767-4.1R	I	1405	0.281880	0.000020	0.000823	0.02442	0.281858	-1.15	0.70	1.92	2.25
194767-5.1	I	1463	0.281903	0.000024	0.001303	0.04198	0.281867	0.47	0.84	1.91	2.20
194767-5.1R	S	1463	0.281889	0.000036	0.001066	0.03098	0.281860	0.21	1.26	1.92	2.21
194767-6.1	M	1154	0.281969	0.000018	0.000670	0.02136	0.281954	-3.37	0.63	1.79	2.20
194767-7.1	D	1317	0.281827	0.000028	0.000957	0.03015	0.281803	-5.08	0.98	2.00	2.43
194767-8.1	D	1296	0.281890	0.000012	0.001075	0.03488	0.281864	-3.40	0.42	1.92	2.31
194767-9.1C	S	1426	0.281983	0.000018	0.000570	0.01784	0.281968	3.21	0.63	1.77	1.99
194767-9.2R	M	1169	0.282072	0.000017	0.000190	0.00693	0.282068	0.97	0.60	1.63	1.94
194767-10.1	S	1381	0.281904	0.000012	0.000998	0.03093	0.281878	-0.98	0.42	1.90	2.22
194767-11.1C	S	1437	0.281902	0.000030	0.000985	0.03039	0.281875	0.17	1.05	1.90	2.19
194767-11.1R	S	1437	0.281862	0.000036	0.000773	0.02304	0.281841	-1.04	1.26	1.94	2.27
194767-13.1C	S	1421	0.281981	0.000027	0.001071	0.03441	0.281952	2.55	0.95	1.79	2.03
194767-13R	S	1421	0.281965	0.000035	0.000790	0.02239	0.281944	2.25	1.23	1.80	2.05
194767-14.1	Y	1308	0.281999	0.000020	0.000736	0.02453	0.281981	1.01	0.70	1.75	2.04
194767-14C	Y	1308	0.281885	0.000025	0.001019	0.03138	0.281860	-3.28	0.88	1.92	2.31
194767-15.1	S	1382	0.281939	0.000013	0.000929	0.02984	0.281915	0.34	0.46	1.84	2.14
194767-16.1	M	1188	0.281940	0.000023	0.000665	0.02269	0.281925	-3.65	0.81	1.83	2.24
194767-17.1C	S	1409	0.282016	0.000027	0.001012	0.03331	0.281989	3.58	0.95	1.74	1.96
194767-17R	S	1200	0.282064	0.000033	0.000783	0.02306	0.282046	0.91	1.16	1.66	1.96
194767-18.1	S	1398	0.281956	0.000024	0.000814	0.02539	0.281935	1.40	0.84	1.81	2.09
194767-18.2R	S	1205	0.281983	0.000023	0.000704	0.02212	0.281967	-1.78	0.81	1.77	2.14
194767-19.1	M	1194	0.281918	0.000015	0.000120	0.00469	0.281915	-3.88	0.53	1.83	2.26
194767-20.1	Y	1323	0.282046	0.000013	0.000893	0.02706	0.282024	2.87	0.46	1.69	1.93
194767-21.1	Y	1372	0.281911	0.000026	0.000779	0.02323	0.281891	-0.73	0.91	1.88	2.20
194764-1.1	I	1401	0.282036	0.000009	0.001010	0.03395	0.282009	4.12	0.30	1.71	1.91
194764-2.1	I	1404	0.281953	0.000010	0.000439	0.01534	0.281941	1.79	0.35	1.80	2.07
194764-3.1	I	1364	0.282040	0.000018	0.001026	0.04500	0.282014	3.44	0.63	1.71	1.93
194764-4.1	I	1417	0.281908	0.000015	0.000545	0.02139	0.281893	0.38	0.53	1.87	2.17
194764-5.1	I	1396	0.282106	0.000020	0.001110	0.04988	0.282077	6.40	0.70	1.62	1.76
194764-6.1	I	1410	0.282091	0.000018	0.001418	0.06204	0.282053	5.89	0.63	1.65	1.81

Table 2. continued

Analysis No.	Group ID	$^{207}\text{Pb}^*/^{208}\text{Pb}^*$ (Ma)	$^{176}\text{Hf}/^{177}\text{Hf}$	1 SE	$^{178}\text{Lu}/^{177}\text{Hf}$	$^{176}\text{Yb}/^{177}\text{Hf}$	$^{176}\text{Hf}/^{177}\text{Hf}$ (i)	ϵHf	1 SE	T_{DM} (Ga)	T_{DM}^2
194764-7.1	I	1399	0.282178	0.000022	0.002469	0.08078	0.282113	7.74	0.77	1.58	1.68
194764-8.1	I	1392	0.282098	0.000013	0.001359	0.05696	0.282062	5.79	0.46	1.64	1.80
194764-9.1	I	1399	0.282048	0.000018	0.000797	0.03237	0.282027	4.70	0.63	1.69	1.88
194764-10.1	I	1381	0.282060	0.000024	0.000925	0.04254	0.282036	4.62	0.84	1.68	1.87
194764-11.1	I	1396	0.282019	0.000023	0.001304	0.06175	0.281985	3.12	0.81	1.75	1.97
194764-12.1	M	1316	0.282037	0.000011	0.001000	0.03466	0.282012	2.30	0.39	1.71	1.96
194764-13.1	I	1404	0.282023	0.000018	0.001365	0.05787	0.281987	3.40	0.63	1.75	1.96
194764-14.1	I	1431	0.282040	0.000022	0.000833	0.03134	0.282017	5.09	0.77	1.70	1.88
194764-15.1	I	1401	0.282161	0.000016	0.001494	0.06423	0.282121	8.10	0.56	1.56	1.66
194764-16.1	I	1406	0.282014	0.000016	0.000859	0.03634	0.281991	3.59	0.56	1.74	1.95
194764-17.1	I	1410	0.282110	0.000016	0.001037	0.03937	0.282082	6.92	0.56	1.61	1.74
194764-18.1	I	1396	0.281941	0.000012	0.000434	0.01331	0.281930	1.17	0.42	1.82	2.10
194764-19.1	I	1397	0.281911	0.000015	0.000639	0.02552	0.281894	-0.05	0.53	1.87	2.18
194764-20.1	I	1401	0.282004	0.000015	0.000547	0.02153	0.281990	3.43	0.53	1.74	1.96
194765-1.1	X	1834	0.281571	0.000020	0.001028	0.03568	0.281535	-2.90	0.70	2.36	2.70
194765-2.1	X	1835	0.281640	0.000040	0.000867	0.03098	0.281610	-0.23	1.40	2.25	2.53
194765-3.1	I	1326	0.282057	0.000041	0.000670	0.02050	0.282040	3.53	1.44	1.67	1.89
194765-3.2	I	1381	0.282175	0.000032	0.001190	0.04183	0.282144	8.44	1.12	1.53	1.62
194765-4.1	X	1343	0.282138	0.000024	0.000858	0.02945	0.282116	6.61	0.84	1.57	1.71
194765-4.2	X	1317	0.282048	0.000022	0.000677	0.02072	0.282031	3.00	0.77	1.68	1.92
194765-5.1C	X	1388	0.282004	0.000017	0.000453	0.01518	0.281992	3.21	0.60	1.73	1.96
194765-5R	X	1388	0.281914	0.000015	0.000350	0.00949	0.281905	0.11	0.53	1.85	2.16
194765-6.1	X	1632	0.281960	0.000009	0.000748	0.02742	0.281937	6.78	0.30	1.81	1.92
194765-7.1	X	1576	0.281633	0.000022	0.000908	0.03084	0.281606	-6.25	0.77	2.26	2.71
194765-8.1C	X	1445	0.281910	0.000010	0.000019	0.00085	0.281909	1.58	0.34	1.84	2.11
194765-8R	X	1445	0.281996	0.000024	0.000706	0.02134	0.281977	3.96	0.84	1.75	1.96
194765-9.1	X	1552	0.281592	0.000014	0.001024	0.03465	0.281562	-8.33	0.49	2.33	2.82
194765-10.1C	X	1534	0.281479	0.000016	0.000831	0.02983	0.281455	-12.54	0.56	2.47	3.07
194765-10R	I	1300	0.281938	0.000018	0.001648	0.04966	0.281898	-2.12	0.63	1.88	2.23
194765-11.1	X	1402	0.281920	0.000039	0.000619	0.02055	0.281904	0.39	1.37	1.86	2.15
194765-12.1C	X	1390	0.282019	0.000031	0.000707	0.02083	0.282000	3.56	1.09	1.72	1.94

Table 2. continued

Analysis No.	Group ID	$^{207}\text{Pb}^*/^{206}\text{Pb}^*$ (Ma)	$^{176}\text{Hf}/^{177}\text{Hf}$	1 SE	$^{176}\text{Lu}/^{177}\text{Hf}$	$^{176}\text{Yb}/^{177}\text{Hf}$	$^{176}\text{Hf}/^{177}\text{Hf}$ (i)	ϵHf	1 SE	T_{DM} (Ga)	T_{DM}^2
194765-12R	X	1390	0.282026	0.000038	0.001537	0.04743	0.281986	3.03	1.33	1.75	1.98
194765-14.1	X	1709	0.281995	0.000012	0.002122	0.08137	0.281926	8.15	0.42	1.82	1.89
194765-15.1	X	1340	0.281990	0.000012	0.001936	0.06344	0.281941	0.33	0.42	1.82	2.11
194765-16.1	X	1366	0.282079	0.000010	0.001588	0.05289	0.282038	4.35	0.35	1.68	1.87
194765-17.1	X	1638	0.281742	0.000016	0.001311	0.03722	0.281701	-1.45	0.56	2.14	2.45
194765-18.1	X	1364	0.281944	0.000008	0.000739	0.02554	0.281925	0.30	0.27	1.83	2.13
194765-20.1C	X	1413	0.282042	0.000018	0.001529	0.05379	0.282001	4.10	0.63	1.73	1.92
194765-20R	X	1413	0.281934	0.000023	0.000501	0.01275	0.281921	1.25	0.81	1.83	2.11
194765-21.1C	X	1417	0.282077	0.000014	0.002029	0.07332	0.282023	4.96	0.49	1.70	1.87
194765-21R	X	1417	0.282031	0.000012	0.001073	0.03390	0.282002	4.23	0.42	1.72	1.92
194765-22.1C	X	1390	0.282089	0.000015	0.000692	0.02406	0.282071	6.06	0.53	1.63	1.78
194765-22R	X	1390	0.282061	0.000021	0.001452	0.04753	0.282023	4.36	0.74	1.70	1.89
194765-23.1R	X	1410	0.281968	0.000010	0.000801	0.02915	0.281947	2.10	0.34	1.80	2.05
194765-23C	X	1410	0.282000	0.000012	0.001914	0.06158	0.281949	2.19	0.42	1.81	2.05
194765-24.1	I	1324	0.282016	0.000025	0.001030	0.02645	0.281990	1.71	0.88	1.74	2.01
194765-24.2	I	1337	0.281985	0.000028	0.000941	0.02733	0.281961	0.98	0.98	1.78	2.07
194765-25.1C	X	1418	0.281917	0.000024	0.000339	0.01106	0.281908	0.91	0.84	1.85	2.13
194765-25.1R	X	1418	0.281956	0.000023	0.000454	0.01606	0.281944	2.18	0.81	1.80	2.05
194765-26.1	X	1682	0.281986	0.000012	0.002014	0.07232	0.281922	7.38	0.42	1.83	1.92
194765-27.1	X	1684	0.281988	0.000023	0.001786	0.06725	0.281931	7.75	0.81	1.82	1.90
194765-28.1	I	1325	0.282071	0.000024	0.002816	0.08408	0.282001	2.10	0.84	1.75	1.98
194765-29.1	X	1680	0.281995	0.000015	0.002594	0.10046	0.281912	7.00	0.53	1.85	1.95
194765-30.1	X	1781	0.281515	0.000012	0.001058	0.03847	0.281479	-6.09	0.42	2.44	2.86

NOTES: Analysis no is the sample number "-"; grain number "*", spot number, $^{176}\text{Hf}/^{177}\text{Hf}$ (i), ϵHf (i) and $T(\text{DM})$ of zircons are calculated using the $^{207}\text{Pb}/^{206}\text{Pb}$ age of grain. $T(\text{DM})$ crustal is calculated using a two-stage evolution assuming a mean $^{176}\text{Lu}/^{177}\text{Hf}$ ratio of crust = 0.015. C and R, appended to the spot number, refer to grain Core and Rim, respectively. Group ID refers to the following I = magmatic; X = xenocrysts; M = metamorphic; D = discordant or interpreted to have undergone radiogenic-Pb loss.

Table 3. Compilation of LA-ICPMS Lu–Hf analytical results for zircon from magmatic rocks of the west Musgrave Province

Analysis No.	Crystallization age	$^{176}\text{Hf}/^{177}\text{Hf}$ measured	1SE	$^{176}\text{Lu}/^{177}\text{Hf}$ measured	$^{176}\text{Yb}/^{177}\text{Hf}$ measured	$^{176}\text{Hf}/^{177}\text{Hf}$ initial	ϵ_{Hf}	1SE	T_{DM} (crustal)	Supersuite
174589-1.2	1080	0.282286	0.000013	0.001692	0.106459	0.282252	5.5	0.46	1.58	Warakurna
174589-4.2	1063	0.282273	0.000018	0.004209	0.249250	0.282189	2.9	0.63	1.73	Warakurna
174589-8.1	1073	0.282186	0.000012	0.002018	0.121272	0.282145	1.6	0.42	1.82	Warakurna
174589-10.1	1077	0.282222	0.000011	0.001576	0.090965	0.282190	3.2	0.39	1.72	Warakurna
174589-11.1	1077	0.282188	0.000013	0.004215	0.251175	0.282102	0.1	0.46	1.92	Warakurna
174589-15.1	1071	0.282197	0.000009	0.003210	0.186929	0.282132	1.1	0.32	1.85	Warakurna
174589-18.1	1070	0.282159	0.000007	0.000831	0.042738	0.282142	1.4	0.23	1.83	Warakurna
174589-19.1	1073	0.282219	0.000011	0.002869	0.167853	0.282161	2.1	0.39	1.79	Warakurna
185583-5.1	1055	0.282146	0.000007	0.000510	0.025352	0.282136	0.8	0.25	1.86	Warakurna
185583-6.1	1046	0.282137	0.000008	0.000528	0.025406	0.282127	0.3	0.27	1.88	Warakurna
185583-7.1	1080	0.282140	0.000007	0.000581	0.028327	0.282128	1.1	0.26	1.86	Warakurna
185583-14.1	1040	0.282116	0.000009	0.000512	0.025164	0.282106	-0.5	0.32	1.93	Warakurna
185583-15.1	854	0.282148	0.000010	0.000614	0.030480	0.282138	-3.6	0.35	1.98	Warakurna
185583-19.1	1098	0.282160	0.000009	0.000541	0.028061	0.282149	2.3	0.33	1.80	Warakurna
185583-23.1	1119	0.282136	0.000007	0.000666	0.034879	0.282122	1.8	0.23	1.85	Warakurna
185583-25.1	1129	0.282132	0.000009	0.000539	0.027810	0.282121	2.0	0.30	1.84	Warakurna
187179-3.1	1169	0.281994	0.000006	0.000275	0.014806	0.281988	-1.9	0.21	2.12	Pitjantjatjara
187179-4.1	1182	0.281995	0.000009	0.000315	0.016155	0.281988	-1.6	0.33	2.11	Pitjantjatjara
187179-5.1	1192	0.281993	0.000007	0.000301	0.010604	0.281986	-1.4	0.25	2.10	Pitjantjatjara
187179-6.1	1203	0.281981	0.000011	0.000363	0.018801	0.281973	-1.6	0.39	2.13	Pitjantjatjara
187179-8.1	1183	0.282095	0.000019	0.000388	0.013379	0.282086	1.9	0.67	1.88	Pitjantjatjara
187179-17.1	1195	0.282024	0.000008	0.000452	0.018587	0.282014	-0.4	0.27	2.04	Pitjantjatjara
187179-21.1	1194	0.281986	0.000017	0.000571	0.021098	0.281973	-1.8	0.60	2.13	Pitjantjatjara
187179-24.1	1215	0.282017	0.000007	0.000322	0.017544	0.282010	0.0	0.23	2.04	Pitjantjatjara
174737-3.1	1234	0.282062	0.000010	0.000527	0.027134	0.282050	1.8	0.35	1.93	Pitjantjatjara
174737-4.1C	1240	0.282051	0.000008	0.000898	0.046654	0.282030	1.2	0.28	1.97	Pitjantjatjara
174737-5.2C	1191	0.282053	0.000007	0.000862	0.043165	0.282034	0.3	0.23	2.00	Pitjantjatjara
174737-5.2R	1264	0.282075	0.000013	0.001339	0.069008	0.282043	2.2	0.46	1.93	Pitjantjatjara
174737-9.1	1238	0.282058	0.000007	0.000909	0.046084	0.282037	1.4	0.25	1.96	Pitjantjatjara
174737-10.1	1207	0.282042	0.000009	0.000431	0.020425	0.282032	0.6	0.30	1.99	Pitjantjatjara

Table 3. continued

Analysis No.	Crystallization age	$^{176}\text{Hf}/^{177}\text{Hf}$ measured	1SE	$^{176}\text{Lu}/^{177}\text{Hf}$ measured	$^{176}\text{Yb}/^{177}\text{Hf}$ measured	$^{176}\text{Hf}/^{177}\text{Hf}$ initial	ϵHf	1SE	T_{DM} (crustal)	Supersuite
174737-14.1	1225	0.282049	0.000008	0.000620	0.032387	0.282035	1.1	0.27	1.97	Pitjantjatjara
174737-23.1C	1212	0.282041	0.000008	0.000579	0.027669	0.282028	0.5	0.27	2.00	Pitjantjatjara
174737-23.1R	1115	0.282039	0.000008	0.000699	0.034253	0.282024	-1.8	0.29	2.07	Pitjantjatjara
174737-24.1	1232	0.282114	0.000012	0.001354	0.063124	0.282083	2.9	0.42	1.86	Pitjantjatjara
185610-1.1	1193	0.282076	0.000015	0.000270	0.013607	0.282070	1.6	0.53	1.91	Pitjantjatjara
185610-5.1	1197	0.282024	0.000014	0.000226	0.009622	0.282019	-0.1	0.49	2.03	Pitjantjatjara
185610-7.1	1175	0.282023	0.000020	0.000502	0.028726	0.282012	-0.9	0.70	2.06	Pitjantjatjara
185610-9.1	1221	0.282023	0.000009	0.000408	0.023464	0.282014	0.2	0.31	2.02	Pitjantjatjara
185610-10.1	1194	0.282040	0.000010	0.000154	0.006483	0.282037	0.4	0.33	1.99	Pitjantjatjara
185610-14.1	1208	0.281931	0.000014	0.000207	0.009777	0.281926	-3.2	0.49	2.23	Pitjantjatjara
185610-17.1	1206	0.282046	0.000008	0.000489	0.025923	0.282035	0.6	0.27	1.99	Pitjantjatjara
185610-18.1	1178	0.281978	0.000015	0.000332	0.017320	0.281971	-2.3	0.53	2.15	Pitjantjatjara
180256-01.01	1172	0.282094	0.000014	0.000735	0.029296	0.282078	1.4	0.49	1.91	Pitjantjatjara
180256-02.01	1152	0.282135	0.000015	0.000807	0.038356	0.282117	2.4	0.53	1.83	Pitjantjatjara
180256-03.01	1116	0.282120	0.000012	0.000523	0.023814	0.282109	1.2	0.42	1.88	Pitjantjatjara
180256-04.01	1145	0.282075	0.000016	0.000491	0.022009	0.282064	0.3	0.56	1.96	Pitjantjatjara
180256-05.01	1191	0.282034	0.000020	0.000546	0.028665	0.282022	-0.2	0.70	2.02	Pitjantjatjara
180256-07.01	1155	0.282181	0.000017	0.000805	0.043616	0.282163	4.1	0.60	1.73	Pitjantjatjara
180256-08.01	1151	0.282068	0.000024	0.000703	0.024271	0.282053	0.0	0.84	1.98	Pitjantjatjara
180256-09.01	1149	0.282125	0.000025	0.000619	0.034358	0.282112	2.1	0.88	1.85	Pitjantjatjara
180256-10.01	1154	0.282040	0.000075	0.000879	0.027740	0.282021	-1.0	2.63	2.05	Pitjantjatjara
180256-11.01	1204	0.282080	0.000010	0.000753	0.034913	0.282063	1.6	0.35	1.92	Pitjantjatjara
180256-12.01	1183	0.282104	0.000013	0.000503	0.022999	0.282093	2.2	0.46	1.87	Pitjantjatjara
180256-13.01	1115	0.282121	0.000018	0.001264	0.046116	0.282094	0.7	0.63	1.91	Pitjantjatjara
180256-14.01	1154	0.282118	0.000008	0.000670	0.031035	0.282103	1.9	0.26	1.86	Pitjantjatjara
180256-15.01	1207	0.282101	0.000009	0.000832	0.039862	0.282082	2.3	0.32	1.88	Pitjantjatjara
180256-17.01	1147	0.282072	0.000022	0.001042	0.037114	0.282049	-0.2	0.77	1.99	Pitjantjatjara
180256-18.01	1234	0.282125	0.000014	0.000732	0.019625	0.282108	3.9	0.49	1.80	Pitjantjatjara
180256-19.01	1096	0.282113	0.000015	0.000671	0.027983	0.282099	0.5	0.53	1.91	Pitjantjatjara
180256-20.01	1161	0.282111	0.000020	0.000821	0.023942	0.282093	1.7	0.70	1.88	Pitjantjatjara
180256-21.01	1084	0.282133	0.000014	0.000532	0.023078	0.282122	1.0	0.49	1.87	Pitjantjatjara

Table 3. continued

Analysis No.	Crystallization age	$^{176}\text{Hf}/^{177}\text{Hf}$ measured	1SE	$^{176}\text{Lu}/^{177}\text{Hf}$ measured	$^{176}\text{Yb}/^{177}\text{Hf}$ measured	$^{176}\text{Hf}/^{177}\text{Hf}$ initial	ϵHf	1SE	T_{DM} (crustal)	Supersuite
180256-24.01	1170	0.282097	0.000010	0.000571	0.021877	0.282084	1.6	0.35	1.90	Pitjantjatjara
180256-22.01	1187	0.282114	0.000015	0.000865	0.039640	0.282095	2.3	0.53	1.86	Pitjantjatjara
180256-25.01	1134	0.282071	0.000012	0.000652	0.020402	0.282057	-0.2	0.42	1.98	Pitjantjatjara
180256-26.01	1179	0.282042	0.000017	0.000772	0.023105	0.282025	-0.3	0.60	2.03	Pitjantjatjara
180256-27.01	1157	0.282092	0.000023	0.000722	0.022594	0.282076	1.0	0.81	1.92	Pitjantjatjara
180256-28.01	1132	0.282098	0.000023	0.000461	0.020650	0.282088	0.9	0.81	1.91	Pitjantjatjara
180256-29.01	1137	0.282100	0.000037	0.000596	0.024367	0.282087	0.9	1.30	1.91	Pitjantjatjara
180256-30.01	1119	0.282111	0.000011	0.000466	0.020607	0.282101	1.0	0.39	1.89	Pitjantjatjara
174558-01.01	1150	0.281995	0.000011	0.000376	0.016459	0.281987	-2.3	0.39	2.13	Pitjantjatjara
174558-02.01	1157	0.282012	0.000009	0.000497	0.021904	0.282001	-1.7	0.33	2.09	Pitjantjatjara
174558-03.01	1209	0.282003	0.000008	0.000462	0.021387	0.281992	-0.8	0.29	2.08	Pitjantjatjara
174558-04.01	1206	0.282013	0.000016	0.000635	0.019632	0.281999	-0.6	0.56	2.07	Pitjantjatjara
174558-06.01	1189	0.282027	0.000011	0.000386	0.017378	0.282018	-0.3	0.39	2.03	Pitjantjatjara
174558-07.01	1191	0.282034	0.000011	0.000428	0.019700	0.282024	-0.1	0.39	2.02	Pitjantjatjara
174558-07.02	1146	0.281992	0.000017	0.000400	0.018710	0.281983	-2.5	0.60	2.14	Pitjantjatjara
174558-08.01	1191	0.282044	0.000014	0.000763	0.025531	0.282027	0.0	0.49	2.01	Pitjantjatjara
174558-08.02	1183	0.281982	0.000018	0.000531	0.017872	0.281970	-2.2	0.63	2.15	Pitjantjatjara
174558-09.01	1174	0.282020	0.000016	0.000442	0.022021	0.282010	-1.0	0.56	2.06	Pitjantjatjara
174558-10.01	1148	0.282026	0.000015	0.000404	0.017823	0.282017	-1.3	0.53	2.06	Pitjantjatjara
174558-10.02	1203	0.282010	0.000011	0.000659	0.031067	0.281995	-0.8	0.39	2.08	Pitjantjatjara
174558-11.02	1207	0.282008	0.000015	0.000495	0.023423	0.281997	-0.7	0.53	2.07	Pitjantjatjara
174558-11.01	1203	0.282016	0.000012	0.000409	0.018584	0.282007	-0.4	0.42	2.05	Pitjantjatjara
174558-12.01	1188	0.282059	0.000012	0.000438	0.019207	0.282049	0.7	0.42	1.96	Pitjantjatjara
174558-12.02	1224	0.282001	0.000014	0.000468	0.021699	0.281990	-0.5	0.49	2.07	Pitjantjatjara
174558-13.02	1215	0.282016	0.000011	0.000458	0.019415	0.282006	-0.2	0.39	2.05	Pitjantjatjara
174558-14.01	1153	0.282001	0.000011	0.000445	0.019176	0.281991	-2.1	0.39	2.12	Pitjantjatjara
174558-14.02	1162	0.282012	0.000011	0.000560	0.019398	0.282000	-1.6	0.39	2.09	Pitjantjatjara
174558-15.01	1242	0.282016	0.000010	0.000524	0.023980	0.282004	0.3	0.33	2.03	Pitjantjatjara
174558-19.01	1168	0.282026	0.000014	0.000374	0.017127	0.282018	-0.8	0.49	2.05	Pitjantjatjara
174558-20.01	1217	0.282033	0.000010	0.000509	0.025564	0.282021	0.4	0.34	2.01	Pitjantjatjara
174558-20.02	1200	0.282026	0.000011	0.000559	0.027196	0.282013	-0.3	0.39	2.04	Pitjantjatjara

Table 3. continued

Analysis No.	Crystallization age	$^{176}\text{Hf}/^{177}\text{Hf}$ measured	1SE	$^{176}\text{Lu}/^{177}\text{Hf}$ measured	$^{176}\text{Yb}/^{177}\text{Hf}$ measured	$^{176}\text{Hf}/^{177}\text{Hf}$ initial	ϵHf	1SE	T_{DM} (crustal)	Supersuite
174558-24.01	1145	0.282004	0.000013	0.000389	0.017415	0.281996	-2.1	0.46	2.11	Pitiantjatjara
174558-25.01	1154	0.282017	0.000015	0.000585	0.019463	0.282004	-1.6	0.53	2.09	Pitiantjatjara
174558-26.02	1200	0.281985	0.000019	0.000568	0.020821	0.281972	-1.7	0.67	2.13	Pitiantjatjara
183509-02.01	1167	0.282107	0.000007	0.001349	0.062753	0.282077	1.3	0.25	1.92	Pitiantjatjara
183509-07.01	1199	0.282094	0.000009	0.000621	0.032682	0.282080	2.1	0.33	1.89	Pitiantjatjara
183509-08.01	1175	0.282114	0.000013	0.000807	0.041690	0.282096	2.1	0.46	1.87	Pitiantjatjara
183509-09.01	1157	0.282095	0.000008	0.000484	0.024602	0.282084	1.3	0.28	1.91	Pitiantjatjara
183509-11.01	1166	0.282020	0.000013	0.000850	0.026525	0.282001	-1.4	0.46	2.09	Pitiantjatjara
183509-13.01	1169	0.282083	0.000006	0.000530	0.021061	0.282071	1.1	0.21	1.93	Pitiantjatjara
183509-15.01	1124	0.282094	0.000007	0.000445	0.020715	0.282085	0.6	0.26	1.93	Pitiantjatjara
183509-16.01	1165	0.282081	0.000009	0.001197	0.057179	0.282055	0.4	0.33	1.97	Pitiantjatjara
183509-18.01	1183	0.282082	0.000009	0.000183	0.009330	0.282078	1.7	0.33	1.90	Pitiantjatjara
183509-21.01	1163	0.282105	0.000009	0.001490	0.072573	0.282072	1.0	0.31	1.93	Pitiantjatjara
183509-22.01	1114	0.281905	0.000009	0.000378	0.017214	0.281897	-6.3	0.30	2.35	Pitiantjatjara
183509-26.01	1170	0.282089	0.000011	0.000452	0.023991	0.282079	1.4	0.39	1.91	Pitiantjatjara
183509-28.01	1098	0.282072	0.000016	0.000941	0.030604	0.282053	-1.2	0.56	2.02	Pitiantjatjara
185339-03.01	1221	0.282043	0.000009	0.001105	0.059493	0.282018	0.4	0.33	2.01	Pitiantjatjara
185339-12.01	1220	0.282022	0.000007	0.000363	0.016839	0.282014	0.2	0.23	2.02	Pitiantjatjara
185339-14.01	1189	0.282059	0.000010	0.000698	0.030311	0.282043	0.6	0.34	1.98	Pitiantjatjara
185339-16.01	1222	0.282073	0.000015	0.000960	0.035973	0.282051	1.6	0.53	1.94	Pitiantjatjara
185339-18.01	1227	0.282042	0.000012	0.001671	0.081582	0.282003	0.0	0.42	2.04	Pitiantjatjara
185339-21.01	1223	0.282037	0.000013	0.001118	0.033346	0.282011	0.2	0.46	2.03	Pitiantjatjara
185339-23.01	1204	0.282046	0.000008	0.000410	0.019781	0.282037	0.7	0.27	1.98	Pitiantjatjara
185339-40.01	1191	0.282056	0.000012	0.000704	0.035970	0.282040	0.5	0.42	1.98	Pitiantjatjara
185339-45.01	1195	0.282035	0.000011	0.000687	0.034979	0.282020	-0.2	0.39	2.03	Pitiantjatjara
194767-4.1	1405	0.281992	0.000020	0.000680	0.021072	0.281974	3.0	0.70	1.99	Papulankutja
194767-4.1R	1405	0.281880	0.000020	0.000823	0.024422	0.281858	-1.2	0.70	2.25	Papulankutja
194767-5.1	1463	0.281903	0.000024	0.001303	0.041980	0.281867	0.5	0.84	2.20	Papulankutja
194767-5.1R	1463	0.281889	0.000036	0.001066	0.030978	0.281860	0.2	1.26	2.21	Papulankutja
194767-10.1	1381	0.281904	0.000012	0.000998	0.030933	0.281878	-1.0	0.42	2.22	Papulankutja
194767-11.1C	1437	0.281902	0.000030	0.000985	0.030386	0.281875	0.2	1.05	2.19	Papulankutja

Table 3. continued

Analysis No.	Crystallization age	$^{176}\text{Hf}/^{177}\text{Hf}$ measured	1SE	$^{176}\text{Lu}/^{177}\text{Hf}$ measured	$^{176}\text{Yb}/^{177}\text{Hf}$ measured	$^{176}\text{Hf}/^{177}\text{Hf}$ initial	ϵHf	1SE	T_{DM} (crustal)	Supersuite
194767-11R	1437	0.281862	0.000036	0.000773	0.023043	0.281841	-1.0	1.26	2.27	Papulankutja
194767-13.1C	1421	0.281981	0.000027	0.001071	0.034411	0.281952	2.6	0.95	2.03	Papulankutja
194767-13R	1421	0.281965	0.000035	0.000790	0.022388	0.281944	2.3	1.23	2.05	Papulankutja
194767-15.1	1382	0.281939	0.000013	0.000929	0.029844	0.281915	0.3	0.46	2.14	Papulankutja
194767-17.1C	1409	0.282016	0.000027	0.001012	0.033310	0.281989	3.6	0.95	1.96	Papulankutja
194767-18.1	1398	0.281956	0.000024	0.000814	0.025389	0.281935	1.4	0.84	2.09	Papulankutja
194764-1.1	1401	0.282036	0.000009	0.001010	0.033954	0.282009	4.1	0.30	1.91	Papulankutja
194764-2.1	1404	0.281953	0.000010	0.000439	0.015340	0.281941	1.8	0.35	2.07	Papulankutja
194764-3.1	1364	0.282040	0.000018	0.001026	0.045000	0.282014	3.4	0.63	1.93	Papulankutja
194764-4.1	1417	0.281908	0.000015	0.000545	0.021395	0.281893	0.4	0.53	2.17	Papulankutja
194764-5.1	1396	0.282106	0.000020	0.001110	0.049878	0.282077	6.4	0.70	1.76	Papulankutja
194764-6.1	1410	0.282091	0.000018	0.001418	0.062035	0.282053	5.9	0.63	1.81	Papulankutja
194764-7.1	1399	0.282178	0.000022	0.002469	0.080783	0.282113	7.7	0.77	1.68	Papulankutja
194764-8.1	1392	0.282098	0.000013	0.001359	0.056956	0.282062	5.8	0.46	1.80	Papulankutja
194764-9.1	1399	0.282048	0.000018	0.000797	0.032372	0.282027	4.7	0.63	1.88	Papulankutja
194764-10.1	1381	0.282060	0.000024	0.000925	0.042542	0.282036	4.6	0.84	1.87	Papulankutja
194764-11.1	1396	0.282019	0.000023	0.001304	0.061750	0.281985	3.1	0.81	1.97	Papulankutja
194764-13.1	1404	0.282023	0.000018	0.001365	0.057870	0.281987	3.4	0.63	1.96	Papulankutja
194764-14.1	1431	0.282040	0.000022	0.000833	0.031337	0.282017	5.1	0.77	1.88	Papulankutja
194764-15.1	1401	0.282161	0.000016	0.001494	0.064230	0.282121	8.1	0.56	1.66	Papulankutja
194764-16.1	1406	0.282014	0.000016	0.000859	0.036343	0.281991	3.6	0.56	1.95	Papulankutja
194764-17.1	1410	0.282110	0.000016	0.001037	0.039370	0.282082	6.9	0.56	1.74	Papulankutja
194764-18.1	1396	0.281941	0.000012	0.000434	0.013314	0.281930	1.2	0.42	2.10	Papulankutja
194764-19.1	1397	0.281911	0.000015	0.000639	0.025519	0.281894	0.0	0.53	2.18	Papulankutja
194764-20.1	1401	0.282004	0.000015	0.000547	0.021532	0.281990	3.4	0.53	1.96	Papulankutja
194765-3.2	1381	0.282175	0.000032	0.001190	0.041831	0.282144	8.4	1.12	1.62	Papulankutja
194765-5.1C	1388	0.282004	0.000017	0.000453	0.015180	0.281992	3.2	0.60	1.96	Papulankutja
194765-5R	1388	0.281914	0.000015	0.000350	0.009492	0.281905	0.1	0.53	2.16	Papulankutja
194765-8.1C	1445	0.281910	0.000010	0.000019	0.000852	0.281909	1.6	0.34	2.11	Papulankutja
194765-8R	1445	0.281996	0.000024	0.000706	0.021337	0.281977	4.0	0.84	1.96	Papulankutja
194765-11.1	1402	0.281920	0.000039	0.000619	0.020553	0.281904	0.4	1.37	2.15	Papulankutja

Table 3. continued

Analysis No.	Crystallization age	$^{176}\text{Hf}/^{177}\text{Hf}$ measured	1SE	$^{176}\text{Lu}/^{177}\text{Hf}$ measured	$^{176}\text{Yb}/^{177}\text{Hf}$ measured	$^{176}\text{Hf}/^{177}\text{Hf}$ initial	ϵ_{Hf}	1SE	T_{DM} (crustal)	Supersuite
194765-12.1C	1390	0.282019	0.000031	0.000707	0.020831	0.282000	3.6	1.09	1.94	Papulankutja
194765-12R	1390	0.282026	0.000038	0.001537	0.047425	0.281986	3.0	1.33	1.98	Papulankutja
194765-16.1	1366	0.282079	0.000010	0.001588	0.052892	0.282038	4.4	0.35	1.87	Papulankutja
194765-18.1	1364	0.281944	0.000008	0.000739	0.025541	0.281925	0.3	0.27	2.13	Papulankutja
194765-20.1C	1413	0.282042	0.000018	0.001529	0.053786	0.282001	4.1	0.63	1.92	Papulankutja
194765-20R	1413	0.281934	0.000023	0.000501	0.012754	0.281921	1.2	0.81	2.11	Papulankutja
194765-21.1C	1417	0.282077	0.000014	0.002029	0.073324	0.282023	5.0	0.49	1.87	Papulankutja
194765-21R	1417	0.282031	0.000012	0.001073	0.033895	0.282002	4.2	0.42	1.92	Papulankutja
194765-22.1C	1390	0.282089	0.000015	0.000692	0.024056	0.282071	6.1	0.53	1.78	Papulankutja
194765-22R	1390	0.282061	0.000021	0.001452	0.047531	0.282023	4.4	0.74	1.89	Papulankutja
194765-23.1R	1410	0.281968	0.000010	0.000801	0.029152	0.281947	2.1	0.34	2.05	Papulankutja
194765-23C	1410	0.282000	0.000012	0.001914	0.061576	0.281949	2.2	0.42	2.05	Papulankutja
194765-25.1C	1418	0.281917	0.000024	0.000339	0.011059	0.281908	0.9	0.84	2.13	Papulankutja
194765-25.1R	1418	0.281956	0.000023	0.000454	0.016058	0.281944	2.2	0.81	2.05	Papulankutja
183496-01.01	1322	0.282070	0.000006	0.000900	0.038279	0.282048	3.7	0.21	1.88	Wankanki
183496-02.01	1330	0.282100	0.000016	0.000961	0.030501	0.282076	4.9	0.56	1.81	Wankanki
183496-03.01	1311	0.282059	0.000009	0.001055	0.044264	0.282033	2.9	0.32	1.92	Wankanki
183496-04.01	1342	0.282088	0.000010	0.001050	0.037560	0.282061	4.6	0.33	1.84	Wankanki
183496-05.01	1315	0.282059	0.000009	0.000881	0.036841	0.282037	3.2	0.32	1.91	Wankanki
183496-07.01	1299	0.282061	0.000008	0.000753	0.032314	0.282043	3.0	0.27	1.91	Wankanki
183496-09.02	1306	0.282108	0.000009	0.000678	0.028153	0.282091	4.9	0.31	1.79	Wankanki
183496-11.01	1319	0.282035	0.000009	0.000622	0.027561	0.282020	2.6	0.30	1.95	Wankanki
183496-14.02	1344	0.282086	0.000011	0.000783	0.035797	0.282066	4.9	0.39	1.82	Wankanki
183496-15.01	1308	0.282044	0.000008	0.000549	0.015589	0.282030	2.8	0.28	1.93	Wankanki
183496-16.02	1321	0.282070	0.000009	0.000573	0.023511	0.282056	4.0	0.33	1.86	Wankanki
183496-16.03	1319	0.282067	0.000012	0.000733	0.032742	0.282049	3.7	0.42	1.88	Wankanki
183496-17.02	1336	0.282078	0.000008	0.000791	0.034470	0.282058	4.4	0.29	1.85	Wankanki
183496-18.02	1310	0.282064	0.000010	0.000818	0.037020	0.282044	3.3	0.35	1.90	Wankanki
183496-19.02	1359	0.282090	0.000008	0.000832	0.036881	0.282069	5.3	0.29	1.81	Wankanki
183496-20.01	1313	0.282062	0.000012	0.000776	0.035102	0.282043	3.3	0.42	1.90	Wankanki
183496-24.02	1311	0.282055	0.000007	0.000591	0.023663	0.282040	3.2	0.25	1.90	Wankanki

Table 3. continued

Analysis No.	Crystallization age	$^{176}\text{Hf}/^{177}\text{Hf}$ measured	1SE	$^{176}\text{Lu}/^{177}\text{Hf}$ measured	$^{176}\text{Yb}/^{177}\text{Hf}$ measured	$^{176}\text{Hf}/^{177}\text{Hf}$ initial	ϵHf	1SE	T_{DM} (crustal)	Supersuite
183496-25.02	1315	0.282065	0.000008	0.001063	0.043437	0.282039	3.2	0.28	1.91	Wankanki
183496-26.02	1307	0.282055	0.000008	0.000880	0.036523	0.282033	2.9	0.27	1.92	Wankanki
183496--7.02	1354	0.282060	0.000010	0.000702	0.029003	0.282042	4.2	0.34	1.87	Wankanki
183496-30.02	1355	0.282084	0.000009	0.001111	0.048002	0.282056	4.7	0.31	1.84	Wankanki
187151-1.1	1320	0.282061	0.000011	0.000940	0.044896	0.282038	3.3	0.39	1.90	Wankanki
187151-3.1	1278	0.282094	0.000029	0.001543	0.053773	0.282057	3.0	1.02	1.89	Wankanki
187151-8.1	1327	0.282064	0.000018	0.002329	0.082535	0.282006	2.3	0.63	1.97	Wankanki
187151-15.1C	1320	0.282042	0.000010	0.000348	0.013972	0.282033	3.1	0.35	1.91	Wankanki
187151-15.1R	1320	0.282045	0.000011	0.000810	0.039889	0.282025	2.8	0.39	1.93	Wankanki
187151-16.1C	1309	0.282031	0.000012	0.000639	0.027419	0.282015	2.3	0.42	1.96	Wankanki
187151-16.1R	1309	0.282056	0.000009	0.000545	0.023612	0.282043	3.2	0.31	1.90	Wankanki
187151-18.1	1310	0.282083	0.000017	0.000981	0.049480	0.282059	3.8	0.60	1.86	Wankanki
187151-20.1	1297	0.282086	0.000012	0.001105	0.053958	0.282059	3.5	0.42	1.87	Wankanki
187151-23.1	1331	0.282021	0.000014	0.001828	0.059616	0.281975	1.3	0.49	2.04	Wankanki
184158-1.1	1310	0.282064	0.000009	0.001421	0.070711	0.282029	2.8	0.33	1.93	Wankanki
184158-2.1	1323	0.282025	0.000011	0.001351	0.059181	0.281991	1.7	0.39	2.01	Wankanki
184158-4.1	1335	0.282065	0.000012	0.001425	0.070421	0.282029	3.3	0.42	1.91	Wankanki
184158-5.1	1336	0.282083	0.000023	0.001580	0.082184	0.282043	3.9	0.81	1.88	Wankanki
184158-7.1	1320	0.282071	0.000009	0.001107	0.058578	0.282043	3.5	0.33	1.89	Wankanki
184158-18.1	1323	0.282080	0.000011	0.001270	0.065320	0.282048	3.8	0.39	1.88	Wankanki
184158-19.1	1326	0.282046	0.000009	0.001624	0.084898	0.282005	2.3	0.31	1.97	Wankanki
184158-22.1	1327	0.282053	0.000012	0.001138	0.056458	0.282024	3.0	0.42	1.93	Wankanki

NOTES: Analysis No. is the sample number "-"; grain number "-"; spot number. $^{176}\text{Hf}/^{177}\text{Hf}$ (i), $\epsilon\text{Hf}(i)$ and T_{DM} crustal of zircons are calculated using the $^{207}\text{Pb}/^{206}\text{Pb}$ age of grain. T_{DM} crustal is calculated using a two-stage evolution assuming a mean $^{176}\text{Lu}/^{177}\text{Hf}$ ratio of crust = 0.015. C and R, appended to the spot number, refer to grain centre and edge respectively. This table is compiled from published datasets available from the Geological Survey of Western Australia (<<http://www.dmp.wa.gov.au/geochron>>).

Table 4. Compilation of TIMS Sm–Nd analytical results for whole rock samples from the west Musgrave Province

Sample No.	Age _(¹⁴⁷Sm/¹⁴⁷Nd) Ma	Method	Lithology	Supersuite	Sm (ppm)	Nd (ppm)	(a) ¹⁴³ Nd/ ¹⁴⁴ Nd	error (2SE)	(b) ¹⁴⁷ Sm/ ¹⁴⁴ Nd	fSm/Nd	εNd at T	T _{DM} (Ga)	T _{DM} ² (Ga)	Easting	Northing
187195	1402	Inferred	granite	Papulanlutja	4.75	19.53	0.512028	0.000005	0.146954	-0.25	-2.96	2.58	2.17	405582	7140874
187171	1180	Inferred	granite	Pitjantjatjara	8.10	45.64	0.511712	0.000005	0.107299	-0.45	-4.57	2.07	2.10	418389	7162276
180262	1180	U–Pb zircon	granite	Pitjantjatjara	13.16	84.37	0.511718	0.000005	0.094300	-0.52	-2.48	1.84	1.95	488835	7141487
180294	1180	Inferred	granite	Pitjantjatjara	15.80	86.69	0.511857	0.000005	0.110100	-0.44	-2.15	1.92	1.92	486458	7136884
184146	1201	U–Pb zircon	granite	Pitjantjatjara	20.98	129.92	0.511740	0.000005	0.097639	-0.50	-2.30	1.87	1.95	408788	7081514
185610	1199	U–Pb zircon	pegmatite	Pitjantjatjara	9.62	73.90	0.511519	0.000005	0.078745	-0.60	-3.72	1.85	2.06	405758	7083884
174538	1178	U–Pb zircon	granite	Pitjantjatjara	16.81	85.41	0.511932	0.000005	0.119000	-0.40	-2.06	1.98	1.91	479442	7142104
174800	1180	Inferred	metagranite	Pitjantjatjara	4.58	23.82	0.511888	0.000005	0.116200	-0.41	-2.47	1.99	1.95	482158	7162624
180256	1176	U–Pb zircon	granite	Pitjantjatjara	16.91	88.59	0.511909	0.000005	0.115400	-0.41	-1.98	1.94	1.91	488577	7143422
180299	1175	U–Pb zircon	granite	Pitjantjatjara	13.58	66.37	0.511960	0.000005	0.123700	-0.37	-2.25	2.03	1.93	499043	7138416
180300	1181	U–Pb zircon	granite	Pitjantjatjara	15.40	80.44	0.511886	0.000005	0.113800	-0.42	-2.14	1.94	1.92	499039	7138293
187166	1180	Inferred	granite	Pitjantjatjara	13.87	86.38	0.511649	0.000005	0.097034	-0.51	-4.25	1.97	2.08	431128	7157580
174594	1190	U–Pb zircon	anorthosite	Pitjantjatjara	3.06	18.75	0.511746	0.000005	0.098600	-0.50	-2.46	1.87	1.95	490563	7133432
183459	1178	U–Pb zircon	granite	Pitjantjatjara	14.74	71.30	0.511943	0.000005	0.125000	-0.36	-2.75	2.09	1.97	494495	7080625
183408	1180	Inferred	granite	Pitjantjatjara	5.42	24.82	0.512004	0.000005	0.132100	-0.33	-2.61	2.16	1.96	473143	7103024
185339	1210	U–Pb zircon	granite	Pitjantjatjara	41.27	194.44	0.511931	0.000005	0.128352	-0.35	-3.20	2.19	2.03	490651	7107248
183509	1165	U–Pb zircon	granite	Pitjantjatjara	28.25	129.41	0.512036	0.000005	0.132000	-0.33	-2.10	2.10	1.91	478093	7108943
190231	1200	Inferred	granite	Pitjantjatjara	44.46	268.26	0.511746	0.000005	0.100187	-0.49	-2.57	1.90	1.97	402399	7155044
194367	1200	Inferred	granite	Pitjantjatjara	44.97	223.22	0.511943	0.000005	0.121781	-0.38	-2.04	2.02	1.93	369783	7166857
174558	1215	U–Pb zircon	granite	Pitjantjatjara	17.63	93.12	0.511811	0.000005	0.114500	-0.42	-3.35	2.07	2.04	466891	7148636
174726	1210	Inferred	granofels	Pitjantjatjara	22.92	116.78	0.511926	0.000005	0.118700	-0.40	-1.81	1.98	1.92	472486	7153181
174737	1219	U–Pb zircon	granite	Pitjantjatjara	20.58	128.27	0.511691	0.000005	0.097000	-0.51	-2.92	1.92	2.01	460511	7147960
180860	1200	Inferred	metagranite	Pitjantjatjara	16.5	73.9	0.512064	0.000005	0.134898	-0.31	-1.71	2.12	1.91	421079	7132084
189523	1157	U–Pb zircon	metagranodiorite	Pitjantjatjara	20.62	105.45	0.511893	0.000013	0.118240	-0.40	-2.92	2.02	1.96	378038	7117710
189523	1157	U–Pb zircon	metagranodiorite	Pitjantjatjara	19.74	102.94	0.511877	0.000005	0.115940	-0.41	-2.88	2.00	1.96	378038	7117710
189452	1200	Inferred	metagranodiorite	Pitjantjatjara	14.75	75.47	0.511883	0.000005	0.118162	-0.40	-2.67	2.04	1.98	377895	7126144
174736	1180	U–Pb zircon	granite	Pitjantjatjara	4.08	33.94	0.511426	0.000005	0.072700	-0.63	-4.92	1.87	2.13	460565	7147986
174747	1205	U–Pb zircon	gabbro	Pitjantjatjara	4.41	17.14	0.512364	0.000005	0.155700	-0.21	0.99	2.10	1.71	463810	7151005
174793	1200	Inferred	gabbro	Pitjantjatjara	3.75	17.36	0.511810	0.000005	0.130700	-0.34	-6.03	2.48	2.23	458064	7146869
174796	1180	Inferred	granite	Pitjantjatjara	3.42	27.09	0.511586	0.000005	0.076300	-0.61	-2.33	1.75	1.94	498865	7138028

Table 4. continued

Sample No.	Age _(t) Ma	Method	Lithology	Supersuite	Sm (ppm)	Nd (ppm)	(a) ¹⁴³ Nd/ ¹⁴⁴ Nd	error (2SE)	(b) ¹⁴⁷ Sm/ ¹⁴⁴ Nd	fSm/Nd	εNd at T	T _{DM} (Ga)	T _{DM} ² (Ga)	Easting	Northing
183508	1175	Inferred	granite	Pitjantjatjara	5.46	49.34	0.511512	0.000005	0.066871	-0.66	-2.44	1.71	1.94	477579	7109355
183510	1200	Inferred	dolerite	Pitjantjatjara	5.32	23.95	0.512032	0.000005	0.134300	-0.32	-2.24	2.17	1.95	476850	7109780
187103	1200	U-Pb zircon	granite	Pitjantjatjara	4.15	27.09	0.511702	0.000005	0.092638	-0.53	-2.28	1.84	1.95	456819	7121725
189494	1067	Inferred	dolerite	Pitjantjatjara	7.07	30.80	0.512198	0.000004	0.138792	-0.29	-0.67	1.96	1.72	365914	7130227
183440	1300	Inferred	granite	Wankanki	8.44	44.93	0.511885	0.000005	0.113600	-0.42	-0.85	1.94	1.92	472469	7111282
183492	1322	U-Pb zircon	granite	Wankanki	7.07	37.69	0.511867	0.000005	0.113400	-0.42	-0.93	1.97	1.95	479065	7108230
183496	1321	U-Pb zircon	granite	Wankanki	4.39	20.46	0.512039	0.000005	0.129600	-0.34	-0.33	2.03	1.90	479680	7106191
183587	1351	U-Pb zircon	granite	Wankanki	6.14	33.46	0.511898	0.000005	0.110900	-0.44	0.42	1.87	1.87	490161	7103173
183726	1300	Inferred	granite	Wankanki	4.45	26.32	0.511794	0.000005	0.102100	-0.48	-0.71	1.87	1.91	481944	7106528
184149	1350	U-Pb zircon	metasilstone	Wankanki	5.38	24.95	0.511960	0.000005	0.130318	-0.34	-1.75	2.19	2.03	408773	7081530
184150	1317	Inferred	metasandstone	Wankanki	5.27	32.49	0.511729	0.000005	0.098052	-0.50	-1.10	1.89	1.96	408801	7081555
184158	1321	U-Pb zircon	monzogranite	Wankanki	6.55	34.21	0.511853	0.000005	0.115737	-0.41	-1.61	2.03	2.00	407493	7076919
185581	1312	U-Pb zircon	monzogranite	Wankanki	2.84	19.76	0.511638	0.000005	0.086872	-0.56	-1.04	1.83	1.95	433456	7090442
185606	1325	U-Pb zircon	monzogranite	Wankanki	2.32	11.42	0.511883	0.000005	0.122710	-0.38	-2.17	2.14	2.04	412136	7088141
180867	1324	U-Pb zircon	metasandstone	Wankanki	6.16	32.81	0.511899	0.000005	0.113461	-0.42	-0.30	1.92	1.90	424133	7146395
189547	1300	Inferred	granodiorite	Wankanki	14.54	72.18	0.511910	0.000005	0.121775	-0.38	-1.74	2.07	1.99	396163	7087440
174547	1067	Inferred	dolerite	Warakurna	5.97	26.38	0.512210	0.000005	0.136800	-0.30	-0.17	1.89	1.68	482749	7156879
185587	1075	Inferred	gabbro	Warakurna	2.25	9.13	0.512251	0.000005	0.147909	-0.25	-0.84	2.11	1.74	401693	7112874
185669	1067	Inferred	gabbro	Warakurna	9.43	39.77	0.512313	0.000005	0.143386	-0.27	0.95	1.84	1.59	407318	7109098
189418	1067	Inferred	gabbro	Warakurna	8.90	38.46	0.512097	0.000005	0.139860	-0.29	-2.80	2.19	1.88	418980	7107216
174524	1067	Inferred	gabbro	Warakurna	5.74	23.69	0.512245	0.000005	0.146482	-0.26	-0.81	2.08	1.73	480073	7140905
174593	1067	Inferred	gabbro	Warakurna	6.62	27.39	0.512359	0.000008	0.146222	-0.26	1.46	1.81	1.56	452221	7136057
194354	1067	U-Pb zircon	granophyre	Warakurna	3.56	14.91	0.512255	0.000010	0.144200	-0.27	-0.30	1.99	1.69	354869	7163642
189416	1067	Inferred	gabbro	Warakurna	6.45	28.19	0.512272	0.000005	0.138274	-0.30	0.84	1.80	1.60	415103	7106931
189417	1067	Inferred	basaltic andesite	Warakurna	9.03	39.47	0.512257	0.000005	0.138355	-0.30	0.54	1.83	1.63	418501	7107240
155615	1075	Inferred	gabbro	Warakurna	1.26	4.07	0.512328	0.000005	0.136883	-0.05	-4.71	4.71	2.03	393746	7094347
155671	1075	Inferred	troctolite	Warakurna	0.56	2.63	0.512230	0.000005	0.129195	-0.34	1.34	1.68	1.57	424324	7121858
183431	1078	Inferred	gabbro	Warakurna	0.74	3.29	0.512254	0.000005	0.136300	-0.31	0.85	1.79	1.61	460953	7109514
183438	1078	Inferred	norite	Warakurna	0.80	2.93	0.512442	0.000005	0.164700	-0.16	0.59	2.24	1.63	457137	7110034
183444	1075	Inferred	dolerite	Warakurna	1.62	4.88	0.512632	0.000005	0.200800	0.02	-0.68	6.21	1.72	486154	7104950
183449	1075	Inferred	norite	Warakurna	1.22	3.49	0.512804	0.000005	0.212100	0.08	1.12	32.81	1.59	486265	7103903

Table 4. continued

Sample No.	Age ₍₇₎ Ma	Method	Lithology	Supersuite	Sm (ppm)	Nd (ppm)	(a) ¹⁴³ Nd/ ¹⁴⁴ Nd	error (2SE)	(b) ¹⁴⁷ Sm/ ¹⁴⁴ Nd	fSm/Nd	εNd at T	T _{DM} (Ga)	T _{DM} ² (Ga)	Easting	Northing
183517	1075	Inferred	gabbro	Warakurna	3.78	6.11	0.512419	0.000005	0.183900	-0.07	-2.52	3.78	1.86	484184	7104374
183532	1075	Inferred	gabbro	Warakurna	1.48	5.56	0.512264	0.000005	0.161000	-0.18	-2.39	2.59	1.85	489736	7110905
185589	1075	Inferred	gabbro	Warakurna	0.29	1.53	0.512012	0.000005	0.115100	-0.41	-0.98	1.78	1.75	484581	7102359
193859	1075	Inferred	gabbro	Warakurna	3.69	14.37	0.512371	0.000005	0.155300	-0.21	0.49	2.06	1.64	494319	7113202
183536	1075	Inferred	gabbro	Warakurna	0.37	1.30	0.512292	0.000005	0.169900	-0.14	-3.07	3.02	1.90	496865	7112102
183702	1075	Inferred	anorthosite	Warakurna	1.25	4.45	0.512381	0.000005	0.169400	-0.14	-1.26	2.68	1.77	483002	7094587
185315	1075	Inferred	gabbro	Warakurna	3.73	17.82	0.511960	0.000005	0.126600	-0.36	-3.59	2.10	1.94	442390	7131159
185316	1075	Inferred	gabbro	Warakurna	1.26	5.64	0.512060	0.000005	0.135200	-0.31	-2.82	2.14	1.88	441166	7131364
155661	1075	Inferred	troctolite	Warakurna	7.13	19.33	0.512496	0.000005	0.223050	0.13	-6.41	-11.19	2.15	424083	7123011
155641	1075	Inferred	gabbro	Warakurna	2.70	8.70	0.512182	0.000005	0.187480	-0.05	-7.65	5.64	2.25	397991	7109490
190276	1075	Inferred	gabbro	Warakurna	1.82	7.36	0.512213	0.000005	0.149424	-0.24	-1.79	2.25	1.81	393034	7139185
190310	1075	Inferred	olivine gabbro	Warakurna	7.01	27.08	0.512378	0.000005	0.156561	-0.20	0.45	2.09	1.64	386521	7142506
190336	1075	Inferred	olivine gabbro	Warakurna	1.18	4.81	0.512216	0.000005	0.148014	-0.25	-1.53	2.19	1.79	399173	7137883
190343	1075	Inferred	olivine gabbro	Warakurna	2.44	10.53	0.512249	0.000005	0.139942	-0.29	0.22	1.89	1.66	375594	7145829
190352	1075	Inferred	olivine gabbro	Warakurna	2.11	7.56	0.512498	0.000005	0.168905	-0.14	1.09	2.26	1.59	372690	7140129
194410	1075	Inferred	gabbro	Warakurna	1.73	7.75	0.512282	0.000005	0.134679	-0.32	1.60	1.70	1.55	354054	7154540
183704	1075	Inferred	gabbro	Warakurna	1.80	6.95	0.512317	0.000005	0.156694	-0.20	-0.76	2.26	1.73	477567	7101349
155659	1075	Inferred	troctolite	Warakurna	1.84	7.59	0.512358	0.000010	0.146751	-0.25	1.42	1.83	1.57	424054	7123409
189321	1075	Inferred	gabbro	Warakurna	0.9	3.1	0.512299	0.000004	0.170267	-0.13	-2.98	3.02	1.90	442219	7159088
189381	1075	Inferred	gabbro	Warakurna	0.8	2.5	0.512575	0.000005	0.200356	0.02	-1.75	6.65	1.80	435126	7152857
194454	1075	Inferred	gabbro	Warakurna	5.34	27.25	0.511966	0.000005	0.118405	-0.40	-2.35	1.91	1.85	465893	7127906
174765	1075	Inferred	granite	Warakurna	6.55	33.04	0.511914	0.000005	0.119800	-0.39	-3.55	2.02	1.94	474450	7116550
174766	1075	Inferred	granite	Warakurna	10.50	55.47	0.511920	0.000005	0.114500	-0.42	-2.70	1.91	1.88	476272	7115792
183885	1075	Inferred	biotite gabbro	Warakurna	5.45	24.72	0.512055	0.000005	0.133400	-0.32	-2.67	2.10	1.87	495020	7108438
174590	1075	Inferred	gabbro	Warakurna	3.30	14.80	0.512118	0.000004	0.134688	-0.32	-1.62	2.01	1.79	450930	7133540
187119	1075	Inferred	gabbro	Warakurna	5.93	27.87	0.512025	0.000005	0.128668	-0.35	-2.60	2.04	1.87	439873	7147066
187256	1062	U-Pb zircon	granite	Warakurna	12.77	64.17	0.511958	0.000005	0.120332	-0.39	-2.88	1.96	1.88	436323	7160678
185576	1075	Inferred	gabbro	Warakurna	2.00	7.87	0.512236	0.000010	0.153568	-0.22	-1.91	2.34	1.82	403645	7114910
187048	1075	Inferred	granite	Warakurna	23.3	102.2	0.512279	0.000005	0.137878	-0.30	1.09	1.78	1.59	341338	7113627
187062	1075	Inferred	granite	Warakurna	17.8	95.6	0.512042	0.000005	0.112496	-0.43	-0.03	1.69	1.67	345512	7111348

Table 4. continued

Sample No.	Age ₍₇₎ Ma	Method	Lithology	Supersuite	Sm (ppm)	Nd (ppm)	(a) ¹⁴³ Nd/ ¹⁴⁴ Nd	error (2SE)	(b) ¹⁴⁷ Sm/ ¹⁴⁴ Nd	fSm/Nd	εNd at T	T _{DM} (Ga)	T _{DM} ² (Ga)	Easting	Northing
194633	1075	Inferred	granite	Warakurna	18.5	91.8	0.512162	0.000004	0.121922	-0.38	1.01	1.66	1.60	342501	7117812
174589	1074	U-Pb zircon	granite	Warakurna	14.98	71.59	0.511971	0.000005	0.126540	-0.36	-3.37	2.08	1.93	451114	7133869
174761	1075	U-Pb zircon	granite	Warakurna	16.41	84.79	0.511913	0.000005	0.117000	-0.41	-3.18	1.97	1.91	473626	7116039
183474	1072	U-Pb zircon	granite	Warakurna	16.39	86.84	0.511846	0.000005	0.114100	-0.42	-4.12	2.01	1.98	467560	7071861
185583	1076	U-Pb zircon	monzogranite	Warakurna	12.34	74.13	0.511847	0.000005	0.100650	-0.49	-2.21	1.77	1.84	435796	7100732
180848	1067	Inferred	dolerite	Warakurna	4.44	18.69	0.512369	0.000004	0.143649	-0.27	2.00	1.73	1.52	439873	7158793
180463	1075	Inferred	gabbro	Warakurna	3.27	12.29	0.512426	0.000005	0.160800	-0.18	0.81	2.12	1.61	476536	7135448
194406	1075	Inferred	basaltic andesite	Warakurna	0.8	2.1	0.513070	0.000006	0.227093	0.15	4.26	-1.05	1.35	358276	7159119
194416	1075	Inferred	basaltic andesite	Warakurna	4.7	20.5	0.512215	0.000005	0.139656	-0.29	-0.40	1.95	1.70	367066	7088420
183476	1075	Inferred	basalt	Warakurna	5.3	23.5	0.512088	0.000005	0.134941	-0.31	-2.24	2.08	1.84	457107	7098015
183480	1075	Inferred	basalt	Warakurna	7.3	37.5	0.511858	0.000005	0.117543	-0.40	-4.33	2.06	2.00	459347	7098624
183480	1075	Inferred	basalt	Warakurna	7.44	37.61	0.511885	0.000005	0.119700	-0.39	-4.10	2.07	1.98	459347	7098624
190292	1075	Inferred	metasandstone	Warakurna	3.9	22.4	0.511804	0.000004	0.105599	-0.46	-3.74	1.91	1.95	388680	7139970
185338	1075	Inferred	basalt	Warakurna	6.85	34.34	0.511911	0.000005	0.120600	-0.39	-3.72	2.04	1.95	442348	7102675
183478	1075	Inferred	basalt	Warakurna	6.68	33.60	0.511921	0.000005	0.120252	-0.39	-3.47	2.02	1.93	457600	7099163
194348	1075	Inferred	basalt	Warakurna	7.83	37.66	0.511954	0.000005	0.125619	-0.36	-3.56	2.09	1.94	354158	7165587
189598	1065	Inferred	volcaniclastic	Warakurna	5.6	22.2	0.512400	0.000005	0.151075	-0.23	1.58	1.86	1.55	344731	7120367
194662	1065	Inferred	basalt	Warakurna	8.7	37.6	0.512349	0.000005	0.140027	-0.29	2.09	1.68	1.51	344097	7095514
183615	1065	Inferred	basalt	Warakurna	3.1	12.9	0.512031	0.000005	0.144033	-0.27	-4.67	2.47	2.01	333097	7096049
194665	1065	Inferred	basalt	Warakurna	15.3	80.6	0.512091	0.000005	0.114445	-0.42	0.55	1.64	1.62	335957	7097905
194674	1065	Inferred	basalt	Warakurna	13.1	69.4	0.511775	0.000005	0.114121	-0.42	-5.60	2.12	2.08	336414	7094721
194678	1065	Inferred	basalt	Warakurna	5.7	25.9	0.511908	0.000006	0.133351	-0.32	-5.61	2.37	2.09	336094	7094301
185323	1065	Inferred	basalt	Warakurna	13.63	59.22	0.512282	0.000005	0.139200	-0.29	0.90	1.80	1.60	436608	7112249
185328	1065	Inferred	komatiite	Warakurna	21.14	94.16	0.512226	0.000005	0.135700	-0.31	0.28	1.83	1.64	435847	7112258
185323	1065	Inferred	basalt	Warakurna	13.68	60.54	0.512226	0.000004	0.136572	-0.31	0.16	1.85	1.65	436608	7112249
185324	1065	Inferred	komatiite	Warakurna	19.76	88.29	0.512220	0.000005	0.135289	-0.31	0.21	1.83	1.65	436597	7112227
185329	1065	Inferred	komatiite	Warakurna	20.18	91.72	0.512224	0.000007	0.133029	-0.32	0.61	1.77	1.62	435569	7112363
185518	1065	Inferred	rhyolite	Warakurna	33.37	155.94	0.512203	0.000006	0.129362	-0.34	0.70	1.73	1.61	436920	7112202
185525	1065	Inferred	rhyolite	Warakurna	19.83	91.34	0.512216	0.000006	0.131203	-0.33	0.71	1.75	1.61	435440	7116374
185565	1065	Inferred	andesite	Warakurna	18.27	80.33	0.512221	0.000005	0.137501	-0.30	-0.07	1.88	1.67	428675	7113706
195723	1070	Inferred	rhyolite	Warakurna	19.1	95.6	0.512122	0.000005	0.121068	-0.38	0.30	1.71	1.65	321577	7112756

Table 4. continued

Sample No.	Age _(<i>t</i>) Ma	Method	Lithology	Supersuite	Sm (ppm)	Nd (ppm)	^(a) ¹⁴³ Nd/ ¹⁴⁴ Nd	error (2SE)	^(b) ¹⁴⁷ Sm/ ¹⁴⁴ Nd	<i>f</i> Sm/Nd	εNd at <i>T</i>	<i>T</i> _{DM} (Ga)	<i>T</i> _{DM} ² (Ga)	Easting	Northing
195784	1070	Inferred	volcaniclastic	Warakurna	22.7	119.9	0.512082	0.000005	0.114296	-0.42	0.44	1.66	1.64	321525	7116800
187060	1065	Inferred	dacite	Warakurna	33.5	161.7	0.512151	0.000005	0.125036	-0.36	0.26	1.74	1.64	344119	7110049
187077	1065	Inferred	dacite	Warakurna	34.3	166.2	0.512141	0.000005	0.124762	-0.37	0.11	1.75	1.66	334693	7106463
187092	1065	Inferred	ignimbrite	Warakurna	22.9	113.0	0.512137	0.000003	0.122732	-0.38	0.31	1.72	1.64	335617	7103422
194661	1065	Inferred	rhyolite	Warakurna	25.2	120.8	0.512208	0.000005	0.126135	-0.36	1.24	1.66	1.57	343543	7095275
194661	1065	Inferred	rhyolite	Warakurna	5.2	24.4	0.512143	0.000005	0.127909	-0.35	-0.28	1.81	1.69	343543	7095275
183605	1065	Inferred	basalt	Warakurna	5.7	26.0	0.512197	0.000005	0.132644	-0.33	0.13	1.81	1.65	326154	7096171
183610	1065	Inferred	basalt	Warakurna	3.2	12.4	0.512381	0.000005	0.158023	-0.20	0.25	2.14	1.65	319184	7098214
183611	1065	Inferred	basalt	Warakurna	5.7	25.0	0.512288	0.000005	0.138187	-0.30	1.16	1.76	1.58	319044	7097578
195732	1065	Inferred	rhyolite	Warakurna	17.7	91.3	0.512135	0.000005	0.117339	-0.40	1.00	1.62	1.59	322311	7111044
195773	1065	Inferred	intrusive rock	Warakurna	19.2	102.3	0.512069	0.000004	0.113284	-0.42	0.28	1.66	1.64	323488	7114311
187177	1065	Inferred	dacite	Warakurna	16.84	76.12	0.511966	0.000005	0.132699	-0.33	-4.39	2.25	1.99	436662	7116045
185530	1065	Inferred	granophyre	Warakurna	19.04	90.54	0.512149	0.000005	0.127100	-0.35	-0.05	1.78	1.67	435703	7116281
185537	1065	Inferred	rhyolite	Warakurna	15.98	78.45	0.512056	0.000005	0.123141	-0.37	-1.34	1.86	1.76	436315	7107744
89561	1065	Inferred	dacite	Warakurna	14.76	77.44	0.511866	0.000005	0.115237	-0.41	-3.97	2.00	1.96	411167	7106763
185523	1065	Inferred	rhyolite	Warakurna	15.90	76.08	0.512056	0.000010	0.126216	-0.36	-1.75	1.92	1.80	436656	7116142
185363	1065	Inferred	dacite	Warakurna	14.1	75.6	0.511795	0.000004	0.112501	-0.43	-4.97	2.05	2.04	435525	7108432
185531	1065	Inferred	rhyolite	Warakurna	14.85	76.00	0.511910	0.000005	0.118200	-0.40	-3.51	2.00	1.93	442497	7116584
183612	1065	Inferred	rhyolite	Warakurna	24.7	120.5	0.512169	0.000005	0.123940	-0.37	0.77	1.69	1.61	315841	7099277
174691	1065	Inferred	rhyolite	Warakurna	25.3	124.3	0.512152	0.000005	0.123142	-0.37	0.55	1.70	1.62	318903	7099390
183606	1065	Inferred	rhyolite	Warakurna	25.3	123.5	0.512182	0.000005	0.123999	-0.37	1.03	1.66	1.59	323517	7098368
187053	1065	Inferred	dacite	Warakurna	23.7	109.7	0.512152	0.000005	0.130477	-0.34	-0.45	1.85	1.70	343084	7113287
194608	1065	Inferred	dacite	Warakurna	19.2	99.0	0.512110	0.000005	0.116976	-0.41	0.58	1.66	1.62	349283	7120550
194613	1065	Inferred	dacite	Warakurna	18.2	96.4	0.512093	0.000005	0.114345	-0.42	0.59	1.64	1.62	347149	7116658
194627	1065	Inferred	dacite	Warakurna	18.5	91.1	0.512145	0.000005	0.122857	-0.38	0.46	1.71	1.63	343163	7119665
194467	1065	Inferred	granite	Warakurna	14.2	92.6	0.512110	0.000005	0.092964	-0.53	3.85	1.33	1.37	350057	7117087
174690	1065	Inferred	dacite	Warakurna	17.6	90.8	0.512110	0.000005	0.117385	-0.40	0.52	1.66	1.62	317681	7101883
189564	1065	Inferred	monzogranite	Warakurna	19.0	99.1	0.512124	0.000005	0.116178	-0.41	0.95	1.62	1.59	352148	7109738
194612	1065	Inferred	volcaniclastic	Warakurna	10.1	52.8	0.511910	0.000005	0.115131	-0.41	-3.08	1.93	1.90	348270	7118322
174662	1065	Inferred	granophyre	Warakurna	16.2	76.0	0.512188	0.000005	0.128863	-0.34	0.47	1.75	1.63	356399	7136167
174667	1065	Inferred	andesite	Warakurna	20.3	89.5	0.512296	0.000005	0.137419	-0.30	1.41	1.73	1.56	351185	7124916

Table 4. continued

Sample No.	Age ⁽⁷⁾ Ma	Method	Lithology	Supersuite	Sm (ppm)	Nd (ppm)	(a) ¹⁴³ Nd/ ¹⁴⁴ Nd	error (2SE)	(b) ¹⁴⁷ Sm/ ¹⁴⁴ Nd	fSm/Nd	εNd at T	T _{DM} (Ga)	T _{DM} ² (Ga)	Easting	Northing
185563	1065	Inferred	dolerite	Warakurna	6.04	24.87	0.512233	0.000005	0.146791	-0.25	-1.10	2.11	1.75	422414	7116487
183572	1300	Min age of deposition	leucogranite	Wirku Metamorphics	0.46	3.76	0.511584	0.000010	0.073835	-0.62	-0.10	1.72	1.87	498625	7092059
194433	1300	Min age of deposition	pelitic gneiss	Wirku Metamorphics	7.98	35.25	0.511856	0.000005	0.136768	-0.30	-5.28	2.58	2.26	368553	7115610
174588	1300	Min age of deposition	felsic gneiss	Wirku Metamorphics	3.17	18.60	0.511699	0.000005	0.102900	-0.48	-2.70	2.01	2.06	494327	7134425
174748	1300	Min age of deposition	gneiss	Wirku Metamorphics	10.87	58.96	0.512022	0.000005	0.111500	-0.43	2.18	1.70	1.70	463945	7150771
174797	1300	Min age of deposition	gneiss	Wirku Metamorphics	5.68	30.69	0.511824	0.000005	0.111900	-0.43	-1.76	2.00	1.99	498605	7137890
174798	1300	Min age of deposition	mafic granulite	Wirku Metamorphics	6.56	28.11	0.512170	0.000005	0.141000	-0.28	0.15	2.08	1.85	494667	7133572
183466	1300	Min age of deposition	migmatite	Wirku Metamorphics	4.93	30.41	0.511132	0.000005	0.098000	-0.50	-12.98	2.66	2.83	496227	7080263
183595	1300	Min age of deposition	gneiss	Wirku Metamorphics	5.26	31.13	0.511160	0.000005	0.102200	-0.48	-13.14	2.72	2.84	496719	7077657
183596	1300	Min age of deposition	granite	Wirku Metamorphics	7.76	41.79	0.511714	0.000005	0.112300	-0.43	-3.98	2.17	2.16	460840	7146470
185508	1300	Min age of deposition	migmatite	Wirku Metamorphics	11.15	54.21	0.511920	0.000005	0.124332	-0.37	-1.96	2.11	2.01	471367	7120871
185508	1300	Min age of deposition	migmatite	Wirku Metamorphics	10.85	52.51	0.511926	0.000005	0.125000	-0.36	-1.95	2.12	2.01	471367	7120871
185591	1300	Min age of deposition	metasiltstone	Wirku Metamorphics	2.17	7.65	0.511632	0.000005	0.171737	-0.13	-15.51	5.49	3.02	496792	7077578
185593	1300	Min age of deposition	migmatite	Wirku Metamorphics	1.07	7.72	0.511733	0.000005	0.084163	-0.57	1.09	1.68	1.78	497287	7087129
185619	1300	Min age of deposition	metasiltstone	Wirku Metamorphics	9.67	54.54	0.511610	0.000005	0.107229	-0.45	-5.17	2.22	2.25	401592	7085320
187109	1300	Min age of deposition	metasandstone	Wirku Metamorphics	4.80	29.88	0.511671	0.000005	0.097073	-0.51	-2.28	1.95	2.03	464816	7122705
187113	1300	Min age of deposition	metagranitic rock	Wirku Metamorphics	0.78	6.63	0.511544	0.000005	0.070810	-0.64	-0.37	1.72	1.89	466258	7121620
187115	1300	Min age of deposition	migmatite	Wirku Metamorphics	6.79	35.53	0.511879	0.000005	0.115528	-0.41	-1.30	1.99	1.96	466258	7121620

Table 4. continued

Sample No.	Age ₍₇₎ Ma	Method	Lithology	Supersuite	Sm (ppm)	Nd (ppm)	(a) ¹⁴³ Nd/ ¹⁴⁴ Nd	error (2SE)	(b) ¹⁴⁷ Sm/ ¹⁴⁴ Nd	fSm/Nd	εNd at T	T _{DM} (Ga)	T _{DM} ² (Ga)	Easting	Northing
187150	1300	Min age of deposition	quartzite	Wiriku Metamorphics	6.87	36.94	0.511502	0.000005	0.112390	-0.43	-8.14	2.49	2.47	442480	7128020
187154	1300	Min age of deposition	metasiltstone	Wiriku Metamorphics	7.36	36.07	0.511938	0.000005	0.123339	-0.37	-1.44	2.06	1.97	485245	7139388
194376	1300	Min age of deposition	granophyre	Wiriku Metamorphics	3.91	16.65	0.512133	0.000008	0.142040	-0.28	-0.75	2.19	1.92	364775	7115309
190245	1300	Min age of deposition	metasandstone	Wiriku Metamorphics	4.26	29.01	0.511634	0.000005	0.088743	-0.55	-1.61	1.86	1.98	410501	7073947
190245	1300	Min age of deposition	metasandstone	Wiriku Metamorphics	3.84	26.64	0.511651	0.000005	0.087059	-0.56	-0.99	1.82	1.94	410501	7073947
189540	1300	Min age of deposition	metagranite	Wiriku Metamorphics	8.46	59.25	0.511156	0.000005	0.086308	-0.56	-10.56	2.39	2.65	380563	7088966

NOTES: (a) Normalized to standard. (b) 2s uncertainty of 1%. Model age parameters $^{147}\text{Sm}/^{144}\text{Nd} = 0.2136$; $^{143}\text{Nd}/^{144}\text{Nd} = 0.513163$; decay constant of $^{147}\text{Sm} = 6.54 \times 10^{-12}$. fSm/Nd = $\{(^{147}\text{Sm}/^{144}\text{Nd})_{\text{sample}} / (^{147}\text{Sm}/^{144}\text{Nd})_{\text{CHUR}}\} - 1$ where $^{147}\text{Sm}/^{144}\text{Nd}_{\text{CHUR}} = 0.1967$. Coordinates refer to MGA Zone 52. The method column refers to how the crystallization age has been determined, where 'U-Pb zircon' indicates SIMS geochronology available at <http://www.dmp.wa.gov.au/geochron>. TIMS = thermal ionization mass spectrometry

Oxygen

Oxygen isotope ratios ($^{18}\text{O}/^{16}\text{O}$; $\delta^{18}\text{O}$; Table 5) were determined using a Cameca IMS 1280 multi-collector ion microprobe located at the Centre for Microscopy, Characterisation and Analysis (CMCA) at the University of Western Australia. Analytical conditions were similar to those outlined in detail by Kita et al. (2009). A static ~3 nA Cs^+ beam with an impact energy of 20 keV was focused to a 15 μm spot on the sample surface. Instrument parameters included: a magnification of 130x between the sample and field aperture, 400 μm contrast aperture, 4000 μm field aperture, 120 μm entrance slit, 500 μm exit slits, and a 40 eV band pass for the energy slit with a 5 eV gap. Secondary O⁻ ions were accelerated to 10 keV and analysed with a mass-resolving power of approximately 2400 using dual Faraday cup detectors. A normal-incidence electron gun was used for charge compensation.

Each analysis spot was pre-sputtered for 10 seconds prior to automated peak centring using secondary deflectors DTFA-X, DTFA-Y, and DTCA-X. Each analysis consisted of 20 four-second cycles through the mass stations, which gave an average internal precision of 0.13‰ (1 SD mean). Bracketing analyses of unknown samples with those of standards permits correction for instrumental mass fractionation (IMF) and drift. IMF was corrected using Temora 2 ($\delta^{18}\text{O} = 8.20 \pm 0.02\text{‰}$; Black et al., 2004). Additionally, zircon standard BR266 (Stern, 2001) was run as an unknown. Blocks of 10 to 20 sample analyses were bracketed with at least seven standard analyses and IMF was calculated using a correction scheme similar to that described by Kita et al. (2009) with propagation of uncertainty as outlined below. The spot-to-spot reproducibility (external precision) for standard spots on Temora 2 zircons was 0.12‰ (1 SD, n=32). Zircon standard BR266 (Stern, 2001), run as an unknown, returned a $\delta^{18}\text{O}$ value of $+13.13 \pm 0.08\text{‰}$ (95% confidence, MSWD = 0.94, probability = 0.50), consistent with the value obtained from BR266 grains calibrated against zircon standard 91500 on numerous other mounts ($\delta^{18}\text{O} = 13.28 \pm 0.17\text{‰}$ (2 SD); UWA and GSWA unpublished data). Corrected $^{18}\text{O}/^{16}\text{O}$ ratios are reported in $\delta^{18}\text{O}$ notation (Table 5), in per mil variations relative to Vienna standard mean ocean water (VSMOW).

Petrography, Hf isotopic signatures, and U–Pb geochronology of the Papulankutja Supersuite and related rocks

This section provides a brief summary of the petrography and U–Pb geochronology of Papulankutja Supersuite magmatic rocks, their derivative clastic sedimentary rocks, and other relevant crosscutting rocks, in the context of Hf isotope measurements for some of this material. This summary provides a temporal framework in which Hf isotope measurements from the entire west Musgrave

Table 5. Oxygen isotope analyses from zircons of the west Musgraves

Sample ID	Grain ID	$^{18}\text{O}/^{16}\text{O}$	1σ	$\delta^{18}\text{O}$	$\delta^{18}\text{O}$	Excluded
<i>Session 1</i>						
TEMORA		0.0020196	0.016	8.42	0.16	
TEMORA		0.0020190	0.015	8.13	0.16	
TEMORA		0.0020195	0.012	8.35	0.12	
TEMORA		0.0020190	0.015	8.13	0.16	
TEMORA		0.0020190	0.012	8.12	0.12	
194765	3.1	0.0020152	0.012	6.24	0.12	
194765	3.2	0.0020155	0.011	6.35	0.11	
194765	4.1	0.0020143	0.013	5.77	0.14	
194765	13.1	0.0020146	0.023	5.92	0.23	
194765	2.1	0.0020177	0.018	7.47	0.19	
194765	14.1	0.0020176	0.014	7.44	0.14	
194765	15.1	0.0020163	0.026	6.78	0.27	
194765	17.1	0.0020155	0.016	6.38	0.16	
BR266		0.0020288	0.013	13.00	0.14	
BR266		0.0020288	0.014	13.00	0.14	
TEMORA		0.0020190	0.013	8.12	0.13	
TEMORA		0.0020191	0.011	8.18	0.11	
TEMORA		0.0020194	0.018	8.32	0.18	
TEMORA		0.0020190	0.011	8.14	0.12	
<i>Session 2</i>						
TEMORA		0.0020194	0.013	8.18	0.13	
TEMORA		0.0020194	0.011	8.21	0.11	
TEMORA		0.0020197	0.018	8.34	0.18	
TEMORA		0.0020193	0.011	8.13	0.12	
194765	7.1	0.0020156	0.012	6.29	0.13	
194765	8.1	0.0020186	0.015	7.82	0.15	
194765	9.1	0.0020156	0.014	6.28	0.14	
194765	29.1	0.0020138	0.013	5.42	0.13	
194765	6.1	0.0020151	0.013	6.05	0.13	
194765	5.1	0.0020170	0.015	6.99	0.15	
194765	21.1	0.0020122	0.018	4.62	0.18	yes
194765	22.1	0.0020115	0.012	4.26	0.12	yes
194765	23.1	0.0020146	0.015	5.80	0.15	
194765	10.1	0.0020168	0.017	6.90	0.17	
BR266		0.0020286	0.021	12.80	0.22	
BR266		0.0020290	0.018	13.00	0.19	
TEMORA		0.0020197	0.020	8.35	0.20	
TEMORA		0.0020195	0.016	8.26	0.16	
TEMORA		0.0020192	0.015	8.07	0.15	
<i>Session 3</i>						
TEMORA		0.0020200	0.018	8.25	0.19	
TEMORA		0.0020199	0.014	8.18	0.14	
TEMORA		0.0020195	0.012	8.01	0.12	
194765	24.2	0.0020154	0.013	5.91	0.13	
194765	24.1	0.0020140	0.013	5.22	0.14	
194765	11.1	0.0020159	0.014	6.17	0.14	
194765	12.1	0.0020128	0.013	4.66	0.14	yes
194765	12.1b	0.0020140	0.036	5.23	0.36	yes
194765	18.1	0.0020163	0.010	6.38	0.11	
194765	28.1	0.0020107	0.013	3.61	0.14	yes
194765	19.1	0.0020169	0.010	6.70	0.11	
194765	25.1	0.0020171	0.011	6.81	0.12	
194765	20.1	0.0020153	0.014	5.88	0.15	
BR266		0.0020296	0.011	13.00	0.12	
BR266		0.0020298	0.012	13.13	0.12	
TEMORA		0.0020202	0.012	8.35	0.13	
TEMORA		0.0020198	0.010	8.16	0.11	

Sample ID	Grain ID	^a ¹⁸ O/ ¹⁶ O	1σ	^b δ ¹⁸ O	^c δ ¹⁸ O	Excluded
TEMORA		0.0020197	0.009	8.08	0.10	
TEMORA		0.0020198	0.010	8.13	0.11	
194765	27.1	0.0020149	0.011	5.67	0.12	
194764	6.1	0.0020158	0.014	6.13	0.14	
194764	4.1	0.0020158	0.012	6.12	0.13	
194764	5.1	0.0020150	0.012	5.76	0.13	
194764	16.1	0.0020151	0.010	5.78	0.11	
194764	3.1	0.0020156	0.013	6.02	0.14	
194764	2.1	0.0020151	0.013	5.77	0.14	
194764	5.1	0.0020153	0.011	5.90	0.12	
194764	7.1	0.0020153	0.011	5.88	0.12	
194764	10.1	0.0020145	0.011	5.47	0.12	
194764	9.1	0.0020162	0.012	6.33	0.13	
BR266		0.0020300	0.015	13.22	0.15	
BR266		0.0020302	0.013	13.34	0.14	
TEMORA		0.0020200	0.012	8.26	0.13	
TEMORA		0.0020200	0.012	8.26	0.12	
TEMORA		0.0020203	0.013	8.39	0.13	
TEMORA		0.0020204	0.013	8.45	0.14	
194764	8.1	0.0020158	0.013	6.12	0.14	
194764	8.1b	0.0020153	0.013	5.87	0.14	
194764	11.1	0.0020159	0.009	6.21	0.10	
194764	12.1	0.0020154	0.012	5.92	0.13	
194764	14.1	0.0020135	0.013	4.97	0.14	yes
194764	15.1	0.0020157	0.012	6.09	0.13	
194764	13.1	0.0020151	0.011	5.81	0.11	
194764	17.1	0.0020148	0.013	5.61	0.14	
194764	19.1	0.0020152	0.010	5.86	0.11	
194764	20.1	0.0020156	0.016	6.02	0.17	
194764	18.1	0.0020116	0.012	4.06	0.13	yes
BR266		0.0020301	0.011	13.29	0.12	
BR266		0.0020298	0.015	13.11	0.16	
TEMORA		0.0020203	0.012	8.37	0.13	
TEMORA		0.0020195	0.010	7.99	0.11	
TEMORA		0.0020200	0.011	8.25	0.12	
TEMORA		0.0020199	0.011	8.21	0.11	
<i>Session 4</i>						
TEMORA		0.0020194	0.012	8.04	0.12	
TEMORA		0.0020199	0.009	8.28	0.09	
TEMORA		0.0020197	0.011	8.20	0.11	
TEMORA		0.0020199	0.011	8.33	0.12	
194765	22.1b	0.0020141	0.013	5.42	0.14	
194765	12.1b	0.0020123	0.011	4.53	0.12	yes
194764	18.1b	0.0020143	0.012	5.53	0.13	
194764	18.1c	0.0020152	0.014	5.97	0.15	
194765	28.1b	0.0020103	0.013	3.49	0.14	yes
BR266		0.0020296	0.013	13.16	0.14	
BR267		0.0020298	0.015	13.26	0.16	
OGC		0.0020147	0.013	5.68	0.14	
OGC		0.0020152	0.013	5.96	0.13	
TEMORA		0.0020197	0.012	8.22	0.12	
TEMORA		0.0020198	0.013	8.28	0.13	
TEMORA		0.0020196	0.016	8.15	0.17	
TEMORA		0.0020196	0.014	8.14	0.14	

NOTES: ^a ¹⁸O/¹⁶O ratios corrected for Faraday Cup yield and background. ¹⁸O/¹⁶O ratios are drift corrected where appropriate. No drift was observed in Sessions 1 and 3. The observed drift for Session 2 was 0.006 ‰ per analysis and 0.03‰ per analysis for Session 4. ^b corrected δ¹⁸O values relative to VSMOW. ^c Each δ¹⁸O error (1σ) represents the propagated uncertainty of the SD_{mean} for 20 analysis cycles acquired for each spot, the external uncertainty of the instrumental mass fractionation, and the reported uncertainty of the reference value for Temora-II (Valley, 2003) as detailed in the text. Excluded analyses were located on metamorphic rims, recrystallized domains, fractures or overlapped inclusions. Letter appended to spot id for additional analyses of zircon domain, where space allowed. Accepted analyses are from grains interpreted to preserve magmatic values.

Province can be evaluated. In this regard, the Papulankutja Supersuite is very important because it represents the oldest known magmatic rocks in the west Musgrave Province and hence potentially has the most direct connection with the primordial basement of the region. Additional information on the geochronology of these samples, including details of the analytical uncertainty from replicate analyses of the standard, are given in the cited Geochronology Records <<http://www.dmp.wa.gov.au/geochron>>.

GSWA 194767: psammitic enclave in gneiss

This sample is from an enclave of psammitic granofels within granitic gneiss (Kirkland et al., 2012d). The gneiss comprises three distinct components, including garnet-bearing neosome veins, biotite–hornblende granite, and rare folded psammitic enclaves. This sample is fine-grained and composed principally of quartz and plagioclase, together with 5% opaque oxide minerals and accessory orthopyroxene. Zircon grains isolated from this sample are subhedral, spherical to acicular, up to 200 µm long, and colourless to pale yellow. Cores of the zircons are idiomorphically zoned and overgrown by low-uranium rims.

Five analyses of three rims indicate low Th/U ratios (0.02–0.12) and yield $^{207}\text{Pb}^*/^{206}\text{Pb}^*$ dates of 1205–1154 Ma, which may indicate prolonged metamorphism (Kirkland et al., 2012d). Six analyses of zircon cores, which exhibit either homogeneous textures or faded oscillatory zoning, yield a weighted mean $^{207}\text{Pb}^*/^{206}\text{Pb}^*$ date of 1313 ± 15 Ma (MSWD = 2.1), reflecting either the age of a young detrital component or the age of metamorphic zircon rim growth and core recrystallization (Fig. 3). Ten analyses of zircon cores yield $^{207}\text{Pb}^*/^{206}\text{Pb}^*$ dates of 1463–1375 Ma, including a significant age component at 1404 ± 15 Ma (nine cores; MSWD = 2.0), interpreted as the ages of older detrital material (Kirkland et al., 2012d).

Oscillatory zoned detrital zircons, interpreted to have an original magmatic genesis, yield a range of ϵHf values from –5.08 to +3.58. The centres of Mesoproterozoic magmatic grains tend to yield more radiogenic signatures. Metamorphic rims yield ϵHf values of –3.88 to +0.91. The metamorphic rims have more radiogenic ϵHf values and lower Lu/Hf ratios than the igneous cores. The edges of Mesoproterozoic magmatic grains are consistently more evolved (less radiogenic) than the centres of the same crystals.

GSWA 194768: migmatitic gneiss

This sample was collected from the same locality as GSWA 194767 and is the migmatitic gneiss host rock to the enclave (Kirkland et al., 2012e). The gneiss is leucocratic, fine-grained, and of syenogranitic composition. It is composed of approximately 54% K-feldspar, 30% quartz, 14% plagioclase, and 2% mafic lenses. The mafic lenses contain hornblende, biotite, opaque oxide minerals rimmed by titanite, amphibole-rimmed clinopyroxene, zoned garnet, and accessory apatite and zircon. Zircons liberated from this sample are

subhedral to euhedral, acicular, up to 300 µm long, and colourless to light brown. Zircon cores are idiomorphically zoned and overgrown by low-uranium rims.

Four analyses of zircon rims with low Th/U ratios (0.11–0.14) yield $^{207}\text{Pb}^*/^{206}\text{Pb}^*$ dates of 1206–1167 Ma, possibly indicating prolonged metamorphism, as also suggested by sample GSWA 194768 (Fig. 3). Three analyses of homogeneous rims with low Th/U ratios (0.06–0.14; Fig. 4) yield a weighted mean $^{207}\text{Pb}^*/^{206}\text{Pb}^*$ date of 1311 ± 21 Ma (MSWD = 1.5), interpreted as the age of a high-grade metamorphic event and migmatization (Kirkland et al., 2012e). Ten analyses of zircon cores indicate $^{207}\text{Pb}^*/^{206}\text{Pb}^*$ dates of 1423–1361 Ma, interpreted as the ages of unmodified detrital components within the gneiss. These 10 analyses include a significant age component at 1402 ± 14 Ma (eight cores; MSWD = 1.8), similar to the ages of detrital zircons in the psammitic enclave (GSWA 194767).

GSWA 187195: leucogranitic gneiss

This sample was collected close to samples GSWA 194767 and GSWA 194768 (Kirkland et al., 2010). The unit sampled is a foliated diatextitic to schlieric leucogranite gneiss comprising 48% quartz, 38% microcline, 10% plagioclase, 1.5% biotite, 1% myrmekite, 1% opaque oxide minerals, and 0.5% garnet. Zircons isolated from this sample are subspherical to euhedral, and colourless to dark brown. The crystals are up to 350 µm long, with aspect ratios up to 4:1. Many have abraded or reabsorbed outer edges with idiomorphic zoning truncated at boundaries with homogeneous overgrowths.

Analyses of two zircons yield $^{207}\text{Pb}^*/^{206}\text{Pb}^*$ dates of 1196 and 1179 Ma, were located in grains that have low CL response, and indicate very high uranium contents (2320 and 3432 ppm, respectively) and low Th/U ratios (about 0.06; Fig. 4). These analyses were interpreted by Kirkland et al., (2010) to reflect the age of metamorphic zircon growth during the prolonged 1219–1155 Ma Musgrave Orogeny (Smithies et al., 2009). One analysis yields a $^{207}\text{Pb}^*/^{206}\text{Pb}^*$ date of 1298 ± 26 Ma (1 σ) and could reflect either a young detrital component or the growth of new zircon associated with melting during the 1345–1293 Ma Mount West Orogeny (Smithies et al., 2009). Twenty-six analyses yield $^{207}\text{Pb}^*/^{206}\text{Pb}^*$ dates of 1561–1351 Ma (Fig. 3) These are interpreted to represent the ages of unmodified detrital components (Kirkland et al., 2010), and include significant age components at c. 1409 and 1375 Ma, defined by 16 and 12 analyses, respectively.

GSWA 194765: granite dyke

This sample was collected from a granite dyke in the same hillside outcrop as GSWA 194764 and 194766. The sample contains approximately 35% microcline, 35% plagioclase, 25% quartz, 5% fine-grained biotite, and accessory muscovite (Kirkland et al., 2012b). Zircons from this sample are euhedral and colourless to yellow. The crystals exhibit a wide variety of internal textures, including idiomorphic zoning and reabsorption features. Several crystals are overgrown by high-uranium rims.

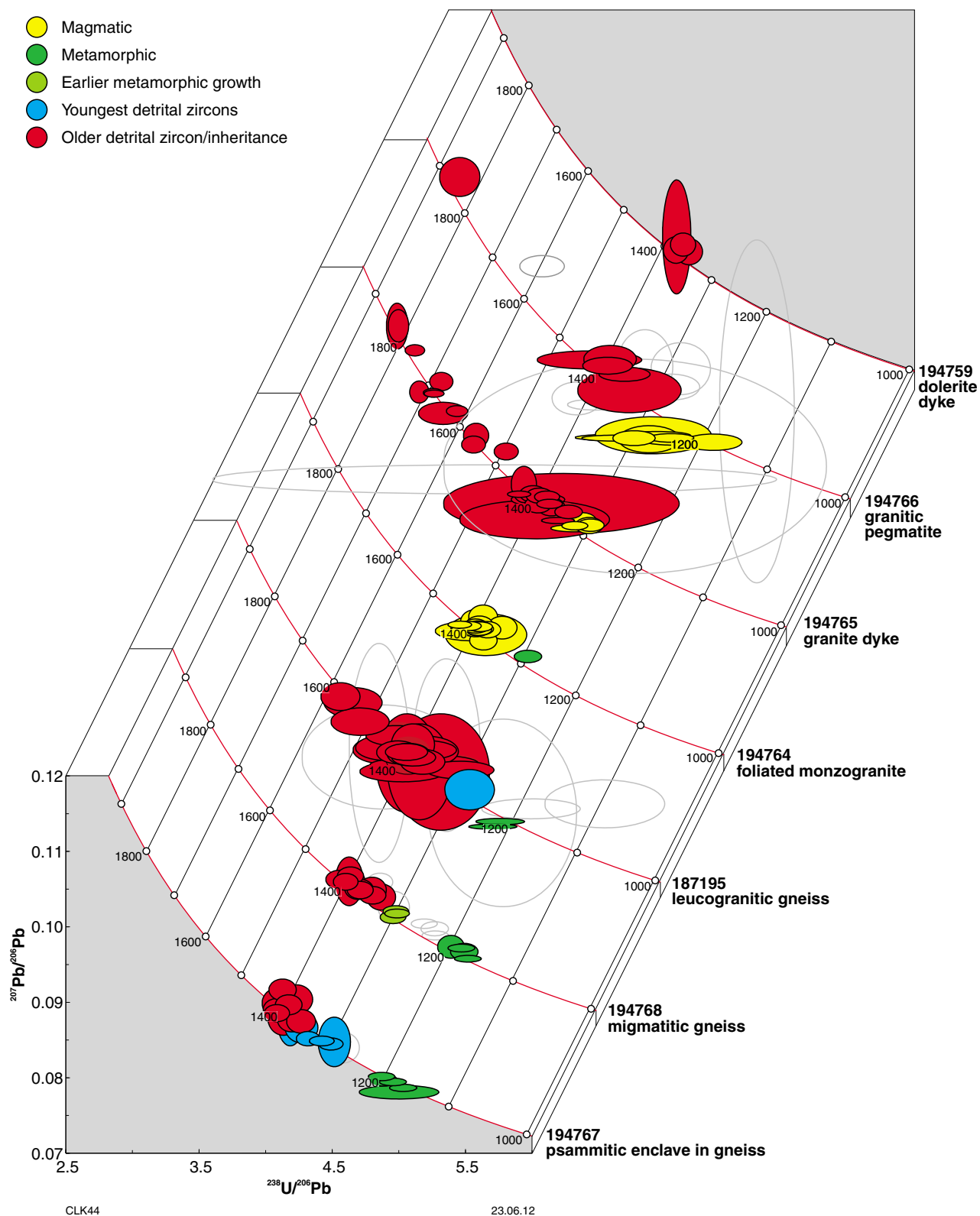


Figure 3. U–Pb analytical data for zircons from Papulankutja Supersuite samples analysed by SHRIMP ion microprobe. Error ellipses are shown at the 2σ level. Grey ellipses refer to Group D data.

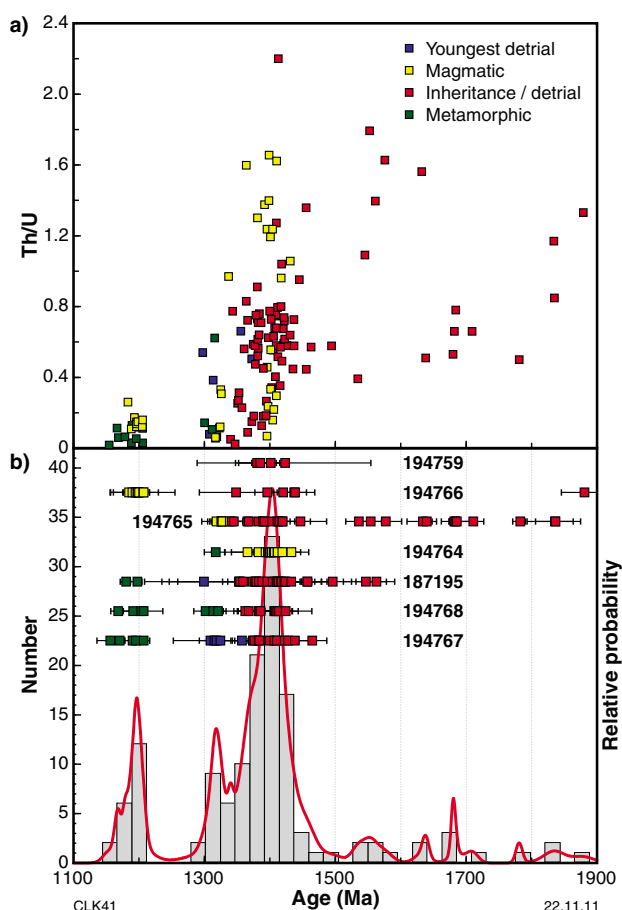


Figure 4. U–Pb zircon geochronology of Papulankutja Supersuite samples: a) Th/U ratios versus $^{207}\text{Pb}^*/^{206}\text{Pb}^*$ ages of zircons; b) Probability density diagram for all seven samples overlain by data from individual samples. Growth mechanism of zircons or zircon domains is indicated by the colour.

Five analyses of zircon rims yield a concordia age of 1318 ± 9 Ma (MSWD = 2.5; Fig. 3), interpreted as the age of magmatic crystallization (Kirkland et al., 2012b). Twenty-six analyses yield $^{207}\text{Pb}^*/^{206}\text{Pb}^*$ dates of 1835–1340 Ma, including significant age components at 1340, 1370, 1390, 1416, and 1681 Ma, defined by 4, 6, 5, 6, and 3 analyses, respectively. These dates are interpreted as the ages of inherited zircons (Kirkland et al., 2012b). The wide age range of inherited zircons is consistent with migration of melt from its source through other lithological units and injection into c. 1400 Ma host rocks (of which GSWA 194764 is representative). The ϵHf values for magmatic zircons from this sample range from evolved values of -12.54 to juvenile values of $+8.44$. The evolved values are only found in zircons older than 1500 Ma. No consistent trends in ϵHf values are evident between the centres and edges of magmatic zircons, and the ϵHf values within individual zircon grains agree to within two ϵHf units.

GSWA 194764: foliated monzogranite

This sample is a foliated monzogranite orthogneiss, crosscut by weakly foliated granite dykes and non-foliated pegmatite dykes, of which samples GSWA 194765 and 194766 are representative (Kirkland et al., 2011b). The monzogranite comprises 25% quartz, 25% microcline, 34% plagioclase, 9% biotite, 6–7% hornblende and recrystallized amphibole after pyroxene, 1% opaque oxide minerals, and accessory apatite and zircon. Zircons isolated from this sample are euhedral, 200–400 μm long, and have aspect ratios up to 6:1. The crystals are colourless and clear to black. In CL images, the crystals exhibit idiomorphic zoning, which in some grains is embayed and contorted. Several display thin high-uranium overgrowths. Nineteen analyses of idiomorphically zoned crystals yield a weighted mean $^{207}\text{Pb}^*/^{206}\text{Pb}^*$ date of 1402 ± 4 Ma (MSWD = 1.4; Fig. 3), interpreted as the age of magmatic crystallization of the monzogranite protolith (Kirkland et al., 2011b). One analysis of a high-uranium zircon rim yields a $^{207}\text{Pb}^*/^{206}\text{Pb}^*$ date of 1316 ± 8 Ma (1σ), interpreted as the age of high-grade metamorphism (Kirkland et al., 2011b). The magmatic zircons from this sample yield a range of juvenile ϵHf values from $+8.10$ to -0.05 .

GSWA 194766: granitic pegmatite dyke

This pegmatite dyke was collected from the same hillside outcrop as, and crosscuts, a 1402 Ma foliated granite (GSWA 194764) and a 1318 Ma granite dyke (GSWA 194765) (Kirkland et al., 2012c). This sample is a partly recrystallized inequigranular monzogranitic pegmatite comprising microcline, antiperthitic plagioclase, and lenses of biotite–epidote–muscovite–opaque oxide minerals, and titanite. Zircons from this sample are subhedral and yellow to brown. The crystals consist of idiomorphically zoned cores overgrown by homogeneous zircon rims. Nine analyses of zircon rims yield a weighted mean $^{207}\text{Pb}^*/^{206}\text{Pb}^*$ date of 1197 ± 4 Ma (MSWD = 0.73; Fig. 3), interpreted as the age of magmatic crystallization of the pegmatite (Kirkland et al., 2012c). Six analyses of zircon cores yield $^{207}\text{Pb}^*/^{206}\text{Pb}^*$ dates of 1879–1347 Ma, which include a coherent component at 1428 ± 13 Ma. These dates are interpreted as the ages of inherited zircons (Kirkland et al., 2012c).

GSWA 194759: dolerite dyke

This sample was collected from a metre-wide dolerite dyke trending 048° on the northern side of the west Hinckley Range (Kirkland et al., 2012a). The dyke is a fine-grained, plagioclase- and olivine-phyric dolerite, containing tremolite–actinolite–phlogopite–magnetite alteration. This sample yielded colourless, rounded, subhedral zircons that exhibit faint idiomorphic zoning in cores and thin low-uranium rims. The rims are too thin (5 μm) for analysis. Four analyses yield a concordia age of 1372 ± 14 Ma (MSWD = 1.6; Fig. 3) and indicate moderate Th/U ratios (0.64 – 0.77). The moderate Th/U ratios and the rounding of the crystals are not typical of primary zircons formed during late-stage crystallization of a mafic magma and suggest that the zircons are inherited

from older rocks. The date of 1372 ± 14 Ma is interpreted as the age of a basement component and provides a maximum age for igneous crystallization of the dolerite dyke (Kirkland et al., 2012a).

Results and interpretation

The c. 1400 Ma Papulankutja Supersuite

In the southwestern part of the Tjuni Purlka Tectonic Zone (Fig. 1), a small outcrop of metamorphosed granite (GSWA 194764) yielded a protolith age of 1402 ± 4 Ma, which is significantly older than the maximum depositional age of the Wirku Metamorphics. The orthogneiss is a moderately foliated, K-feldspar porphyritic, orthopyroxene–clinopyroxene–biotite granodiorite to monzogranite, metamorphosed at or near granulite-facies conditions. A single zircon rim yielded a date of 1316 ± 8 Ma (1σ), similar to crystallization ages for the Wankanki Supersuite of the Mount West Orogen. The granodiorites and monzogranites of the Papulankutja Supersuite are indistinguishable petrographically and geochemically from the calc-alkaline granites of the Wankanki Supersuite. However, the Wankanki Supersuite rocks do not typically contain significant quantities of inherited zircon, implying that the Wankanki magmas were undersaturated in zirconium (Smithies et al., 2010).

Those Wankanki samples that do exhibit zircon inheritance yield xenocryst ages within the broad timeframe of the Mount West Orogeny (1345–1293 Ma; Evins et al., in press). This has been interpreted as indicating that emplacement of the Wankanki Supersuite was mainly within essentially coeval rocks of the same supersuite (Howard et al., 2011a). The granodiorites and monzogranites from the area south of Mount Scott intrude paragneisses that contain a dominant detrital component of c. 1400 Ma zircons, although they also include components as old as c. 1550 Ma (e.g. GSWA 187195, 194767, and 194768). If these metagranites belong to the geochemically similar Wankanki Supersuite, they must have selectively inherited only the c. 1400 Ma detrital component from the surrounding country rock. A more likely explanation is that the c. 1400 Ma zircon age represents the true crystallization age of the granodiorites and monzogranites. If this interpretation is correct, then this metagranite sample represents hitherto unrecognized igneous basement rocks significantly older than the Wankanki Supersuite. On this basis, the granodiorites and monzogranites from the area south of Mount Scott were assigned to the Papulankutja Supersuite by Howard et al., (2011b).

The 1318 ± 9 Ma leucogranite dyke (GSWA 194765), which cuts foliated granodiorites and monzogranites of the c. 1400 Ma Papulankutja Supersuite, is assigned to the Wankanki Supersuite. The c. 1318 Ma date also represents a minimum age for deformation of the host Papulankutja

Supersuite granodiorites and monzogranite, whereas the c. 1400 Ma zircon age for those host rocks represents a maximum age constraint on that deformation, irrespective of how that date is interpreted. This deformation at some time between c. 1400 and 1318 Ma represents the first temporal constraint on deformation events either associated with, or older than, the Mount West Orogeny.

The age of 1197 ± 4 Ma for the granite pegmatite, which crosscuts the c. 1400 Ma monzogranite and c. 1300 Ma granite dykes (Kirkland et al., 2012c), corresponds to the c. 1220 to c. 1120 Ma, ultrahigh-temperature Musgrave Orogeny. The Musgrave Orogeny caused both widespread development of leucosomes, representing local partial melts, in the Wirku Metamorphics, and generation of extensive $\geq 1000^\circ\text{C}$ granites of the Pitjantjatjara Supersuite.

Metasedimentary rocks related to the Papulankutja Supersuite

Garnetiferous diatexite, approximately 10 km north of Mount Scott, contains enclaves of psammitic metasediment. A sample of a psammitic enclave (GSWA 194767) from the diatexite yielded a detrital zircon age component of 1404 ± 15 Ma (Kirkland et al., 2012d), and two samples of the host diatexite (GSWA 187195, 194768) also contain a dominant 1400 Ma zircon age component. In all three samples, a minor component of younger zircons (mainly rims) was dated at 1313 ± 15 Ma (GSWA 194767), 1298 ± 26 Ma (GSWA 187195, one zircon), and 1311 ± 21 Ma (GSWA 194768). These younger age components can be interpreted as detrital material constraining the maximum age of deposition of the protolith or, alternatively, they may reflect local incipient migmatization during the Mount West Orogeny.

If these zircons represent detritus, then the psammitic enclave and diatexite belong to the Wirku Metamorphics, the sedimentary protoliths of which were deposited between c. 1340 and 1270 Ma (Howard et al., 2011a). However, zircons dated at c. 1400 Ma dominate the samples in the area around Mount Scott, which also includes granitic intrusions of this age (Fig. 4), suggesting that the protoliths to these rocks contain a volcanic component emplaced at c. 1400 Ma and related to the Papulankutja Supersuite. In this scenario, the c. 1300 Ma age component would be related to metamorphism and local in situ melting during the Mount West Orogeny. This alternative is supported by the homogeneous textures of the c. 1300 Ma zircons (dominantly rims), and their low Th/U ratios, which are features consistent with growth during metamorphism (Fig. 4).

Inheritance in the dolerite dyke

The plagioclase- and olivine-phyric dolerite dyke (GSWA 194759) yields a unimodal 1372 ± 14 Ma zircon age component, which is interpreted as the age of inherited material (Kirkland et al., 2012a) (Fig. 3). Based on geochemistry and field relationships, the dyke is assigned

to the Kullal Suite, which elsewhere yielded an imprecise Sm–Nd mineral isochron of c. 1000 Ma (Glikson et al., 1996). Although this 1372 Ma inherited zircon component is younger than Papulankutja Supersuite magmatism, it nonetheless demonstrates that magmatic rocks older than the Wankanki Supersuite (Mount West Orogeny) exist within the hidden basement of the west Musgrave Province.

Evolution of Hf isotope ratios within individual zircons

Zircons from psammitic enclave sample GSWA 194767 (Kirkland et al., 2012d) display consistent intragrain patterns in Hf isotopic ratios. The metamorphic rims are always more radiogenic than the corresponding magmatic cores in the same crystal, although the rims are not all more radiogenic than all igneous cores within the sample. Metamorphic rims also have lower Lu/Hf ratios than corresponding magmatic cores (Fig. 5). This indicates that the metamorphic zircon rims grew within a metamorphic medium that had a higher $^{176}\text{Hf}/^{177}\text{Hf}$ ratio than the magma within which the zircon cores grew. Lutetium, a heavy REE (HREE), is partitioned into garnet much more strongly than is Hf, a HFSE (Chen et al., 2010; Zheng et al., 2005). Garnet crystallization during high-grade metamorphism can significantly deplete the metamorphic medium in HREE to produce a metamorphic fluid or melt with a low Lu/Hf ratio. Garnet is a constituent of the leucosomes that transect the host rock of the psammitic enclave. If garnet coprecipitates with zircon, the metamorphic zircons will acquire a lower $^{176}\text{Lu}/^{177}\text{Hf}$ ratio than the older igneous zircons because of preferential partitioning of Lu into garnet (Hoskin and Schaltegger, 2003). However, breakdown of garnet will lead to a metamorphic fluid with high $^{176}\text{Hf}/^{177}\text{Hf}$ ratios as a result of time-integrated high Lu/Hf ratios in the garnet (Zheng et al., 2005). The higher $\epsilon\text{Hf}(t)$ values for the metamorphic rims compared to the igneous cores indicate metastable breakdown of garnet in the garnet-bearing leucosomes, with transport of elements within metamorphic fluids into newly crystallizing metamorphic zircon rims in the psammitic enclave. In this sample, this relationship is only observed on an intragrain level. However, it does not hold for all metamorphic rims compared to all magmatic cores, implying inhomogeneous Hf concentration in localized metamorphic fluids.

The Hf isotopic signatures of the centres of detrital magmatic zircon grains in sample GSWA 194767 are consistently more evolved than those in the edges of the same crystals (Fig. 5). This suggests that the magma from which the zircon crystallized evolved towards more unradiogenic compositions (lower time-integrated Lu/Hf ratios) over a time scale shorter than the typical uncertainties (c. 5–10 Ma at 1400 Ma) of ion microprobe (SHRIMP) U–Pb zircon dates. Such a situation could imply greater incorporation of unradiogenic sediment into magma through time.

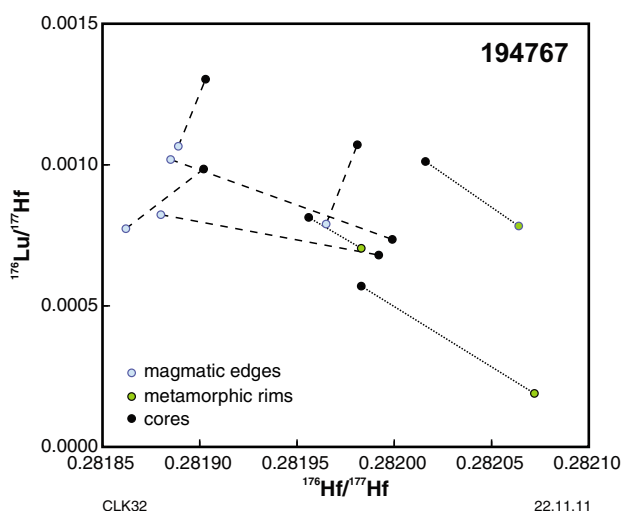


Figure 5. Intragrain Hf isotopic values in zircons from GSWA 194767. Metamorphic zircon rims are more radiogenic than zircon cores and also have lower $^{176}\text{Lu}/^{177}\text{Hf}$ ratios. The edges of magmatic zircons are consistently more evolved than the magmatic cores of the same crystals.

Evolution of Hf isotope ratios between samples: the case for c. 1900 Ma crust formation

The initial $^{176}\text{Hf}/^{177}\text{Hf}$ isotopic composition of 1400 Ma zircons in rocks of the Papulankutja Supersuite defines a field that extends between values corresponding to CHUR1400 Ma and 0.28215 ($\epsilon\text{Hf}1400$ Ma values from approximately 0 to +9). This range is compared with that of other magmatic suites within the west Musgrave Province in Figure 6, which shows that the isotopic composition of all younger magmas lies essentially within the envelope defined by normal crustal isotopic evolution from a Papulankutja Supersuite composition. Thus, the Hf-isotope range of all rocks younger than c. 1400 Ma can be explained entirely through recycling of pre-existing crust during several orogenies. Only the data for the Warakurna Supersuite show a trend to initial $^{176}\text{Hf}/^{177}\text{Hf}$ values slightly above this evolution line, which could additionally be interpreted to reflect renewed juvenile input.

For zircons from spatially related samples, well-defined Hf-isotope evolution arrays can be used to suggest genetic relationships through processes such as repeated recycling of an isotopically homogeneous source or variable mixing between two source components. In the former case, the array defines the average $^{176}\text{Lu}/^{177}\text{Hf}$ composition of the source melt, and the time that this source separated from the mantle. Regressing all data from magmatic rocks of the west Musgrave Province (weighted by conservative analytical uncertainties) yields a slope of 0.011 ± 0.02 (Fig. 7), corresponding to a $^{176}\text{Lu}/^{177}\text{Hf}$ ratio of 0.018, which

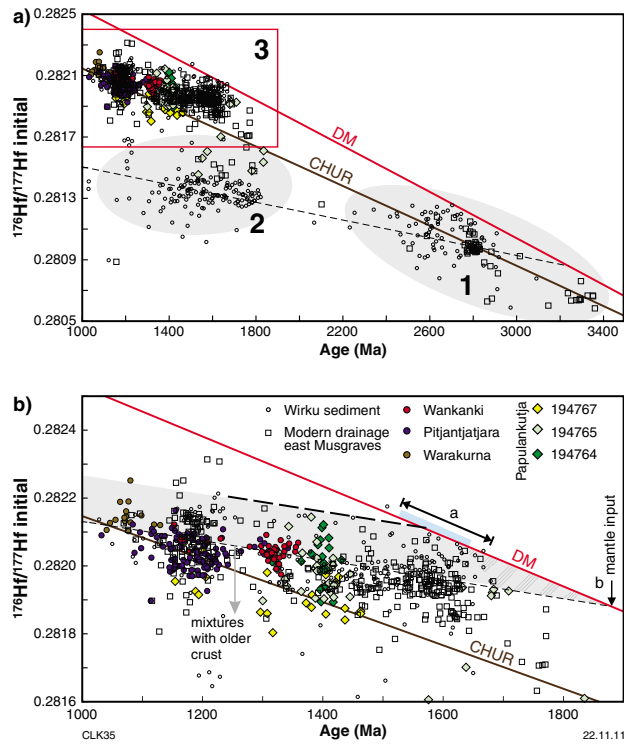


Figure 6. $^{176}\text{Hf}/^{177}\text{Hf}$ (i) evolution diagram for zircons from the west Musgrave Province: a) Musgrave data from GSWA's online geochronology database <<http://dmp.wa.gov.au/geochron>>, Woodhouse et al. (in prep) and Gum and Belousova (2006). The dashed line is a reference evolution line corresponding to a $^{176}\text{Lu}/^{177}\text{Hf}$ ratio of 0.015. Fields 1, 2, and 3 are discussed in the text; b) Data for 1900–1000 Ma zircons (coloured) from magmatic rocks and samples presented in this paper. The line 'a' indicates the timing of juvenile addition at 1650–1550 Ma, corresponding to possible arc magmatism (blue bar; Wade et al., 2006); 'b' indicates a crust formation event at 1950–1900 Ma. DM indicates depleted mantle. CHUR indicates chondritic uniform reservoir.

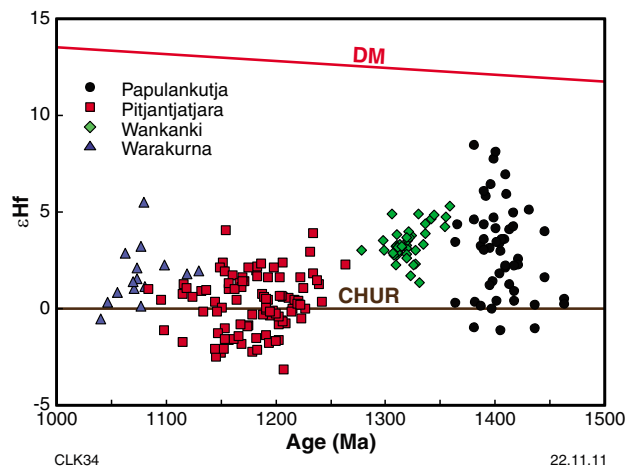


Figure 7. Hf-evolution diagram for magmatic rocks of the west Musgrave Orogen. DM indicates depleted mantle. CHUR indicates chondritic uniform reservoir.

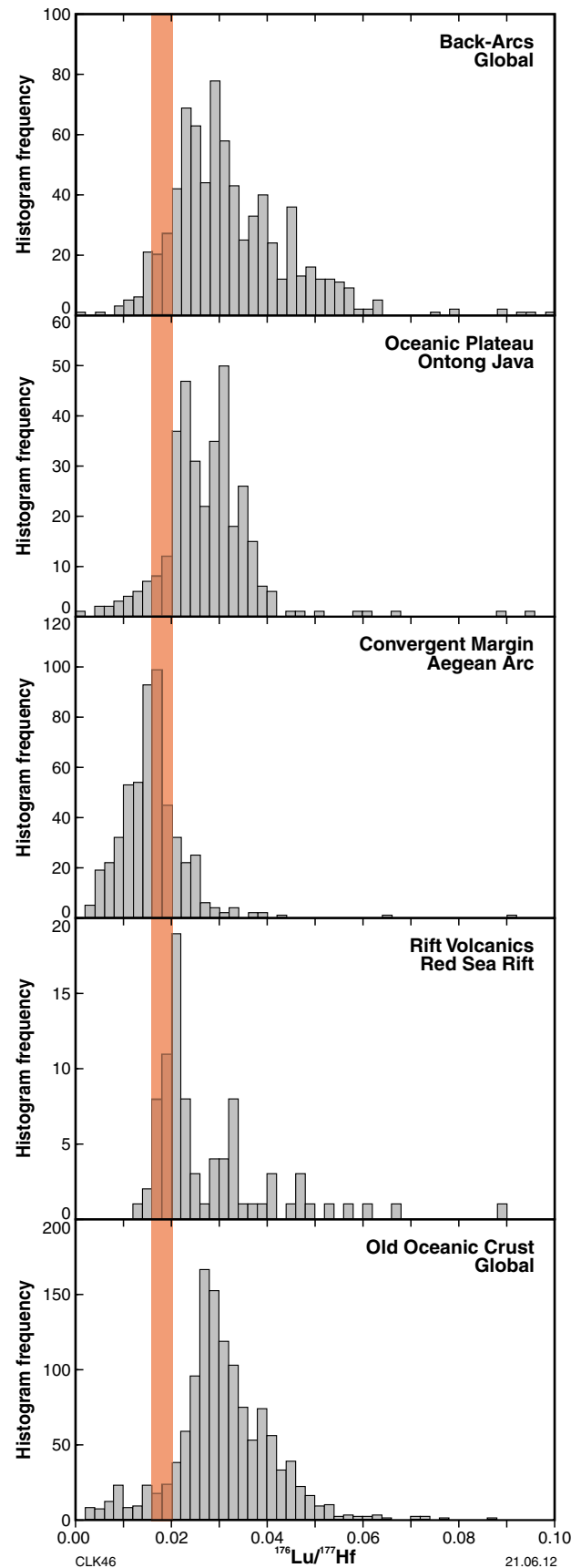


Figure 8. Histograms of $^{176}\text{Lu}/^{177}\text{Hf}$ values for a range of different geological settings (data from <<http://www.earthchem.org>>). Vertical bar represents the average $^{176}\text{Lu}/^{177}\text{Hf}$ ratio of a c. 1950–1900 Ma source in the west Musgrave Province.

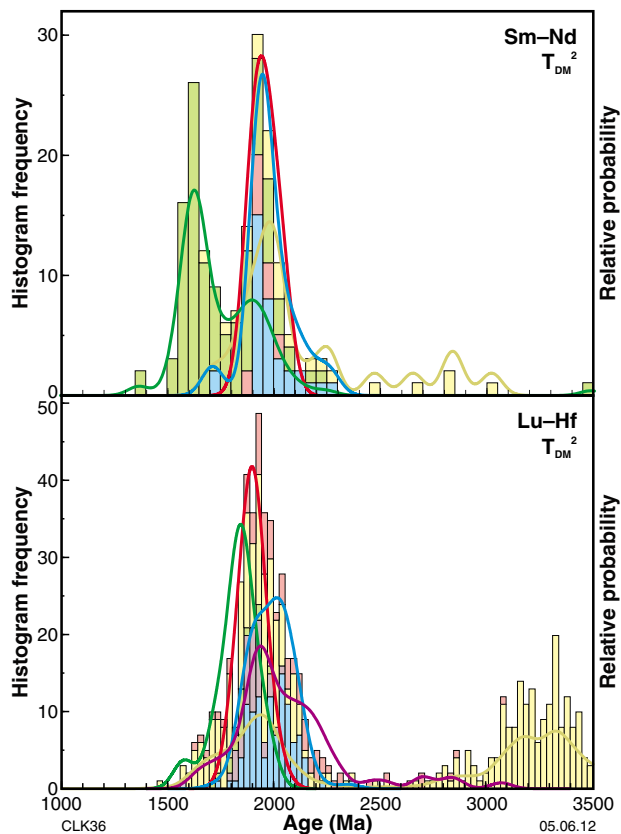


Figure 9. Probability density diagram of two-stage model ages from the west Musgrave Province: a) Whole-rock Sm-Nd; b) zircon Lu-Hf. Blue = Pitjantjatjara Supersuite, red = Wankanki Supersuite, green = Warakurna Supersuite, yellow = Wirku Metamorphics, purple = Papulankutja Supersuite.

intersects CHUR at 1110 ± 36 Ma (MSWD = 65; see below). An average source $^{176}\text{Lu}/^{177}\text{Hf}$ of 0.018 is higher than that of time-integrated upper continental crust (Rudnick and Gao, 2003), indicating that clastic sediments or differentiated igneous rocks are not the sole magma source. A $^{176}\text{Lu}/^{177}\text{Hf}$ ratio of 0.018 is typically observed in measurements of convergent margin arc magmas and is indicative of mafic to intermediate crust (cf. Blichert-Toft and Albarede, 2008) (Fig. 8). The array for west Musgrave Province magmatic rocks forms a very well defined apparent crustal evolution line from a c. 1950–1900 Ma mantle extraction event. The evolution line clearly corresponds to the peak in model ages in Figure 9.

Several significant observations arise from a comparison of Wirku Metamorphics detrital zircon data with those from spatially related magmatic rocks (Fig. 6). Wirku Metamorphics Hf isotope values define radiogenic and distinctly non-radiogenic groups, with very few data lying between the groups. The non-radiogenic group reflects material that does not appear to have been assimilated by the magmatic rocks. However, the radiogenic group overlaps and extends the array defined by the magmatic rocks, yielding a slope corresponding

to a $^{176}\text{Lu}/^{177}\text{Hf}$ ratio of approximately 0.015. Therefore, the Wirku Metamorphics detrital zircon data suggest that the sedimentary protoliths of these paragneisses were derived through erosion of at least two main hinterlands, one of which was the same c. 1950–1900 Ma mafic to intermediate material from which the Musgrave Province granites were derived. A small subset of the radiogenic group also plots on the depleted mantle evolution line at c. 1650–1550 Ma (Fig. 6b area of graph indicated by 'a'). This subset provides evidence for a central Australian juvenile mantle source component derived within that period and is consistent with the suggestion of a c. 1650–1550 Ma juvenile arc component within the basement source of the Musgrave Province (Wade et al., 2006).

Justification of the inferred c. 1950–1900 Ma mafic to intermediate source of the granites of the Musgrave Province raises further questions. In particular, can the apparent evolution trend be better explained as indicating mixing of source components? If not, what is the cause of dispersion around the c. 1950–1900 Ma evolution array?

To assess whether the apparent c. 1950–1900 Ma evolution array is best attributed to isotopic evolution from a mantle extraction event or to mixing between a range of source components, time-series analysis was carried out on the model ages derived from all dated igneous zircons in the magmatic supersuites (Fig. 10). Progressive mixing of depleted mantle with unradiogenic crustal material should result in a model-age trend through time (Fig. 11). The only exception to this would be in the unlikely case that contributions from individual source components systematically changed by both radiogenic and unradiogenic additions to yield a constant model age

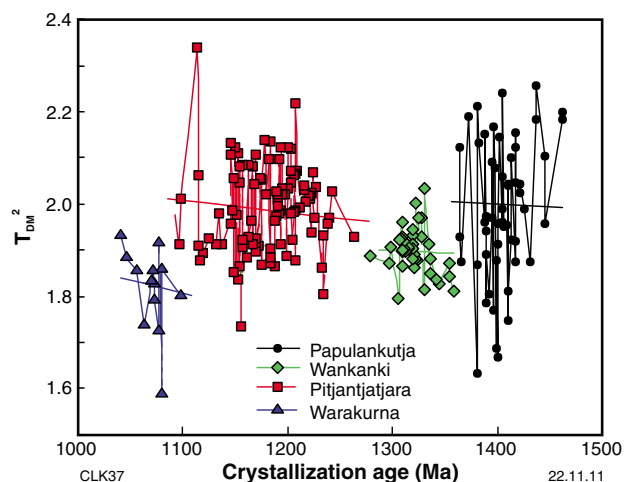


Figure 10. Two-stage model-age evolution of magmatic supersuites of the west Musgrave Province. Best-fit lines through each supersuite are shown. The Warakurna Supersuite shows somewhat younger model ages consistent with renewed juvenile input. However, as a whole and within individual time segments, no statistically significant temporal trend is apparent. This implies a consistent source which either has some degree of crustal or mantle input causing minor heterogeneity.

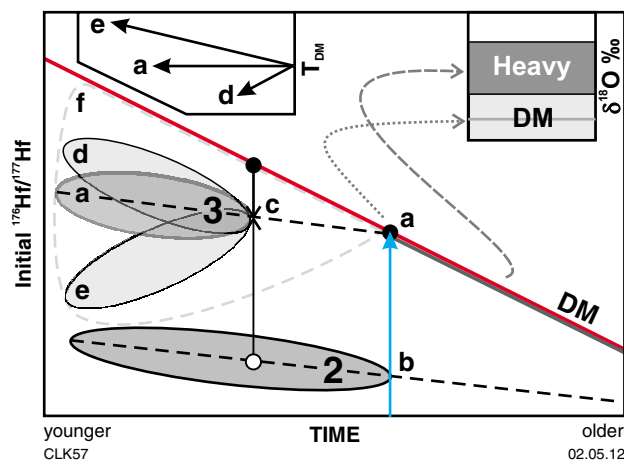


Figure 11. Schematic initial Hf evolution diagram. A real mantle extraction event is indicated at 'a'. Coeval reworking of older material commences at 'b'. Mixing of mantle and crustal sources could produce a homogenous reservoir, although crustal influence should be diagnosed in heavy oxygen isotopes (top-right inset). Juvenile addition into a homogenized basement would result in increasing radiogenic input 'd' and decreasing model ages (top-left inset). In contrast, increasing addition of crustal material would increase unradiogenic input 'e' and increase model ages. A heterogeneous Lu–Hf source would lead to increasing dispersion in initial ratios 'f'. Fields 2 and 3 correspond to Fields 2 and 3 in Figure 6.

that nonetheless represents a mixture. However, if a single, or homogenized, source was tapped, no such trend would be expected and the dispersion could then be attributed to localized mixing with radiogenic or unradiogenic sources. The model-age time-series was statistically evaluated in 1, 3, 4, 5 ... 22 intervals. Calculated r^2 and P values from the time-integrated regressions for all intervals are presented in Table 6. No r^2 values are ≥ 0.65 at $P \leq 0.05$ for any of these regressions; hence no statistically meaningful trend was observed in the dataset, either within individual time segments or collectively (see Bryhn and Dimberg, 2011). Nonetheless, it is clear that the Warakurna Supersuite incorporated more radiogenic material, and consequently yields younger model ages, than do the other supersuites.

The large MSWD of 65 associated with the regression to calculate the source $^{176}\text{Lu}/^{177}\text{Hf}$ ratio reflects the presence of components with contrasting $^{176}\text{Lu}/^{177}\text{Hf}$ ratio or source extraction age. This could indicate a source comprising several contemporaneous components with dissimilar $^{176}\text{Lu}/^{177}\text{Hf}$ ratios (i.e. mixed mafic and felsic rocks). However, this should lead to a systematic divergence (increasing spread) in isotopic composition with decreasing age, which is not observed (Fig. 10). Rather, the high MSWD of the regression can be better interpreted as reflecting very minor assimilation of isotopically contrasting material through time into the magmas. The composition of this material can be accounted for by the sources of the Wirku Metamorphics (i.e. an unradiogenic component and a juvenile c. 1650–1550 Ma component).

Table 6. Statistical time series analysis of Nd and Hf model ages from magmatic rocks of west Musgrave Province

<i>Linear trend analysis of Nd T_{DM}^2 time series</i>					
<i>Supersuite</i>	<i>Intervals</i>	r^2	P	n	<i>Statistically meaningful trend?</i>
Pitjantjatjara	1 (entire)	0.07	0.12	33	No
Wankanki	1 (entire)	0.61	0.00	12	No
Warakurna	1 (entire)	0.10	0.00	108	No
Warakurna	3	0.48	0.51	108	No
Warakurna	4	0.55	0.26	108	No
Warakurna	5	0.00	0.97	108	No
All data	1 (entire)	0.29	0.00	154	No

<i>Linear trend analysis of Hf T_{DM}^2 time series</i>					
<i>Supersuite</i>	<i>Intervals</i>	r^2	P	n	<i>Statistically meaningful trend?</i>
All data	1 (entire)	0.01	0.18	206	No
All data	3	0.65	0.40	206	No
All data	4	0.15	0.61	206	No
All data	5	0.15	0.52	206	No
All data	6	0.21	0.36	206	No
All data	7	0.23	0.28	206	No
All data	8	0.23	0.22	206	No
All data	9	0.24	0.18	206	No
All data	10	0.20	0.19	206	No
All data	11	0.25	0.12	206	No
All data	12	0.29	0.07	206	No
All data	13	0.25	0.08	206	No
All data	14	0.24	0.07	206	No
All data	15	0.22	0.07	206	No
All data	16	0.21	0.07	206	No
All data	17	0.18	0.09	206	No
All data	18	0.25	0.03	206	No
All data	19	0.18	0.07	206	No
All data	20	0.18	0.07	206	No
All data	21	0.19	0.05	206	No
All data	22	0.23	0.02	206	No

NOTES: r^2 and P values calculated from time integrated regressions for time segments and entire time intervals. No r^2 values are ≥ 0.65 at $P \leq 0.05$ for any of these regressions (Bryhn and Dimberg, 2011).

Therefore, time-series analysis of data for the Papulankutja, Wankanki, and Pitjantjatjara Supersuites supports the hypothesis that the 1950–1900 Ma array reflects either a source that separated from the mantle at that time, or a combination of sources (e.g. a juvenile c. 1800 Ma component and a >1900 Ma unradiogenic component) that were homogenized between 1800 and 1900 Ma to consistently yield 1950–1900 Ma model ages. This hypothesis can be further evaluated using a Musgrave Province dataset that includes Hf-isotope data from modern river sediments (Gum and Belousova, 2006), magmatic rocks (this work and Smithies et al., 2011), and sedimentary rocks (Woodhouse, E, written comm., 2012).

This dataset defines three main fields (Fig. 6). Field 1 records Archean detritus from 3400–2400 Ma sources with initial $^{176}\text{Hf}/^{177}\text{Hf}$ isotopic values that lie on CHUR. A distinct mantle extraction event at 2800–2600 Ma is recorded by data within this field with initial $^{176}\text{Hf}/^{177}\text{Hf}$ values between 0.280779 and 0.281256 ($\epsilon\text{Hf}(t) \leq +7$). Field 2 encompasses 1800–1200 Ma detrital zircons derived from isotopically evolved sources, with initial $^{176}\text{Hf}/^{177}\text{Hf}$ values mostly between 0.281050 and 0.281491 ($\epsilon\text{Hf}(t)$ about -13) and model ages clustering around 3200 Ma. The Hf-evolution pattern defined by this field is consistent with crustal reworking of Archean material (Field 1) during Proterozoic events. Field 3 encompasses data from juvenile sources with 1800–1000 Ma crystallization ages. Field 3 data lie along an apparent reworking trend from a dominant 1950–1900 Ma mantle extraction event or an event reflecting 1800–1900 Ma isotopic homogenization. It is significant that the time at which reworking of Archean material commences (Field 2) closely corresponds to the hypothesized 1950–1900 Ma juvenile crust-forming event defined by Field 3. This correspondence increases confidence that this hypothesized event is real and indicates a coupling between lower and upper crustal processes.

Minor dispersion of data between Fields 2 and 3 (Fig. 6) is consistent with variable mixing of evolved unradiogenic crust and juvenile mantle-derived material during all Mesoproterozoic magmatic events. However, the lack of a more continuous spread of data between the older components of Fields 2 and 3 suggests that the 1950–1900 Ma array does not reflect systematic mixing between Field 2 and a juvenile component between 1900 and 1800 Ma to consistently yield 1950–1900 Ma model ages. Such a source would require remarkably efficient isotopic homogenization of consistently precise proportions of components throughout the entire basement of the Musgrave Province. Accordingly, we prefer to interpret the 1950–1900 Ma array as reflecting a single homogeneous source that separated from the mantle at that stage.

Whole-rock Sm–Nd isotopic record of the Musgrave Province: support for c. 1900 Ma crust formation

A first-order coherency between Hf and Nd isotopes has been widely recognized in terrestrial datasets, reflecting the similar fractionation of Lu–Hf and Sm–Nd in the crust and mantle (Bouvier et al., 2008; van De Flierdt et al., 2007). None of the minerals that account for substantial fractionation of Sm–Nd and Lu–Hf (e.g. garnet) achieves extensive Hf–Nd decoupling on a crustal scale within the terrestrial system. This has been interpreted as evidence of an efficient mixing process on a dynamic Earth (Bouvier et al., 2008). The coherent trend between Sm–Nd and Lu–Hf, where $\text{Hf} = 1.36 \times \text{Nd} + 2.95$, is referred to as the terrestrial array (Fig. 12). A robust regression of whole-rock ϵNd versus each individual zircon ϵHf value for magmatic rocks and sedimentary rocks within the west Musgrave Province defines a similar trend to the

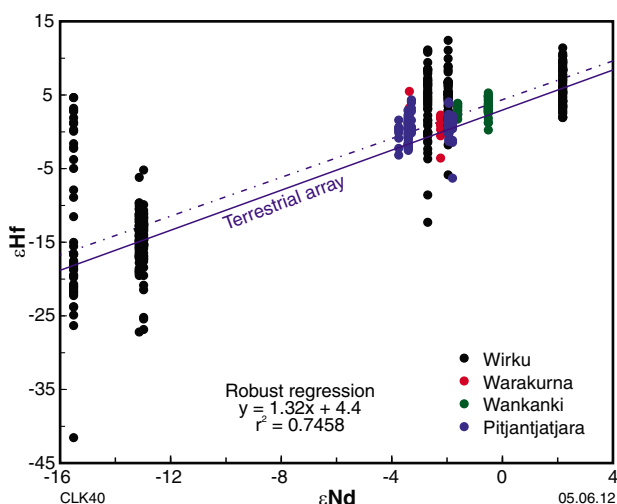


Figure 12. Whole-rock ϵNd vs zircon ϵHf for samples from the west Musgrave Province. The dashed line through the data indicates a robust regression (York, 1966). Greater variability is evident in data for metasedimentary rocks of the Wirku Metamorphics compared to those for magmatic supersuites.

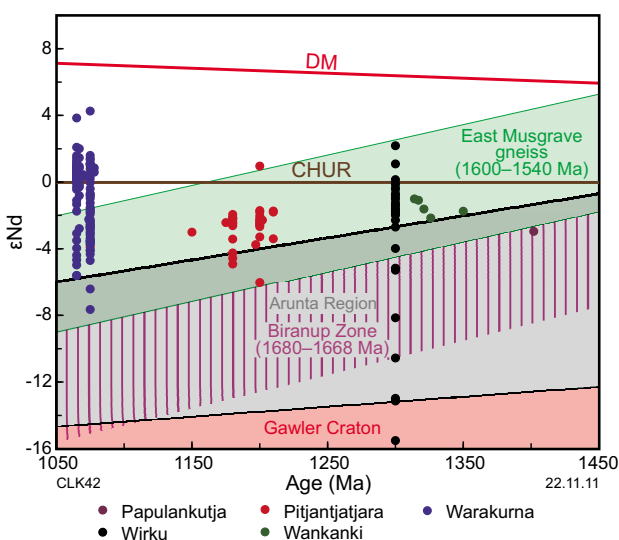


Figure 13. Nd-evolution plot for whole-rock samples from the west Musgrave Province. Values for the Wirku Metamorphics are calculated at 1300 Ma. Potential source regions are from Wade et al. (2006, 2008), Foden et al. (1995), Sun et al. (1995), Zhao and McCulloch (1995), Spaggiari et al. (2009), Kirkland et al. (2011a), and Close et al. (2003). The field for the Biranup Zone is indicated by vertical stripes. DM indicates depleted mantle. CHUR indicates chondritic uniform reservoir.

terrestrial array. This implies no decoupling of the Nd and Hf systems in these rocks and therefore that the magmas from which the zircons crystallized developed outside the garnet-stability field. Thus, the Nd-isotopic evolution trend for magmatic rocks closely matches that for Hf-isotopic values from zircons within those rocks. Generally most Nd-isotopic analyses lie between CHUR and $\epsilon\text{Nd} -4$, although greater variance is noted in Warakurna Supersuite samples, which yield values as radiogenic as $\epsilon\text{Nd} +4$ (Fig. 13). The Wirku Metamorphics display the largest variance and dispersion towards evolved values as low as $\epsilon\text{Nd} -16$, consistent with the incorporation of unradiogenic Archean material, as is also indicated by the presence of Archean detrital zircons in these rocks (Fig. 6; Howard et al., 2011a; Kirkland et al., 2009a; Kirkland et al., 2009b).

Nd isotopes are commonly used to calculate ‘crust-formation’ ages, which refer to the time at which magma was extracted from the mantle (DePaolo, 1988). The key assumption of these model ages is that the ratio of the parent-to-child isotope (Lu–Hf and Sm–Nd) changes during generation of new crust, and subsequently is not fractionated further by remelting, erosion, and sedimentation within the continental crust. Nd isotopic data for the west Musgrave Province were compiled from GSWA datasets. All samples have their formation ages determined either directly by U–Pb zircon geochronology or inferred from geological observations. All Nd isotopic data (Table 4) indicate depleted-mantle Sm–Nd model ages (calculated assuming linear isotopic growth for a depleted mantle reservoir) that range from $\epsilon\text{Nd}(t) = 0$ at 4.55 Ga to $\epsilon\text{Nd}(0) = +10$ ($^{143}\text{Nd}/^{144}\text{Nd} = 0.513163$) at the present day, with $^{147}\text{Sm}/^{144}\text{Nd} = 0.2136$.

In a situation analogous to that of Hf model ages, rocks derived from mixed sources extracted from the mantle at different times will yield Nd model ages that reflect only a minimum age of extraction for the oldest component and maximum age of extraction for the youngest component. Furthermore, the assumption that a Sm–Nd model age represents the time of mantle extraction is only valid if no Sm–Nd fractionation has taken place since the first separation of its protolith from the mantle source. The relatively uniform Sm–Nd ratios observed in most crustal rocks have been inferred to suggest that no significant Sm–Nd fractionation has occurred during most crustal melting and sedimentary processes on Earth (Vervoort et al., 2000). However, there are exceptions in highly evolved melts and most material in the Musgrave Province indicates fractionated Sm/Nd ratios outside normal crustal values. To circumvent this problem, two-stage depleted mantle Nd model ages (T_{DM}^2) are calculated on the assumption that the sources of all rocks follow the isotopic evolution of the average continental crust, regardless of their true lithological characteristics.

As with the Hf model ages, a mantle-extraction event is inferred by Nd isotopes at 1950–1900 Ma in rocks of the Papulankutja, Wankanki, and Pitjantjatjara Supersuites and also in the Wirku Metamorphics (Fig. 9). The Warakurna Supersuite displays a slightly younger Nd model-age mode at 1700 Ma, although there is also a secondary Nd model-age peak at 1950–1900 Ma. As with the Hf isotopic evolution of zircons, it is important to evaluate the extent to which the whole-rock Nd system might reflect a mixture as opposed to an actual 1950–1900 Ma

mantle-extraction event (or at least the minimum age of source homogenization). We apply a similar trend-evaluation approach as used with the Hf dataset: each magmatic supersuite is evaluated individually and then all are evaluated collectively. As with the Hf dataset, no statistically meaningful trend ($r^2 \geq 0.65$ at $P \leq 0.05$; Bryhn and Dimberg, 2011) is defined. Therefore, we consider that the peak in Nd model-ages at 1950–1900 Ma does not reflect mixing of magma sources through time; it rather reflects a real mantle extraction event at 1950–1900 Ma.

Oxygen isotopes in zircons: evaluating the degree of crustal input into mantle magma sources

Analysis of oxygen isotopes in dated zircons can be used to trace both the evolution of crustal recycling and crust–mantle interaction (Valley et al., 2005). Zircon crystals diffuse oxygen slowly, even under high-temperature conditions; hence their measured $\delta^{18}\text{O}_{\text{VSMOW}}$ values approximate the crystallization values provided that no late alteration has occurred (Peck et al., 2001). Incorporation of high $\delta^{18}\text{O}$ material (e.g. rocks or minerals altered by low-temperature near-surface processes) will increase the $\delta^{18}\text{O}$ value of a melt, so that zircons crystallized from such melts will also have elevated $\delta^{18}\text{O}$ values. Zircons in equilibrium with mantle-derived melts have $\delta^{18}\text{O}_{\text{VSMOW}}$ values of approximately $5.3 \pm 0.6\text{‰}$ (two standard deviations of the mean, 2σ ; Valley, 2003). A $\delta^{18}\text{O}$ value greater than about 6.3–6.5‰ is commonly taken as indicating incorporation of an elevated $\delta^{18}\text{O}$ component (Hawkesworth and Kemp, 2006a; Kemp et al., 2007; Valley, 2003; Valley et al., 1994). We use oxygen isotopes as a tool to identify zircons that crystallized from magmas that contained a contribution from near-surface rocks (those with $\delta^{18}\text{O}_{\text{SMOW}} > 6.3\text{‰}$), because these are likely

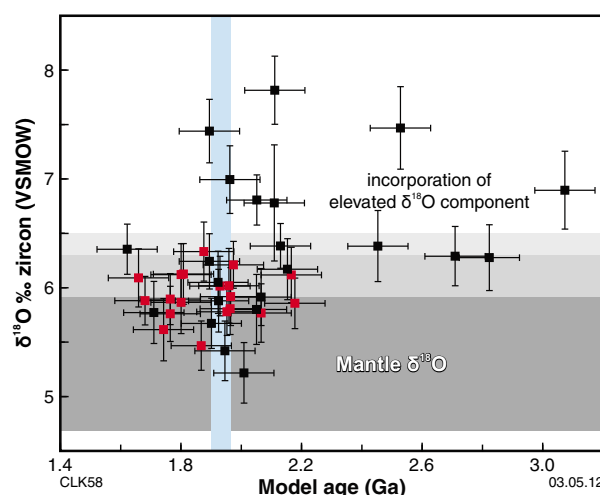


Figure 14. Zircon $\delta^{18}\text{O}_{\text{VSMOW}}$ against Hf crustal model age (Ga) from the same zircon grains. Blue vertical bar indicates the timing of hypothesized crust-formation event. Grey horizontal bars indicate values for zircons with minimal (<6.3‰) and no influence of crustal material. Note divergence to heavy oxygen values for model ages >1950 Ma. Red squares indicate data from sample GSWA 194764, black squares indicate data from sample GSWA 194765.

to yield mixed model ages that are unlikely to represent discrete crust-forming events (Fig. 14).

The pattern of $\delta^{18}\text{O}$ values from two Papulankutja gneisses implies that melts at 1950–1900 Ma were not contaminated by near-surface material. Zircons with the oldest model ages typically have the most elevated $\delta^{18}\text{O}$ components, consistent with incorporation of unradiogenic sedimentary material into those magmas. Zircons with model ages of c. 1950–1900 Ma indicate a range of $\delta^{18}\text{O}$ values, from 7.5 to 5.0‰, with a substantial component indicating $\delta^{18}\text{O}$ values <6.3‰ (Table 5). There are even many zircons within uncertainty of mantle values, implying derivation from source rocks with variable contamination, including a substantial fraction of source rocks with negligible or no sedimentary contamination, consistent with these model ages reflecting crust generation.

Masking of juvenile Hf input by high-field-strength element (HFSE) magma enrichment

Processes of crustal recycling and juvenile addition to the crust can operate independently or together; however, identifying their relative influence is critical in evaluating the tectonic evolution of ancient terrains. Hf-isotope data, particularly in conjunction with Nd-isotope data, have proved a very powerful tool in this regard because magmatic processes can produce distinctive patterns of isotopic change that track changes in source composition (Be'eri-Shlevin et al., 2010).

For the west Musgrave Province, a first-order conclusion that can readily be drawn from the Hf- and Nd-isotope data is that a regionally isotopically homogeneous and juvenile source developed in the middle to lower crust between 1950 and 1900 Ma. This source strongly controlled isotope evolution trends for c. 800 Ma thereafter, through at least four subsequent orogenic events. Thus, although this region is likely to represent Australia's most isotopically juvenile Proterozoic terrain, the granites produced throughout this c. 800 Ma period appear to reflect crustal recycling. This is consistent with the evidence that the tectonic evolution of the region, at least after (although possibly also including) the Mount West Orogeny, was intracontinental (Evins et al., 2010; Smithies et al., 2011; Wade et al., 2006; Wade et al., 2008). However, this is inconsistent with a range of geological data that point to a very large mantle input — particularly after the Mount West Orogeny.

For example, Smithies et al. (2011) suggest that the source of the Pitjantjatjara Supersuite, which was emplaced continuously throughout the c. 1220 and 1150 Ma Musgrave Orogeny, was dominated by new mantle additions. Intrusion of these voluminous, high-temperature (approximately >900°C), anhydrous granites into the middle crust, over an area of >15 000 km², was associated with UHT metamorphism that persisted for a similar period (Smithies et al., 2011; Smithies et al., 2010). Even in regions little affected by advective heat from granite intrusion, metamorphic temperatures

exceeded 1000°C (at 7–8 kbar; Kelsey et al., 2009; King, 2008). The granites show no geochemical evidence for residual garnet, which limits pressures during melting to approximately <10 kbar, and constrains the crustal column separating the source from the emplacement level to 7–10 km. However, metamorphic temperatures at the level of intrusion are already at the limit of those attainable in the lower crust through conduction of mantle heat alone — even assuming total removal of the lithospheric mantle (Brown, 2008). This further limits the amount of crust (i.e. potential granite source material) that was sustainable below the level of granite emplacement, almost certainly to significantly less than 7 km. However, throughout large parts of the Musgrave Province, the Pitjantjatjara Supersuite forms a sheet up to 5 km thick. To derive this granite volume entirely through melting of crust, particularly from the mafic to intermediate bulk source composition required to produce the least evolved granites (<60 wt% SiO₂), would likely require a crustal column >20 km thick (assuming approximately 20% partial melting producing a 5-km-thick regional granite sheet). Moreover, the melting temperatures (>900°C) determined for the granites would need to have been achieved throughout that column. Accordingly, Smithies et al. (2011) suggested that the granites were extracted from lower-crustal crystal-mush (melting, assimilation, storage, and homogenization or MASH) chambers. Based on mixing calculations using Nd-isotopic data, it was estimated that the granites incorporated at least 50% mantle material (Smithies et al., 2011).

An even greater juvenile addition to the crust occurred during the c. 1085 to 1040 Ma Giles Event, when mafic to felsic magmas were intruded and extruded. In the west Musgrave Province alone, these included a layered-mafic intrusion (including local ultramafic cumulates) estimated to have originally been up to 10 km thick, >170 km long, and about 60 km wide (Howard et al., 2011b); an extensive series of massive gabbro bodies and granite intrusions; and a succession of bimodal volcanic rocks with a minimum preserved extent of 3500 km². In nearly all cases, the felsic magmas of the Warakurna Supersuite have strongly ferroan, alkali-calcic compositions and represent tholeiitic lines of descent — either fractionated from contemporaneous mafic magmas or partially melted from a nearly contemporaneous mafic intraplate (Howard et al., 2011a).

Therefore, although formation of both the Pitjantjatjara and Warakurna Supersuites clearly involved a component of recycled crust, these supersuites also represent enormous mantle contributions to the intracontinental Mesoproterozoic crust of central Australia (Smithies et al., 2011). The Warakurna Supersuite yields high initial ¹⁷⁶Hf/¹⁷⁷Hf and ¹⁴³Nd/¹⁴⁴Nd values that could be interpreted as reflecting renewed juvenile input, although the data do not require that interpretation and are entirely consistent with an apparent crustal reworking trend. In the case of the Pitjantjatjara Supersuite, zircon Hf and whole-rock Nd isotopes show no clear indication of any juvenile input at all. Therefore, first-order interpretations of isotopic data for the west Musgrave Province do not appear to be consistent with the geological evolution of this region.

Two main factors cause the Hf- and Nd-isotopic systematics of rocks in the west Musgrave Province to be insensitive to renewed juvenile crustal contributions through time. First is the highly juvenile initial isotopic composition of the 1950–1900 Ma source to the west Musgrave crust, with bulk crustal compositions remaining relatively close to depleted-mantle compositions for at least the first few 100 Ma of crustal evolution. The second factor is perhaps more widely relevant to intracontinental orogenic events in general, and in particular to central Australian Proterozoic terrains, and is related to the effects of high-temperature crustal recycling on HFSE budgets.

Both the Musgrave Orogeny and the Giles Event involved high-temperature (ultrahigh in the case of the Musgrave Orogeny at least) melting, or remelting, of dry crustal material (Smithies et al., 2011; Smithies et al., 2010). Under such conditions, the resulting felsic melts are typically anhydrous (although often F-rich), ferroan, alkali-calcic to alkaline magmas. These show very strong enrichment in incompatible trace elements such as Th, U, REE, and HFSE, previously concentrated in accessory minerals (zircon, apatite, titanite, etc.) that remained in the crustal source throughout earlier periods of high-grade metamorphism, including dehydration melting to produce earlier calc-alkaline magmas (e.g. Wankanki Supersuite). However, most important from the perspective of Hf- and Nd-isotopic systematics in the rocks of the west Musgrave Province is a comparison of average compositions of successive supersuites — from the Wankanki to Pitjantjatjara and then Warakurna — that shows that this intracontinental reworking clearly established a significant HFSE-enrichment trend (a HFSE-enriched intracontinental province). In any instance where these extreme HFSE-enriched crustal magmas interact (e.g. mixing, assimilation) with mantle-derived magmas they clearly have the capacity to overwhelmingly dominate the Hf and Nd budget, and thus the isotopic composition. Because the bulk isotopic composition of the west Musgrave Province basement, and also the HFSE-enriched crustal magmas, are themselves relatively juvenile, the capacity to mask the similarly radiogenic isotopic contributions from mantle-derived magmatism is enhanced yet further.

Simple mixing calculations (Langmuir et al., 1978) illustrate this point (Fig. 15). Model mixtures based on bulk assimilation of average Pitjantjatjara Supersuite (crust) into mid-ocean ridge basalt (MORB)-like magmas indicate that >50% MORB contribution is required before the isotopic composition of the hybrid varies by more than one ϵHf unit from the crustal component. Such a scenario is perhaps relevant to the formation of the Warakurna Supersuite, in which mantle-derived magmas intrude crust dominated by rocks of the Pitjantjatjara Supersuite. If we consider that mixing involves partial melts of the (Pitjantjatjara) crustal component (rather than simple bulk assimilation), then the proportion of MORB required to change the ‘crustal’ isotopic signature is then increased even further.

The Pitjantjatjara Supersuite was modelled as a homogenized mix (MASH) of crustal material (an average Wirku Metamorphics metasediment composition) and

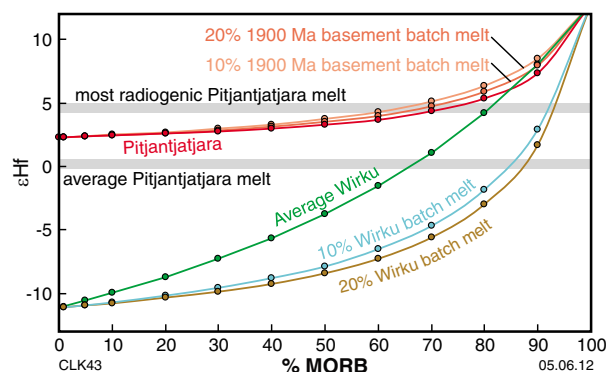


Figure 15. Mixture-modelling of batch melts and bulk melting between Musgrave lithologies and average mid-ocean ridge basalt (MORB). The figure indicates that large amounts of MORB can be accommodated in high-field-strength (HFSE)-enriched magmas prior to ϵHf signatures being deflected towards more juvenile values.

MORB-like mantle melt (Smithies et al., 2011). If the crustal component in this model was an approximately 20% partial melt (rather than bulk assimilation), then the Hf-isotopic data indicate that the bulk source must have incorporated approximately 85% MORB to achieve the isotopic composition of the average Pitjantjatjara Supersuite (Fig. 15). The calculated 15% crustal material is a minimum estimate because it assumes an already moderately unradiogenic crustal source component. A more realistic regional basement crustal component is the 1950–1900 Ma juvenile crust identified in this study. Assuming that Hf concentrations in this component are broadly similar to the average for the Wirku Metamorphics and that a 20% partial melt is assimilated, 70% MORB would be required to account for the most juvenile zircon Hf values in the Pitjantjatjara Supersuite. Additional contamination by unradiogenic Archean material only increases the required proportion of mantle component.

For this reason, realistic estimates of the proportion of juvenile mantle that contributed to the Pitjantjatjara Supersuite and to the felsic units of the Warakurna Supersuite are in the order of 70–85%. This contribution is largely hidden within the Hf- and Nd-isotopic data. In provinces that show significant HFSE-enrichment trends it is possible that the true amount of juvenile crustal growth is often greatly underestimated. Such provinces are typically regions of intracontinental extension, although they possibly also include far-field continental back-arc settings like those that Giles et al. (2002) suggested characterized Paleoproterozoic Australia.

Isotopic constraints on the geological architecture of Proterozoic Australia

Models for the evolution of late Archean to early Mesoproterozoic Australian crust were initially dominated

by intracontinental processes and the assumption of a single cratonic mass (Etheridge et al., 1987; Gee, 1979; Oliver et al., 1991; Rutland, 1973; Wyborn et al., 1988). Crust formation was envisaged by vertical accretion, involving underplating, and by extensional tectonism, driven through mantle plumes.

More recent studies from the Arunta region, Capricorn Orogen, Musgrave Province, and the Albany–Fraser Orogen have recognized either accreted fragments or extensional back-arcs linked to convergent plate margin processes (Cawood and Tyler, 2004; Kirkland et al., 2011a; Korsch et al., 2011; Scrimgeour and Close, 1999; Zhao and Bennett, 1995; Zhao and McCulloch, 1995). Within this accretionary and collisional tectonic framework, existing models for the amalgamation of the North and South Australian Cratons suggest that the early evolution (Stage I) of the Albany–Fraser Orogeny coincided with the Mount West Orogeny in the Musgrave Province and that this reflects the collision of the two cratonic masses during the assembly of Rodinia at c. 1300–1100 Ma (Betts and Giles, 2006; Clark et al., 2000; Giles et al., 2004; Myers et al., 1996). Alternatively, amalgamation of the two cratons has been proposed much earlier at c. 1730 Ma (Şener et al., 2005) or between 1800 and 1500 Ma (Giles et al., 2004).

A comparison of the Hf-isotope data from the Musgrave Province with data from other southern and central Australian terrains places several constraints on the Proterozoic tectonic evolution of Australia.

Comparison with the Albany–Fraser Orogen

Several geological events in the Musgrave Province and Albany–Fraser Orogen appear to be synchronous after c. 1400 Ma. For example, the 1345–1293 Ma Mount West Orogeny was coeval with Stage I of the Albany–Fraser Orogeny and the 1220–1150 Ma intracontinental Musgrave Orogeny was coeval with Stage II of the Albany–Fraser Orogeny (Kirkland et al., 2011a; Spaggiari et al., 2009; Wade et al., 2008; White et al., 1999) (Fig. 16). However, the crustal evolution of these two regions prior to 1400 Ma is distinctly different (Fig. 17). Hafnium isotopic evolution trends between c. 1900 and 1400 Ma contrast apparent crustal reworking for the Musgrave Province with progressive juvenile input into unradiogenic Archean crust in the Albany–Fraser Orogen. The Hf-isotopic data also indicate that the crust forming the Musgrave Province and the Albany–Fraser Orogen was distinctly different in composition and likely evolved under different tectonic regimes. The Albany–Fraser Orogen has a strong connection to the Yilgarn Craton through both the Hf-isotopic signature of Proterozoic magmas, the presence of isolated Archean tectonic fragments within new Proterozoic crust, and the Proterozoic reworking of Archean lithologies on the margin (Kirkland et al., 2011a; Spaggiari et al., 2011). No such relationship is clear for the Musgrave Province, which instead appears to be dominated by reworking of c. 1950–1900 Ma juvenile crust, with punctuated voluminous input of additional juvenile material. Archean

material is also observed within the Musgrave Province (i.e. Archean zircons) and it also formed a minor crustal component at all stages. This implies that if Archean crust does not actually form a minor basement component to the Musgrave Province, then the province was not far removed from Archean crust.

Comparison with the Arunta Orogen

The Proterozoic Arunta Orogen lies along the southern margin of the North Australian Craton (Black and Shaw, 1995; Collins and Shaw, 1995; Cross et al., 2005; Scrimgeour, 2006). It has been divided into a southern exotic terrane, referred to as the Warumpi Province, and the autochthonous Aileron Province (Scrimgeour, 2006). The Warumpi Province records two Paleoproterozoic magmatic events: high-K calc-alkaline magmatism during the 1690–1670 Ma Argilke Igneous Event, and magmatism associated with a 1640–1635 Ma accretion event known as the Liebig Orogeny (Scrimgeour, 2006; Scrimgeour et al., 2005) (Fig. 16). The Argilke Event is believed to correspond to the formation of a magmatic arc outboard of the North Australian Craton (Close et al., 2006; Scrimgeour et al., 2005).

Felsic and mafic gneisses from the eastern Musgrave Province have subduction-like geochemical signatures and juvenile Nd-isotopic compositions and have been interpreted as the remnants of a 1600–1540 Ma magmatic arc, suggested to have formed along the southern edge of the Warumpi Province (Wade et al., 2006; Wade et al., 2008). This arc is a fundamental component of models for the Proterozoic evolution of Australia and has been inferred as the source for younger intracontinental magmatic suites of the Musgrave Province. Data presented here also indicate that juvenile material of that age range contributed to the bulk crust of the Musgrave Province. However, the bulk source for all magmas in the west Musgrave Province was considerably more radiogenic than the source of Warumpi Province magmas (Kirkland et al., 2009c; 2009d; Kirkland et al., 2009e, and <<http://www.dmp.wa.gov.au/geochron>>) (Fig. 17). This indicates that neither the Warumpi Province itself, nor a significant component from it, forms basement to the Musgrave Province. Furthermore, the Warumpi Province Hf-isotope dataset indicates that the bulk source to the Ininti Granite in the western Arunta Orogen included an unradiogenic Archean component that was similar to magmatic sources from which the western Aileron Province evolved (Kirkland et al., 2009f). This perhaps signifies that the Warumpi Province has some original proximity to the western Aileron Province during the Argilke Event.

Comparison with the Gawler Craton

The Gawler Craton occupies a large portion of central South Australia and preserves a record of Neoproterozoic to Mesoproterozoic crustal evolution. Early Mesoproterozoic (c. 3150), Latest Archean (2560–2500 Ma) and Paleoproterozoic (2000–1850 Ma) units make up the basement, which is intruded and overlain by late Paleoproterozoic (1750–1600 Ma) to early Mesoproterozoic (1600–1550 Ma) rocks (Daly et al., 1998; Fraser et al.,

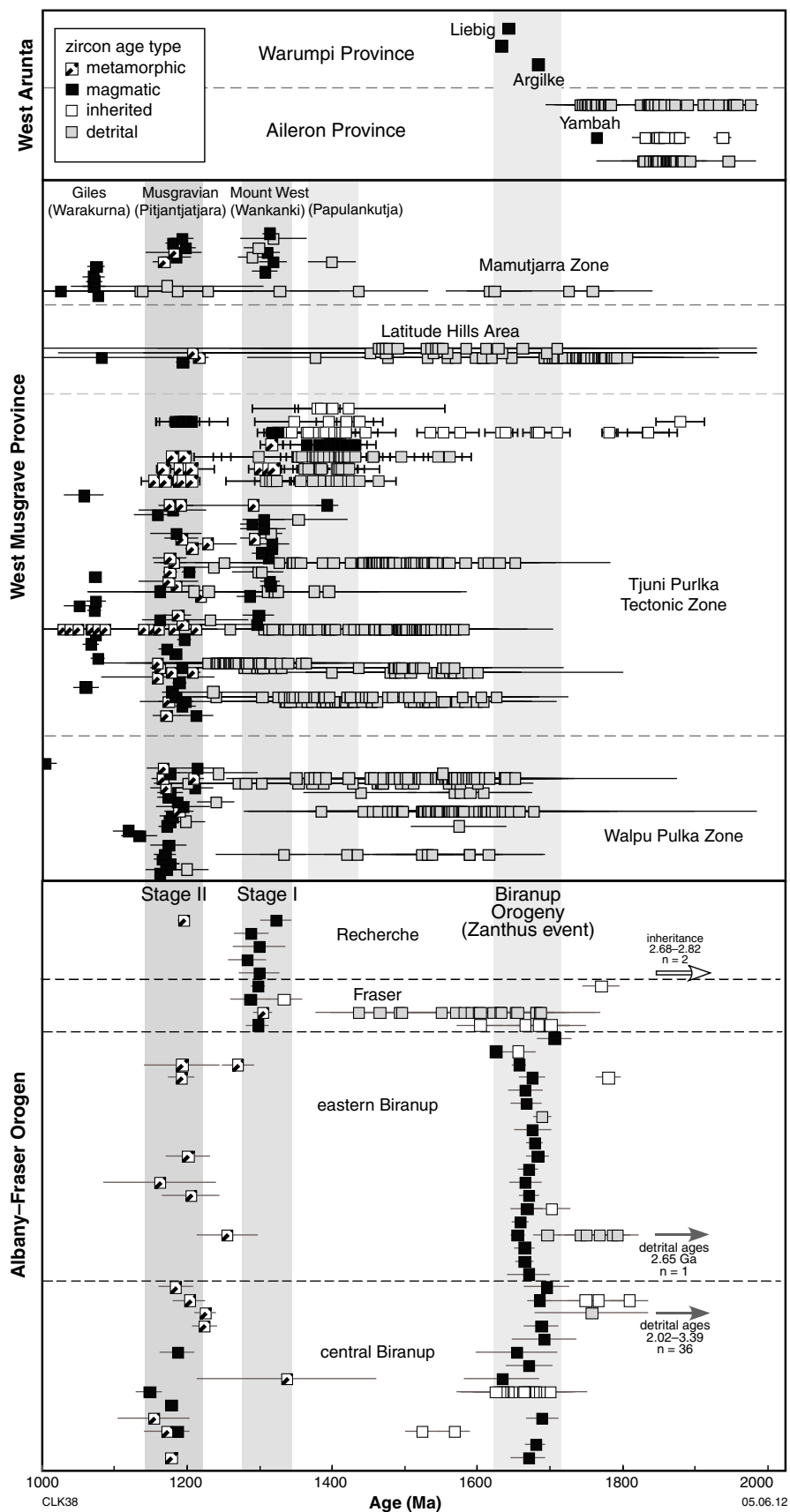


Figure 16. Time-space diagram for the west Musgrave Province, Albany-Fraser Orogen, and west Arunta Orogen (modified from Kirkland et al., 2011a). The diagram includes ion microprobe (SHRIMP) U-Pb zircon and baddeleyite ages determined by GSWA within each region. All data available from <<http://www.dmp.wa.gov.au/geochron>>.

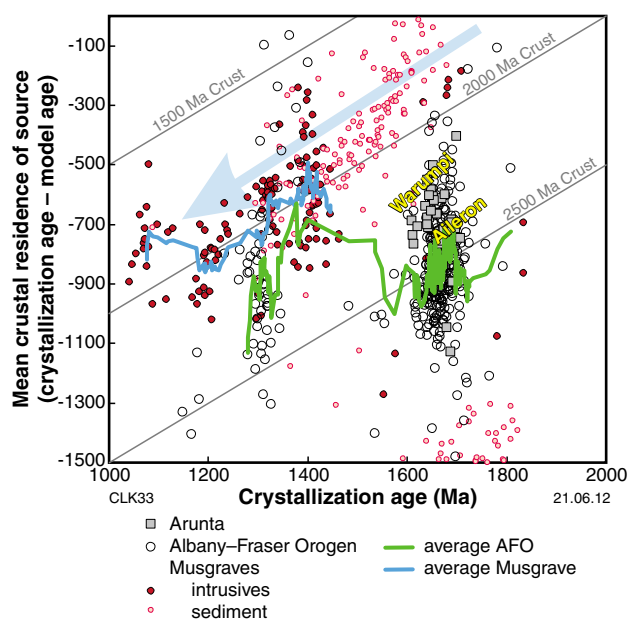


Figure 17. Event signature diagram showing the general trend of reworking (downwards), mixing (horizontal), or juvenile input (upwards). Note the indication of mantle extraction at 1950–1900 Ma in the Musgrave Province, which is dissimilar to events in the Albany–Fraser Orogen (AFO) and the Warumpi Province of the west Arunta Orogen. Blue curve indicates the best-fit average of west Musgrave Hf in zircons from magmatic supracrusts; green curve indicates the best-fit average of Hf isotopes in zircons from the AFO; blue arrow indicates predominant 1900 Ma crustal reworking.

2010; Howard et al., 2011c; Howard et al., 2011d; Howard et al., 2011e). Along the northern margin of the Gawler Craton, 1780–1730 Ma paragneisses have Hf isotopic values similar to packages in the Arunta Region (Hollis et al., 2010) and reflect reworking of a 2600–2200 Ma source (Armit et al., 2010). However, a small component of 1550–1500 Ma zircons indicates a juvenile 2000–1800 Ma source (Armit et al., 2010), similar to the dominant component identified in the Musgrave Province. Although this could indicate a link between the northern Gawler Craton and the Musgrave Province, data for the Gawler Craton come from sediments that may have been transported significant distances. Nonetheless, some degree of proximity between the northern Gawler Craton and the Musgrave Province is indicated prior to at least the late Mesoproterozoic.

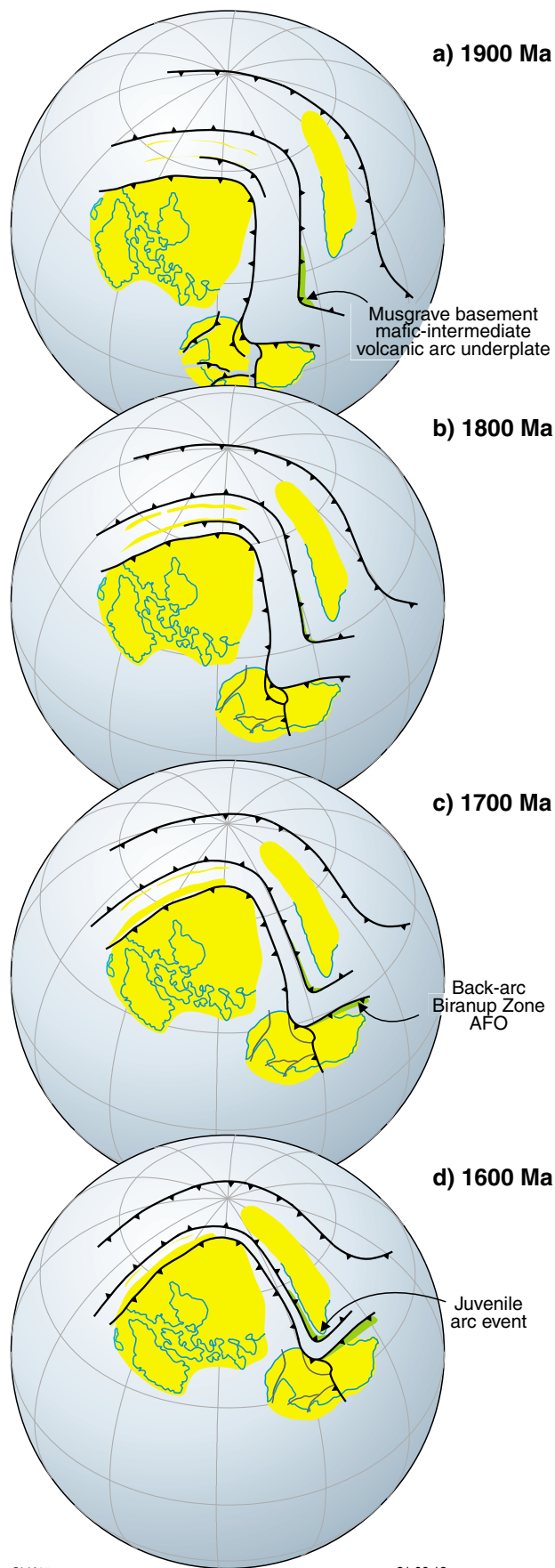
The Proterozoic development of the Musgrave Province

Whereas the tectonic evolution of Proterozoic Australia is presently described in terms of modern plate tectonic processes of subduction and arc accretion (Cawood and Korsch, 2008), earlier models stressed intracontinental processes involving asthenosphere-driven vertical

accretion (Etheridge et al., 1987). However, there appears to be nothing in the isotopic datasets presented here, or in the geological or geochemical data presented elsewhere (Betts and Giles, 2006; Giles et al., 2004; Smithies et al., 2011), that uniquely identifies either of these two types of processes for the Musgrave Province. In this respect, the region is similar to other Australian Proterozoic belts that show a ‘diffuse’ tectonic style in which the role of plate-boundary forcing is obscured (Giles et al., 2002). McLaren et al. (2005) relate this to the extraordinarily elevated thermal regimes that characterized much of Proterozoic Australia. Certainly, between c. 1300 and 1040 Ma, evolution of the west Musgrave Province involved low-pressure and high- to ultrahigh-temperature metamorphism, crustal melting, and voluminous juvenile mantle input in what appears to have been essentially an extensional intracontinental environment (Evins et al., 2010; Smithies et al., 2011) or, conceivably, some form of far-field continental back-arc setting (Giles et al., 2002). A large proportion of the heat responsible for these processes was advected mantle heat (i.e. underplating and intraplate during the Musgrave Orogeny and Giles Event; Smithies et al., 2011; Smithies et al., 2010). Heat-producing elements (U, Th, K) were also redistributed to upper crustal levels such that, following the Giles Event, tectonic styles were high-pressure and low- to moderate-temperature.

In terms of placing constraints on the early crustal evolution of the Musgrave Province, and of Proterozoic central Australia in general, the following observations are critically important. A major mantle extraction event at 1950–1900 Ma formed the mafic to intermediate lower crust that became the dominant basement component to the Musgrave Province. Neither this juvenile crust, nor the subsequent 1650–1550 Ma juvenile component also identified in the basement to the Musgrave Province, provide any evidence of a direct tectonic link between the province and currently proximal Proterozoic terrains to the north (Arunta, and specifically the Warumpi Province) and southwest (Albany–Fraser Orogen) prior to c. 1400 Ma. Archean material formed a minor crustal component at all stages during the evolution of the Musgrave Province, and significant reworking of the Archean source of this material was near-synchronous with formation of the 1950–1900 Ma mafic to intermediate basement to the Musgrave Province.

Collectively, these observations support a model in which the formation of 1950–1900 Ma juvenile mafic to intermediate crust was isolated from processes occurring along the southern margin of the North Australian Craton, but which operated in proximity to Archean crust, possibly the Gawler Craton to the south (Fig. 18). Because zircons resulting from remelting of this mafic to intermediate crust retain mantle $\delta^{18}\text{O}$ values, the 1950–1900 Ma crust is likely to comprise intrusive, rather than volcanic, rocks. We suggest that it represents a regional underplate related to subduction along the northern margin of the Gawler Craton. Reworking of Archean crust also commenced at this stage, and it continued for 300–400 Ma. On that basis, it might be argued that a long-lived active margin environment is more likely, although the younger, 1220 to <1040 Ma, evolution of the Musgrave Province itself



shows that prolonged apparent crustal reworking can also occur within an intracontinental environment.

A small amount of juvenile material was again added to the Musgrave Province basement between 1650 and 1550 Ma. Although this is consistent with the putative record of 1600–1500 Ma subduction along the northern margin of the Musgrave Province (Wade et al., 2008), it is not directly related to formation of the Warumpi Province of the Arunta Orogen further to the north. One possibility is that these two regions formed on either side of a closing ocean (Fig. 18).

The origins of the Papulankutja and Wankanki Supersuites are also not clear. Whereas their calc-alkaline chemistry is similar to that of continental arc rocks, their model ages indicate 500–600 Ma of crustal history. Whether or not either of these supersuites (rather than their sources) was subduction-related, their isotopic compositions are overwhelmingly dominated by the 1950–1900 Ma juvenile mafic to intermediate basement of the Musgrave Province. Episodic additions of isotopically evolved material are recognized in the modern American Cordilleran Orogenic System, where continental lower crust is thrust beneath the arc, resulting in episodic magmatism dominated by recycled crust (DeCelles et al., 2009). At the same time that the Wankanki Supersuite was formed, the lateral extension of the Musgrave Province basement, including an overlying Archean and reworked Archean component, was uplifted, eroded, and redeposited to form the protolith to the Wirku Metamorphics. It is likely that subduction processes leading to craton amalgamation were underway at c. 1400 Ma and continued until c. 1300 Ma, which represents the final accretion of a southern continental mass, including the Gawler Craton and the Musgrave Province basement, with the North Australian Craton.

Conclusions

The Papulankutja Supersuite of calc-alkaline granodiorite and monzogranite represents the c. 1400 Ma igneous basement rocks, which are significantly older than the Wankanki Supersuite of the 1345–1293 Ma Mount West Orogeny. A foliated 1402 ± 4 Ma monzogranite has its solid-state fabric crosscut by a 1318 ± 9 Ma granite dyke, indicating a deformation phase prior to or early in the

Figure 18. (left) Schematic continental reconstruction of Proterozoic Australia for the interval 1900–1600 Ma (modified from Betts et al., 2008). The possible position of a Musgrave volcanic-arc underplate is shown developing outboard of the Mawson Craton at c. 1900 Ma. The development of a back-arc (Biranup Zone) of the Albany–Fraser Orogen (AFO) is displayed developing at 1700–1600 Ma. The reconstruction generates Musgrave Province basement in an allochthonous position, isolated from the West Australian Craton and the North Australian Craton.

Mount West Orogeny. The Papulankutja Supersuite may represent subduction-related magmatism associated with the beginning of South Australian Craton impinging on the North Australian Craton.

Sm–Nd and Lu–Hf data imply an isotopically homogeneous juvenile source with a mafic to intermediate bulk composition, isolated from the mantle at 1950–1900 Ma. This bulk source effectively forms basement to the Musgrave Province and dominates the subsequent isotopic evolution of the province through apparent recycling events at c. 1400, 1345–1293, 1220–1150, and 1085–1040 Ma.

The absence of mixing arrays diverging from a 1950–1900 Ma source and the near-coeval initiation of Archean reworking implies a crust generation event at 1950–1900 Ma, consistent with $\delta^{18}\text{O}$ values of <6.3‰ in zircons that define this age component. This illustrates that, in certain tectonic environments, information on crust formation events may only be preserved in their isotopic legacy, because no juvenile crystals may have been preserved.

The 1950–1900 Ma Musgrave crust formation event is distinct from autochthonous processes recorded in the Albany–Fraser Orogen and from the crustal development of the Arunta region. Additional juvenile material formed at 1650–1550 Ma. It was locally mixed with either the 1950–1900 Ma component or with melts derived from that source to produce dispersion of data about the 1950–1900 Ma isotopic array. Unradiogenic Archean material is a locally available component that also mixed with magmas to produce dispersion towards unradiogenic values.

Although Hf- and Nd-isotope arrays for the Musgrave Province are clearly dominated by apparent recycling trends, a range of geological data requires significant mantle contributions associated with the Musgrave Orogeny and the Giles Event. This younger magmatic period coincides with marked changes in felsic magma composition from calc-alkaline to ferroan, alkali-calcic magmas, with extreme HFSE enrichment. This HFSE enrichment in crustal melts effectively subdues any renewed juvenile isotopic signature.

Crust formation is implied by strong linear evolution patterns pointing to juvenile addition at the same time as isotopically distinct reworking. Mantle-like oxygen isotope values in zircon crystals corroborate this finding. Oxygen isotopes, time-series analysis of model ages, and holistic interpretation of isotopic evolution patterns, are all able to address the well-known ambiguity of both Hf and Nd model ages where mixing of old and young material produces intermediate model ages that do not correspond to crust formation.

Although the Musgrave Province is an extreme case of a HFSE-enriched magmatic province, it is quite possible that considerable amounts of juvenile input into other intracontinental orogens have gone undetected in isotopic data. A corollary to this is that the amounts of juvenile crustal growth in intracontinental extensional settings may also have been underestimated.

References

- Aitken, A and Betts, P 2009, Constraints on the Proterozoic supercontinent cycle from the structural evolution of the south-central Musgrave Province, central Australia: *Precambrian Research*, v. 168, p. 284–300.
- Arculus, RJ 1999, Origins of the continental crust: *Journal and Proceedings of the Royal Society of New South Wales*, v. 132, p. 83–110.
- Armit, R, Betts, P and Schaefer, B 2010, Lu–Hf isotope characteristics of the marginal terranes of the northern Gawler Craton, in *GOMA (Gawler Craton–Officer Basin–Musgrave Province–Amadeus Basin) Seismic and MT Workshop 2010* edited by RJ Korsch and N Kositsin: Geoscience Australia, Record 2010/39, p. 118–127.
- Arndt, NT and Goldstein, SL 1987, Use and abuse of crust-formation ages: *Geology*, v. 15, p. 893–895.
- Be’eri-Shlevin, Y, Katzir, Y, Blichert-Toft, J, Kleinhanns, I and Whitehouse, M 2010, Nd–Sr–Hf–O isotope provinciality in the northernmost Arabian–Nubian Shield; implications for crustal evolution: *Contributions to Mineralogy and Petrology*, v. 160, p. 181–201.
- Betts, PG and Giles, D 2006, The 1800–1100 Ma tectonic evolution of Australia: *Precambrian Research*, v. 144, p. 92–125.
- Betts, PG, Giles, D and Schaefer, BF 2008, Comparing 1800–1600 Ma accretionary and basin processes in Australia and Laurentia: possible geographic connections in Columbia: *Precambrian Research*, v. 166, p. 81–92.
- Black, LP, Kamo, SL, Allen, CM, Davis, DW, Aleinikoff, JN, Valley, JW, Mundil, R, Campbell, IH, Korsch, RJ, Williams, IS and Foudoulis, C 2004, Improved Pb/U microprobe geochronology by the monitoring of a trace-element-related matrix effect; SHRIMP, ID-TIMS, ELA-ICP-MS and oxygen isotope documentation for a series of zircon standards: *Chemical Geology*, v. 205, p. 115–140.
- Black, LP and Shaw, RD 1995, An assessment, based on U–Pb zircon data, of Rb–Sr dating in the Arunta Inlier, central Australia: *Precambrian Research*, v. 71, p. 3–15.
- Blichert-Toft, J and Albarede, F 1997, The Lu–Hf isotope geochemistry of chondrites and the evolution of the mantle–crust system: *Earth and Planetary Science Letters*, v. 27, p. 243–258.
- Blichert-Toft, J and Albarede, F 2008, Hafnium isotopes in Jack Hills zircons and the formation of the Hadean crust: *Earth and Planetary Science Letters*, v. 265, p. 686–702.
- Bouvier, A, Vervoort, JD and Patchett, PJ 2008, The Lu–Hf and Sm–Nd isotopic composition of CHUR: Constraints from unequilibrated chondrites and implications for the bulk composition of terrestrial planets: *Earth And Planetary Science Letters*, v. 273, p. 48–57.
- Brown, M 2008, Characteristic thermal regimes of plate tectonics and their metamorphic imprint throughout Earth history: When did Earth first adopt a plate tectonics mode of behaviour? in *When did plate tectonics begin on planet Earth?* edited by K Condie and V Pease: Geological Society of America, Special Paper, v. 440, p. 97–128.
- Bryhn, AC and Dimberg, PH 2011, an operational definition of a statistically meaningful trend: *PLoS One*, v. 6, p. e19241.
- Camacho, A and Fanning, C 1995, Some isotopic constraints on the evolution of the granulite and upper amphibolite facies terranes in the eastern Musgrave Block, central Australia: *Precambrian Research*, v. 71, p. 155–183.
- Camacho, A, Hensen, B and Armstrong, R 2002, Isotopic test of a thermally driven intraplate orogenic model, Australia: *Geology (Boulder)*, v. 30, p. 887–890.
- Cawood, PA and Korsch, RJ 2008, Assembling Australia: Proterozoic building of a continent: *Precambrian Research*, v. 166, p. 1–35.

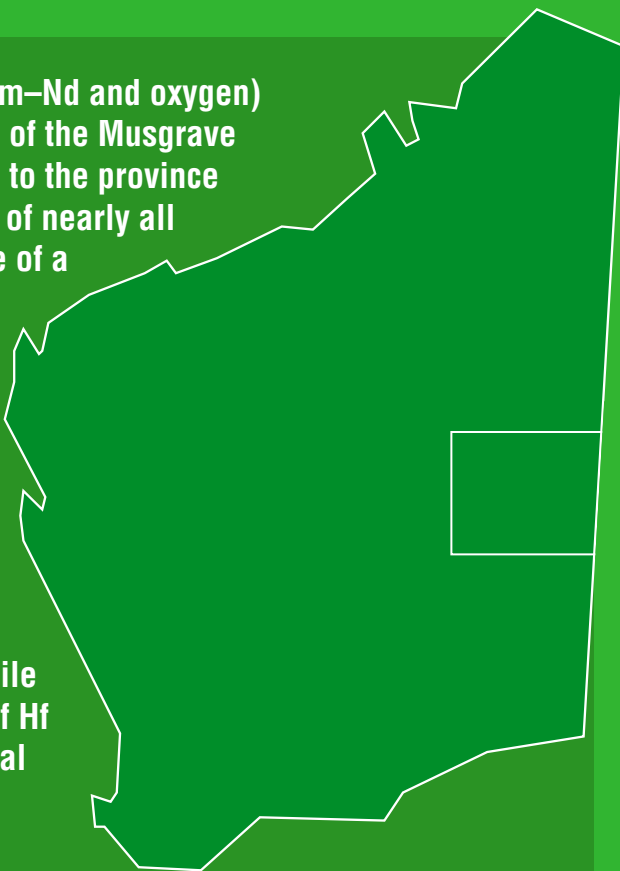
- Cawood, PA and Tyler, IM 2004, Assembling and reactivating the Proterozoic Capricorn Orogen: lithotectonic elements, orogenies, and significance: *Precambrian Research*, v. 128, p. 201–218.
- Chen, RX, Zheng, YF and Xie, LW 2010, Metamorphic growth and recrystallization of zircon: Distinction by simultaneous in-situ analyses of trace elements, U–Th–Pb and Lu–Hf isotopes in zircons from eclogite-facies rocks in the Sulu orogen: *Lithos*, v. 114, p. 132–154.
- Clark, DJ, Hensen, BJ and Kinny, PD 2000, Geochronological constraints for a two-stage history of the Albany–Fraser Orogen, Western Australia: *Precambrian Research*, v. 102, p. 155–183.
- Clarke, G and Powell, R 1991, Decompressional coronas and symplectites in granulites of the Musgrave Complex, central Australia: *Journal of Metamorphic Geology*, v. 9, p. 441–450.
- Close, D, Scrimgeour, I and Edgoose, C 2006, Evolution and mineral potential of the Palaeoproterozoic Warumpi Province, in *Evolution and metallogenesis of the North Australian Craton edited by P Lyons and DL Huston DL: Geoscience Australia Record 2006/16*, p. 9–10.
- Close, D, Scrimgeour, I, Edgoose, C, Cross, A, Claoue-Long, J, Kinny, P and Meixner, A 2003, Redefining the Warumpi Province: Annual GeoScience Exploration Seminar (AGES) 2003: Record of Abstracts, Northern Territory Geological Survey Record 2003-001.
- Collins, WJ, Belousova, EA, Kemp, AIS and Murphy, JB 2011, Two contrasting Phanerozoic orogenic systems revealed by hafnium isotope data: *Nature Geoscience*, v. 4, p. 333–337.
- Collins, WJ and Shaw, RD 1995, Geochronological constraints on orogenic events in the Arunta Inlier: a review: *Precambrian Research*, v. 71, p. 315–346.
- Condie, KC 1998, Episodic continental growth and supercontinents: A mantle avalanche connection?: *Earth and Planetary Science Letters*, v. 163, p. 97–108.
- Cross, A, Claoue-Long, JC, Scrimgeour, IR, Crispe, A and Donnellan, N 2005, Summary of results. Joint NTGS-GA geochronology project northern Arunta and Tanami Regions: Northern Territory Geological Survey Record 2005-003.
- Daly, SJ, Fanning, CM and Fairclough, MC 1998, Tectonic evolution and exploration potential of the Gawler Craton, South Australia: *AGSO Journal of Australian Geology and Geophysics*, v. 17, p. 145–168.
- Daniels, J 1974, The geology of the Blackstone region, Western Australia: Geological Survey of Western Australia, Bulletin, v. 123, 257 p.
- DeBievre, P and Taylor, P 1993, Table of the isotopic composition of the elements: *International Journal of Mass Spectrometry and Ion Processes*, v. 123, p. 149.
- DeCelles, PG, Ducea, MN, Kapp, P and Zandt, G 2009, Cyclicity in cordilleran orogenic systems: *Nature Geoscience*, v. 2, p. 251–257.
- DePaolo, DJ 1988, Neodymium Isotope Geochemistry An Introduction. Minerals and Rocks Series no. 20: Tokyo, Berlin, Heidelberg, New York, London, Paris, Springer-Verlag, 187p.
- Edgoose, C, Scrimgeour, I and Close, D 2004, Geology of the Musgrave Block, Northern Territory: Northern Territory Geological Survey, Report 15, 48p.
- Etheridge, MA, Rutland, RWR and Wyborn, LA 1987, Orogenesis and tectonic process in the early to middle Proterozoic of northern Australia, in *Proterozoic lithospheric evolution edited by A Kroner: American Geophysical Union, Washington, DC*, p. 131–147.
- Ernst, RE, Buchan, KL and Campbell, IH 2005, Frontiers in large igneous province research, in *Kerr, A, England, R and Wignall, P, Mantle plumes: physical processes, chemical signatures, biological effects: Lithos*, v. 79, p. 271–297.
- Evins, PM, Smithies, RH, Howard, HM, Kirkland, CL, Wingate, MTD and Bodorkos, S 2010, Devil in the detail: The 1150–1000 Ma magmatic and structural evolution of the Ngaanyatjarra Rift, west Musgrave Province, Central Australia: *Precambrian Research*, v. 183, p. 572–588.
- Evins, PM, Smithies, RH, Howard, HM and Maier, WD 2009, HOLT, WA Sheet 4546: Geological Survey of Western Australia, 1:100 000 Geological Series.
- Fishwick, S and Reading, A 2008, Anomalous lithosphere beneath the Proterozoic of western and central Australia; a record of continental collision and intraplate deformation?: *Precambrian Research*, v. 166, p. 111–121.
- Foden, J, Mawby, J, Kelley, S, Turner, S and Bruce, D 1995, Metamorphic events in the eastern Arunta Inlier. Part 2: Nd–Sr–Ar isotopic constraints, in *Time limits on tectonic events and crustal evolution using geochronology; some Australian examples edited by WJ Collins and RD Shaw: Precambrian Research, Elsevier, Amsterdam*, p. 207–227.
- Fraser, GL, and Neumann, NL 2010, New SHRIMP U–Pb zircon ages from the Gawler Craton and Curnamona Province, South Australia, 2008 – 2010: *Geoscience Australia, Record, 2010/16*, p. 256.
- Frost, B, Barnes, C, Collins, W, Arculus, R, Ellis, D and Frost, C 2001, A geochemical classification for granitic rocks: *Journal of Petrology*, v. 42, p. 2033–2048.
- Frost, B and Frost, C 2008, On charnockites: *Gondwana Research*, v. 13, p. 30–44.
- Gee, RD 1979, Structure and tectonic style of the Western Australian Shield: *Tectonophysics*, v. 58, p. 327–369.
- Giles, D, Betts, PG and Lister, GS 2002, Far-field continental backarc setting for the 1.80–1.67 Ga basins of northeastern Australia: *Geology*, v. 30, p. 823–826.
- Giles, D, Betts, P and Lister, G 2004, 1.8–1.5-Ga links between the North and South Australian cratons and the early-middle Proterozoic configuration of Australia: *Tectonophysics*, v. 380, p. 27–41.
- Glikson, A, Stewart, A, Ballhaus, G, Clarke, G, Feecken, E, Level, J, Sheraton, J and Sun, S-S 1996, Geology of the western Musgrave Block, central Australia, with reference to the mafic-ultramafic Giles Complex: Australian Geological Survey Organisation, Bulletin, v. 239, p. 135–143.
- Goldfarb, RJ, Groves, DI and Gardoll, S 2001, Orogenic gold and geologic time: A global synthesis: *Ore Geology Reviews*, v. 18, p. 1–75.
- Gray, C 1978, Geochronology of granulite-facies gneisses in the western Musgrave Block, central Australia: Geological Society of Australia, v. 25, p. 403–414.
- Gray, C and Compston, W 1978, A Rb–Sr chronology of the metamorphism and prehistory of central Australian granulites: *Geochimica et Cosmochimica Acta*, v. 42, p. 1735–1748.
- Gregory, C, Buick, I, Hermann, J and Rubatto, D 2009, Mineral-scale trace element and U–Th–Pb age constraints on metamorphism and melting during the Petermann Orogeny (central Australia): *Journal of Petrology*, v. 50, p. 251–287.
- Griffin, WL, Belousova, EA, Shee, SR, Pearson, NJ and O'Reilly, SY 2004, Archean crustal evolution in the northern Yilgarn Craton: U–Pb and Hf-isotope evidence from detrital zircons: *Precambrian Research*, v. 127, p. 19–41.
- Griffin, W, Pearson, N, Belousova, E and Saeed, A 2006, Comment: Hf-isotope heterogeneity in standard zircon 91500: *Chemical Geology*, v. 233, p. 358–363.

- Griffin, W, Pearson, N, Belousova, E and Saeed, A 2007, Reply to 'Comment to short-communication: Hf-isotope heterogeneity in zircon 91500' by WL Griffin, NJ Pearson, EA Belousova, A Saeed (Chemical Geology 233 (2006) p. 358–363)' by F Corfu: Chemical Geology, v. 244, p. 354–356.
- Griffin, WL, Wang, X, Jackson, S, Pearson, N, O'Reilly, S, Xu, X and Zhou, X 2002, Zircon chemistry and magma genesis, SE China: in-situ analysis of Hf isotopes, Pingtan and Tonglu igneous complexes: Lithos, v. 61, p. 237–269.
- Groves, DI, Goldfarb, RJ, Robert, F and Hart, CJR 2003, Gold deposits in metamorphic belts: Overview of current understanding, outstanding problems, future research, and exploration significance: Economic Geology, v. 98, p. 1–29.
- Gum, J and Belousova, E 2006, Musgrave Province reconnaissance using TerraneChron: ASEG Extended Abstracts, v. 1, p. 1–7.
- Haines, PW, Hand, M and Sandiford, M 2001, Palaeozoic syn-orogenic sedimentation in central and northern Australia: a review of distribution and timing of intracontinental orogens. Australian Journal of Earth Science, v. 48, no. 6, p. 911–928.
- Hawkesworth, C, Cawood, P, Kemp, T, Storey, C and Dhuime, B 2009, A matter of preservation: Science, v. 323, p. 49–50.
- Hawkesworth, C and Kemp, A 2006a, Using hafnium and oxygen isotopes in zircons to unravel the record of crustal evolution: Chemical Geology, v. 226, p. 144–162.
- Hawkesworth, CJ and Kemp, AIS 2006b, The differentiation and rates of generation of the continental crust: Chemical Geology, v. 226, p. 134–143.
- Hofmann, AW 1988, Chemical differentiation of earth: the relationship between mantle continental crust and oceanic crust: Earth and Planetary Science Letters v. 90, p. 297–314.
- Hollis, JA, Beyer, EE, Whelan, JA, Kemp, AIS, Scherstén, A and Greig, A 2010, Summary of results. NTGS laser U–Pb and Hf geochronology project: Pine Creek Orogen, Murphy Inlier, McArthur Basin and Arunta Region: Northern Territory Geological Survey, Record, 2010-001.
- Hoskin, PWO and Schaltegger, U 2003, The Composition of zircon and igneous and metamorphic petrogenesis: Reviews in Mineralogy and Geochemistry, v. 53, p. 27–62.
- Howard, HM, Smithies, RH, Evins, PM, Kirkland, CL, Werner, M, Wingate, MTD and Pirajno, F 2011a, The west Musgrave Province: 1:100 000 Explanatory Notes, Geological Survey of Western Australia, p. 359.
- Howard, HM, Smithies, RH, Kirkland, CL, Evins, P and Wingate, MTD 2009, Age and geochemistry of the Alcurra Suite in the west Musgrave Province and implications for orthomagmatic Ni–Cu–PGE mineralization during the Giles Event: Geological Survey of Western Australia, Record 2009/16, p. 16.
- Howard, KE, Hand, M, Barovich, KM and Belousova, E 2011c, Provenance of late Paleoproterozoic cover sequences in the central Gawler Craton: Exploring stratigraphic correlations in eastern Proterozoic Australia using detrital zircon ages, Hf and Nd isotopic data: Australian Journal of Earth Sciences, v. 58, p. 475–500.
- Howard, KE, Hand, M, Barovich, KM, Payne, JL and Belousova, EA 2011d, U–Pb, Lu–Hf and Sm–Nd isotopic constraints on provenance and depositional timing of metasedimentary rocks in the western Gawler Craton: Implications for Proterozoic reconstruction models: Precambrian Research, v. 184, p. 43–62.
- Howard, KE, Hand, M, Barovich, KM, Payne, JL, Cutts, KA and Belousova, EA 2011e, U–Pb zircon, zircon Hf and whole-rock Sm–Nd isotopic constraints on the evolution of Paleoproterozoic rocks in the northern Gawler Craton: Australian Journal of Earth Sciences, v. 58, p. 615–638.
- Howard, HM, Werner, M, Smithies, RH, Kirkland, CL, Kelsey, DL, Hand, M, Collins, A, Pirajno, F, Wingate, MTD, Maier, WD and Raimondo, T 2011b, The geology of the west Musgrave Province and the Bentley Supergroup – a field guide: Geological Survey of Western Australia, Record 2011/4, 119p.
- Kelly, N, Clarke, G, Harley, S and Baldwin, J 2006, Monazite behaviour and age significance in poly-metamorphic high-grade terrains; a case study from the western Musgrave Block, central Australia, Lithos, v. 88, p. 100.
- Kelsey, DE, Hand, M, Smithies, H, Evins, P, Clark, C and Kirkland, CL 2009, High-temperature, high geothermal gradient metamorphism in the Musgrave Province, central Australia; potential constraints on tectonic setting, in Kangaroo Island 2009, Biennial Conference of the Specialist Group for Geochemistry, Mineralogy and Petrology, November 2009 edited by NE Timms, J Foden, KE Evans and C Clark: Geological Society of Australia Abstracts, v. 96, p. 28.
- Kemp, A, Hawkesworth, C, Foster, G, Paterson, B, Woodhead, J, Hergt, J, Gray, C and Whitehouse, M 2007, Magmatic and crustal differentiation history of granitic rocks from Hf–O isotopes in zircon: Science, v. 315, p. 980–983.
- Kilpatrick, J and Ellis, D 1992, C-type magmas: igneous charnockites and their extrusive equivalents: Transactions of the Royal Society of Edinburgh, Earth Sciences, v. 83, p. 155–164.
- King, RJ 2008, Using calculated pseudosections in the system NCKFMASHTO and SHRIMP II U–Pb zircon dating to constrain the metamorphic evolution of paragneisses in the Latitude Hills West Musgrave Province, Western Australia: Geological Survey of Western Australia, Record 2009/15, 116p.
- Kirkland, CL, Bodorkos, S, Wingate, MTD and Smithies, RH 2009a, 185592: banded quartz-rich psammite, Latitude Hill; Geochronology Record 763, Geological Survey of Western Australia, 5p.
- Kirkland, CL, Spaggiari, CV, Pawley, MJ, Wingate, MTD, Smithies, RH, Howard, HM, Tyler, IM, Belousova, EA and Poujol, M 2011a, On the edge: U–Pb, Lu–Hf, and Sm–Nd data suggests reworking of the Yilgarn craton margin during formation of the Albany–Fraser Orogen: Precambrian Research, v. 187, p. 223–247.
- Kirkland, CL, Wingate, MTD, Bodorkos, S and Smithies, RH 2009b, 185591: garnet-rich leucogranite, Latitude Hill; Geochronology Record 761: Geological Survey of Western Australia, 4p.
- Kirkland, CL, Wingate, MTD, Howard, HM and Smithies, RH 2012a, 194759: dolerite dyke, Hinckley Range; Geochronology Record 1057 Geological Survey of Western Australia, 4p.
- Kirkland, CL, Wingate, MTD and Smithies, RH 2010, 187195: leucogranitic gneiss, Mount Scott; Geochronology Record 912: Geological Survey of Western Australia, 5p.
- Kirkland, CL, Wingate, MTD and Smithies, RH, 2011b, 194764: monzogranite, Mount Scott; Geochronology Record 965: Geological Survey of Western Australia, 4p.
- Kirkland, CL, Wingate, MTD and Smithies, RH, 2012b, 194765: syenogranite, Mount Scott; Geochronology Record 1040: Geological Survey of Western Australia, 4p.
- Kirkland, CL, Wingate, MTD and Smithies, RH 2012c, 194766: granite pegmatite vein, Mount Scott; Geochronology Record 1039: Geological Survey of Western Australia, 4p.
- Kirkland, CL, Wingate, MTD, Smithies, RH and Evins, PM 2012d, 194767: psammitic enclave in gneiss, Mount Scott; Geochronology Record 1025, 4p.
- Kirkland, CL, Wingate, MTD, Smithies, RH and Evins, PM, 2012e, 194768: migmatitic paragneiss, Mount Scott; Geochronology Record 1028: Geological Survey of Western Australia, 4p.

- Kirkland, CL, Wingate, MTD, Spaggiari, CV and Tyler, IM 2009c, 184353: monzogranite, Kiwirrkurra: Geochronology Record 820: Geological Survey of Western Australia, 4p.
- Kirkland, CL, Wingate, MTD, Spaggiari, CV and Tyler, IM 2009d, 184359: metarhyodacite, Dovers Hills: Geochronology Record 815, Geological Survey of Western Australia, 4p.
- Kirkland, CL, Wingate, MTD, Spaggiari, CV and Tyler, IM 2009e, 184364: metasyenogranite, Buck Hills: Geochronology Record 845: Geological Survey of Western Australia, 4p.
- Kirkland, CL, Wingate, MTD, Tyler, IM and Spaggiari, CV 2009f, 184367: metagranodiorite, Dwarf Well: Geochronology Record 846: Geological Survey of Western Australia, 4p.
- Kita NT, Ushikubo T, Fu B and Valley JW, 2009. High precision SIMS oxygen isotope analysis and the effect of sample topography. *Chemical Geology*: 264(1-4), p. 43–57.
- Korsch, R, Kositsin, N and Champion, D 2011, Australian island arcs through time; geodynamic implications for the Archean and Proterozoic: *Gondwana Research*, v. 19, p. 716–734.
- Langmuir, C, Vocke, R and Hanson, G, 1978, A general mixing equation with applications to Icelandic basalts: *Earth and Planetary Science Letters*, v. 37, p. 380–392.
- McLaren, S, Sandiford, M and Powell, R 2005, Contrasting styles of Proterozoic crustal evolution: A hot-plate tectonic model for Australian terranes: *Geology*, v. 33, p. 673–676.
- Myers, JS, Shaw, RD and Tyler, IM 1996, Tectonic evolution of Proterozoic Australia: *Tectonics*, v. 15, p. 1431–1446.
- O’Nions, RK, Carter, SR, Evensen, NM and Hamilton, PJ 1979, Geochemical and cosmochemical applications of Nd isotope analysis: *Annual Review of Earth and Planetary Science*, v. 7, p. 11–38.
- Oliver, NHS, Holcombe, RJ, Hill, EJ and Pearson, PJ 1991, Tectono-metamorphic evolution of the Mary Kathleen fold belt, Northwest Queensland: a reflection of mantle plume processes? *Australian Journal of Earth Sciences*, v. 38, p. 425–455.
- Paul, M 1992, Nature of the crust beneath magmatically active continental rifts: *Tectonophysics*, v. 213, p. 269–284.
- Peck, WH, Valley, JW, Wilde, SA and Graham, CM 2001, Oxygen isotope ratios and rare earth elements in 3.3 to 4.4 Ga zircons: Ion microprobe evidence for high $\delta^{18}\text{O}$ continental crust and oceans in the Early Archean: *Geochimica et Cosmochimica Acta*, v. 64, p. 4215–4229.
- Rogers, N, Macdonald, R, Fitton, JG, George, R, Smith, M and Barreiro, B, 2000, Two mantle plumes beneath the East African rift system: Sr, Nd and Pb isotope evidence from Kenya Rift basalts: *Earth and Planetary Science Letters*, v. 176, p. 387–400.
- Rudnick, RL and Gao, S, 2003, Composition of the continental crust, *in* The crust: treatise on geochemistry Volume 3 *edited by* RL Rudnick: Elsevier, Amsterdam, p. 1–64.
- Rutland, RWR 1973, Tectonic evolution of the continental crust of Australia: implications of continental drift to the earth sciences, *Continental evolution*, Volume 2: Academic Press, London, p. 1011–1033.
- Scherer, E, Munker, C and Mezger, K 2001, Calibration of the lutetium-hafnium clock: *Science*, v. 293, p. 683–687.
- Scrimgeour, IR 2006, The Arunta Region: Links between tectonics and mineralisation, *in* Annual Geoscience Exploration Seminar (AGES) *edited by* TJ Munson and IS Scrimgeour: Northern Territory Geological Survey Record 2006-002, p. 7–10.
- Scrimgeour, IR and Close, D 1999, Regional high-pressure metamorphism during intracontinental deformation; the Petermann Orogeny, central Australia: *Journal of Metamorphic Geology*, v. 17, p. 557–572.
- Scrimgeour, IR, Kinny, PD, Close, DF and Edgoose, CJ 2005, High-T granulites and polymetamorphism in the southern Arunta Region, central Australia: evidence for a 1.64 Ga accretional event: *Precambrian Research*, v. 142, p. 1–27.
- Şener, AK, Young, C, Groves, DI, Krapez, B and Fletcher, IR, 2005, Major orogenic gold episode associated with Cordilleran-style tectonics related to the assembly of Paleoproterozoic Australia?: *Geology*, v. 33, p. 225–228.
- Smithies, RH, Howard, HM, Evins, PM, Kirkland, CL, Kelsey, DE, Hand, M, Wingate, MTD, Collins, AS and Belousova, E 2011, High-temperature granite magmatism, crust-mantle interaction and the mesoproterozoic intracontinental evolution of the Musgrave Province, central Australia: *Journal of Petrology*, v. 52, p. 931–958.
- Smithies, RH, Howard, HM, Evins, PM, Kirkland, CL, Kelsey, DE, Hand, M, Wingate, MTD, Collins, AS, Belousova, E and Allchurch, S 2010, Geochemistry, geochronology and petrogenesis of Mesoproterozoic felsic rocks in the western Musgrave Province of central Australia and implication for the Mesoproterozoic tectonic evolution of the region: *Geological Survey of Western Australia, Report 106*, p. 73.
- Smithies, RH, Howard, HM, Evins, PM and Maier, WD 2009, BLACKSTONE, WA Sheet 4545: Geological Survey of Western Australia, 1:100 000 Geological Series.
- Spaggiari, CV, Bodorkos, S, Barquero-Molina, M, Tyler, IM and Wingate, MTD 2009, Interpreted bedrock geology of the south Yilgarn and central Albany–Fraser Orogen, Western Australia: *Geological Survey of Western Australia, Record 2009/10*, p. 84.
- Spaggiari, CV, Kirkland, CL, Pawley, MJ, Smithies, RH, Wingate, MTD, Doyle, MG, Blenkinsop, TG, Clark, C, Oorschot, CW, Fox, LJ and Savage, J 2011, The Geology of the East Albany–Fraser Orogen — A field guide, *Geological Survey of Western Australia, Record 2011/23*, p. 98.
- Stern, RA 2001, A new isotopic and trace-element standard for the ion microprobe: preliminary thermal ionization mass spectrometry (TIMS) U–Pb and electron microprobe data, *Geological Survey of Canada, Report 2001-F1*, 11p.
- Stern, RA, Bodorkos, S, Kamo, SL, Hickman, AH and Corfu, F 2009, Measurement of SIMS instrumental mass fractionation of Pb isotopes during zircon dating: *Geostandards and Geoanalytical Research*, v. 33, p. 145.
- Sun, S-S and McDonough, WF 1989, Chemical and isotopic systematics of oceanic basalts; implications for mantle composition and processes, *in* *Magmatism in the ocean basins* *edited by* AD Saunders and MJ Norry: Geological Society of London, London v. 42, p. 313–345.
- Sun, S-S, Warren, RG and Shaw, RD 1995, Nd isotope study of granites from the Arunta Inlier, central Australia; constraints on geological models and limitation of the method, *in* *Time limits on tectonic events and crustal evolution using geochronology; Some Australian Examples* *edited by* WJ Collins and RD Shaw: Precambrian Research, Elsevier, Amsterdam, p. 310–314.
- Valley, J 2003, Oxygen isotopes in zircon, *in* *Zircon* *edited by* JM Hanchar and PWO Hoskin: Reviews in Mineralogy and Geochemistry, v. 53, Geological Society of America, p. 343–385.
- Valley, J, Chiarenzelli, J and McLelland, J 1994, Oxygen isotope geochemistry of zircon: *Earth and Planetary Science Letters*, v. 126, p. 187–206.
- Valley, JW et al. 2005, 4.4 billion years of crustal maturation: oxygen isotope ratios of magmatic zircon: *Contributions to Mineralogy and Petrology*, v. 150, p. 561–580.

- van de Fliedert, T, Goldstein, SL, Hemming, SR, Roy, M, Frank, M and Halliday, AN 2007, Global neodymium-hafnium isotope systematics – revisited: *Earth and Planetary Science Letters*, v. 259, p. 432–441.
- Vervoort, JD, Patchett, PJ, Albarede, F, Blichert-Toft, J, Rudnick, R and Downes, H 2000, Hf–Nd isotopic evolution of the lower crust: *Earth and Planetary Science Letters*, v. 181, p. 115.
- Wade, B, Barovich, K, Hand, M, Scrimgeour, I and Close, D 2006, Evidence for early Mesoproterozoic arc magmatism in the Musgrave Block, central Australia; implications for Proterozoic crustal growth and tectonic reconstructions of Australia: *Journal of Geology*, v. 114, p. 43–63.
- Wade, B, Kelsey, D, Hand, M and Barovich, K 2008, The Musgrave Province; stitching north, west and south Australia: *Precambrian Research*, v. 166, p. 370–386.
- Watson, EB 1996, Dissolution, growth and survival of zircons during crustal fusion: kinetic principles, geological models and implications for isotopic inheritance: *Geological Society of America Special Papers*, v. 315, p. 43–56.
- Wendt, I and Carl, C 1991, The statistical distribution of the mean squared weighted deviation: *Chemical Geology*, v. 86, p. 275–285.
- White, R, Clarke, G and Nelson, D 1999, SHRIMP U–Pb zircon dating of Grenville-age events in the western part of the Musgrave Block, central Australia: *Journal of Metamorphic Geology*, v. 17, p. 465–481.
- Wingate, MTD and Kirkland, CL 2010, Introduction to geochronology information released in 2010: *Geological Survey of Western Australia*, p. 5.
- Wingate, M, Pirajno, F and Morris, P 2004, Warakurna large igneous province; a new Mesoproterozoic large igneous province in west-central Australia: *Geology (Boulder)*, v. 32, p. 105–108.
- Woodhouse, A, Hand, M, Barovich, K, Kirkland, CL, Smithies, RH, Belousova, E in prep, Isotopically distinct source terrains of sedimentary protoliths in the west Musgrave Province.
- Wörner, G 1999, Lithospheric dynamics and mantle sources of alkaline magmatism of the Cenozoic West Antarctic Rift System: *Global and Planetary Change*, v. 23, p. 61–77.
- Wyborn, LAI, Page, RW and McCulloch, MT 1988, Petrology, geochronology and isotope geochemistry of the post-1820 Ma granites of the Mount Isa Inlier: mechanisms for the generation of Proterozoic anorogenic granites: *Precambrian Research*, v. 40/41, p. 509–541.
- York, D 1966, Least-squares fitting of a straight line: *Canadian Journal of Physics* v. 44, p. 1079–1086.
- Zhao, J-X and Bennett, V 1995, SHRIMP U–Pb zircon geochronology of granites in the Arunta Inlier, central Australia; implications for Proterozoic crustal evolution: *Precambrian Research*, v. 71, p. 17–43.
- Zhao, J-X and McCulloch, M 1995, Geochemical and Nd isotopic systematics of granites from the Arunta Inlier, central Australia; implications for Proterozoic crustal evolution: *Precambrian Research*, v. 71, p. 265–299.
- Zheng, Y-F, Wu, Y-B, Zhao, Z-F, Zhang, S-B, Xu, P and Wu, F-Y 2005, Metamorphic effect on zircon Lu–Hf and U–Pb isotope systems in ultrahigh-pressure eclogite-facies metagranite and metabasite: *Earth and Planetary Science Letters*, v. 240, p. 378.

This report uses a multi-isotopic (Lu–Hf, Sm–Nd and oxygen) approach to constrain the crustal evolution of the Musgrave Province. Although the nature of basement to the province is cryptic, the Nd and Hf isotopic evolution of nearly all rocks in the province requires the presence of a Paleoproterozoic to early Mesoproterozoic juvenile basement, along with a minor Archean component. Nd and Hf isotopic model ages from magmatic rocks and sediments throughout the Musgrave Province indicate a major juvenile crust formation event at 1950–1900 Ma. Later during the Musgrave Orogeny (1220–1150 Ma) crust in this region became HFSE-enriched so that it was insensitive to juvenile input, which has very low concentrations of Hf and Nd. Hence, addition of juvenile material during and after the Musgrave Orogeny is difficult to distinguish. Although the Musgrave Province is an extreme case of a HFSE-enriched magmatic province, it is possible that considerable amounts of juvenile input into other intracratonic orogens have gone undetected in isotopic data.



Further details of geological products and maps produced by the Geological Survey of Western Australia are available from:

Information Centre

Department of Mines and Petroleum

100 Plain Street

EAST PERTH WA 6004

Phone: (08) 9222 3459 Fax: (08) 9222 3444

<http://www.dmp.wa.gov.au/GSWApublications>